2011

Accurate and Efficient Modeling of Interconnects in Lossy Layered Media

Sidharath Jain
Iowa State University

Accurate and efficient modeling of interconnects in lossy layered media

by

Sidharath Jain

A dissertation submitted to the graduate faculty

in partial fulfillment of the requirements for the degree of

DOCTOR OF PHILOSOPHY

Major: Electrical Engineering

Program of Study Committee:
Jiming Song, Major Professor
Gary L. Tuttle
Nicola Bowler
Jaeyoun Kim
Santosh Pandey

Iowa State University

Ames, Iowa

2011

TABLE OF CONTENTS

LIST OF TABLES

LIST OF FIGURES

ACKNOWLEDGEMENTS

I am very grateful to Prof. Jiming Song for his valuable guidance and keeping his office door open so that I could talk to him when ever I had any questions. I am also thankful to him for freedom he gave me to think and explore new ideas. I am also very grateful to Prof. Gary Tuttle, Prof. Nicola Bowler, Prof. Jaeyoun Kim and Prof. Santosh Pandey for their time and valuable suggestions. I am also very grateful to Prof. Sumit Chaudhary who was a part of my committee but was not available for my PhD defence for his time, for his valuable guidance and support.

I am also grateful to Dr. Telesphor Kamgaing, from Intel Corporation, Chandler, Arizona for his valuable suggestions about the current needs of the electronic design automation (EDA) industry so that we could contribute something valuable which could be integrated into the current EDA tools in order to make them more efficient. I am thankful to Intel Corporation, Arizona, USA and the National Science Foundation for funding my PhD research.

I am thankful to Dr. Fu Gang Hu, Hui Xie, Teng Zhao and Hongsheng Xu and other students in Dr. Song's group for their kind and friendly association and enlightening discussions. I thank all the departmental staff for their timely help.

I am also very grateful to my friends Dr. Siddhartha Khaitan, Sandeep Krishnan, Dr. Abhisek Mudgal, Dr. Venkat Krishnan, Yang Li, Aditya Jain and others who provided a very loving and friendly atmosphere without which all this would not have been possible.

I am extremely grateful to my parents and my sister for their loving support and encouragement throughout.

ABSTRACT

Semiconductor-based integrated circuits have become the mainstream for very-large-scale integration (VLSI) systems such as high-speed digital circuits, radio-frequency integrated circuits (RFIC), and even monolithic microwave integrated circuits (MMIC). The shrinking feature size and increasing frequency promote high integration density and interconnection complexity that demand high accuracy modeling techniques. The current design paradigm has shifted from the transistor-driven design to the interconnect-driven design. Thus the accurate and efficient modeling of on-chip interconnect becomes critical for the computer-aided design tools to analyze the overall system performance.

In this research, we focus on implementing the full wave spectral domain approach (SDA) for accurate modeling of shielded microstrip interconnects. Two new techniques, the mid-point summation (MPS) and the super convergent series (SCS) approach have been developed to accelerate the SDA by nearly five to six orders of magnitude. It involves the leading term extraction of the Green's function and the Bessel's function and using the above two methods to accelerate the summation of slowly convergent infinite spectral series.

An accelerated SDA has been developed using two superconvergent series to handle the more general case of multilayered shielded microstrip interconnects in which the signal strip can be displaced from the center. In addition to this, closed form expressions have been developed to dynamically choose the number of terms and the value of the parameters as a function of the argument, to adaptively obtain the best convergence of the second type of superconvergent series for a given accuracy and argument.

The accelerated spectral domain formulation using two super convergent series was extended to handle multiple metal lines on the same interface and very accurate results have been obtained for the propagation constant using a few terms of the infinite summation.

Also an equivalent model for a lossy shielded microstrip line on layered media is constructed by replacing the layered media with a single effective medium and a detailed analysis of its validity at different frequencies and different range of dimensions has been presented for application to on chip interconnects. The relative permittivity for a single layer microstrip which results in the same propagation constant for the dominant mode as the layered one at a given frequency is considered to be the equivalent. The results show that this model is frequency independent for layered structures when the given frequency and frequency of operation are less than the transition frequency (i.e. the frequency at which there is a significant change in the equivalent dielectric constant (ϵ_{req})). For frequencies higher than the transition frequency the equivalent model is not frequency independent but it gives good results for the higher order mode although it is derived using the dominant mode. Also it is seen that at low frequency ϵ_{req} depends on the layers near to the signal metal but at higher frequencies it depends on the layer with the highest value of ϵ_{r} irrespective of its location w.r.t to the metal strip. For the case, when some of the layers have a finite conductivity we see two transition frequencies. The first transition frequency just depends on the layer with the highest $\sigma_{ri}/\epsilon_{ri}$ ratio and the second transition frequency is the same as that for the lossless case and occurs when the thickness of the layer with the highest value of ϵ_{ri} becomes comparable to the wavelength.

The spectral domain immitance approach (SDIA) was extended to handle multiple metal lines in different layers. Also, several techniques to account for the finite thickness and conductivity of the metal lines have been studied. The pulse-triangle and triangle-triangle basis functions were developed so as to include this effect into the SDA. This, is because entire domain basis functions such as Chebyshev polynomials will lead to nonconvergent infinite series summation while calculating the elements of the MoM matrix.

CHAPTER 1. Introduction

In the last three decades there has been a rapid advancement in semiconductor based integrated circuits such as VLSI cicuits, RFIC's, MMIC circuits and high speed digital circuits. With the rapid increase in the frequency and the reduction in feature size, newer technologies such a multichip modules, multi level and multilayered interconnect modules have been developed to support higher integration density.

Due to the reduction of device size and increase of overall chip size, the signal delays on interconnect networks become critical in determining the overall circuit performance. Currently the VLSI design paradigm is shifting from the conventional transistor-driven to the interconnect-driven design to satisfy the total technical requirements. Moreover, the high integration density makes circuits vulnerable to the harsh electromagnetic interference (EMI). The requirement of signal integrity demands that the computer-aided design (CAD) tools should accurately and efficiently predict the electrical properties of interconnects. In order to cope up with the advancement in these technologies, the accurate modeling of electromagnetic (EM) properties of interconnects is the key.

1.1 Research Motivation

With the increasing demands on the speed and accuracy in electronic design automation (EDA) tools, there is need for fast and accurate modeling of interconnects over a wide frequency range. As we know, the 3-D integrated interconnect structures are very complex consisting of multiple layers of metal lines, vias, etc. embedded in multiple layers of lossy medium. In order to increase

the speed and accuracy domain decomposition methods are being used in recent electromagnetic solvers like HFSS 13. In the future versions of electromagnetic solvers the whole problem will be split into domains using the domain decomposition method and each domain would be analyzed using a problem specific approach on a separate core [5]. The techniques proposed in this thesis and its extensions can improve the speed and accuracy in the modeling of metal lines and patches embedded in a multilayered lossy material which constitute a major portion of any chip. Also in the modeling and simulation of multilayered interconnects as shown in Figure 1.1, one needs to combine many thin layers together to increase mesh uniformity and reduce computation time and memory requirements. It is very handy to be able to model the structure as using a single effective medium. In most packages and semiconductor backends, dummy metallization, ground planes and vias are typically placed around the signal interconnects for both process optimization and electrical coupling reduction. In high density packaging, external electromagnetic interference (EMI) shielding may be used to limit interaction between components or a die may be flip-chip assembled above the power or ground plane of an underlaying package substrate. In such cases, microstrip transmission lines on the silicon can be considered as being in a shielded environment.

In MMIC circuits it is common to use packaging to provide isolation so the circuits need to be modeled keeping into account the enclosing shielding box. Metallic shielding is commonly used to give mechanical support and to improve heat dissipation. The effects of the shielding become considerable in the following two situations [6]. Firstly, when the frequency of operation exceeds the cut off frequency for the higher order modes. Secondly, when the side walls and top of the metal box are very close to the circuitry [7], these are referred to as proximity effects. In the first case the occurrence of high Q resonances can cause an abrupt change in the response around the resonance frequency. The proximity of the side walls to the circuit metallization usually causes a shift in the frequency and certain other global perturbations in the response of the circuit. The proximity effects are more prominent at a lower frequency because when the frequency is lower the electrical distance between the side wall and the metal strip is very small but it increases with

increase in frequency. If the box size is reduced the effective dielectric constant (ϵ_{reff}) will reduce because more and more electric field lines will terminate on the side walls and the top surface so the concentration of field lines in the dielectric region will reduce and a larger percentage of energy will propagate in the air region. This makes the accurate modeling of multilayered shielded interconnect structures all the more important.

1.2 Problem Statement

In this thesis an attempt has been made to accurately and efficiently extract the effective medium parameters for multilayered interconnect structure with multiple dummy metallizations or multiple metal lines with finite thickness and conductivity in different layers as shown in Figure 1.1. We have used the spectral domain approach (SDA) to accomplish this. SDA is much more efficient and accurate as compared to using the finite element method (FEM) [8], finite difference (FD) [8] because it uses the Green's function which already takes into account the boundary conditions very accurately. Also the grid dispersion error is absent in the SDA. Also by using the entire domain basis instead of sub domain basis very accurate results for the propagation constant can be obtained using a few basis functions. But in spite of these advantages of small matrix sizes the accurate computation of the matrix elements can be computationally intensive as it requires infinite summation of slowly convergent spectral series. Also as the complexity increases drastically as the number of metal lines increases. In addition, to this the resistive thin sheet approximation and impedance boundary condition (IBC) [9],[10] can be used to model very thin and very thick metal lines, respectively. Also a R-Card/IBC formulation proposed by [11] can be used to model strip thickness less than skin depth (δ) and greater than nearly three times δ. But there are no accurate models reported which can model metal lines with metal thickness of the order of its width which is the case in modern interconnects.

So at first we consider a simplified problem of a single layer shielded microstrip with a single

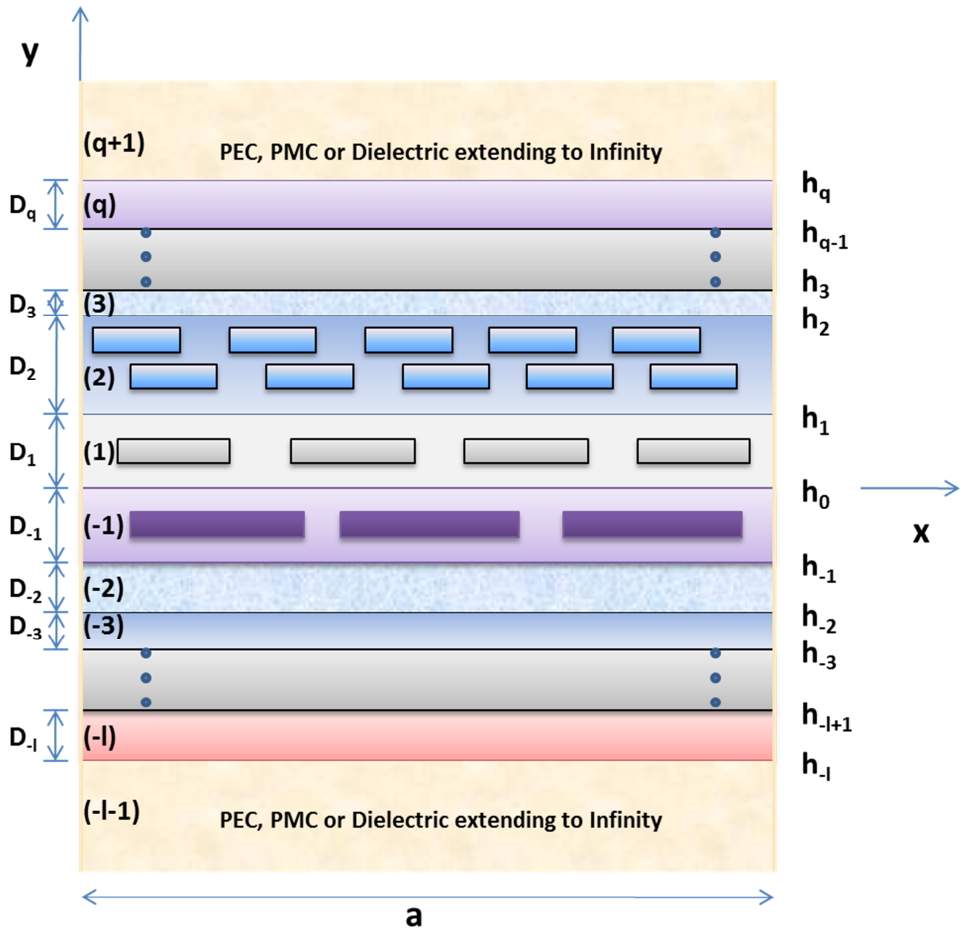

Figure 1.1 Shielded multilayered interconnects with multiple dummy metallizations or multiple metal lines in different layers

signal strip at the center to demonstrate the acceleration of the convergence of the matrix elements. We then increase the complexity of the problem by considering a generalized multilayered shielded microstrip in which the signal strip is displaced from one of the side walls by a distance c.

In the next step we will look at the multilayered shielded microstrip with multiple conductors on the same plane as shown in Figure 6.1. Finally we will consider the case of a multilayer shielded microstrip when we have multiple conductors located in different layers as shown in Figure 1.1. Also, we will consider some approximations to model the metal lines with a finite thickness and conductivity.

1.3 Literature Review

1.3.1 Spectral Domain Approach for Shielded Microstrip Lines and Acceleration of Infinite Series Summation

The spectral domain approach (SDA) results in accurate results for propagation constants for shielded microstrip lines using a few basis functions. However, as the required accuracy increases the computation time increases very rapidly because of the slow convergence of the spectral series summation making this approach computationally intensive for computer aided design (CAD) purposes. In order to accelerate the convergence of spectral series summation several techniques have been used ([3], [12]). Also for open microstrip with double negative materials an approach based on leading term extraction has been demonstrated [13]. The time intensive part in the SDA is the calculation of the matrix elements and not finding the determinant as the matrix size is small [3]. By using appropriate basis functions and adding the asymptotic tails of the series involved improvement in accuracy and CPU time can be obtained [14]. Cano et al. [3] have proposed a leading term extraction technique for accelerating but it involves the computation of the Green's function in the space domain and a time intensive double integral to find each element of the Galerkin matrix. Tsalamengas and Fikioris [12] have proposed a leading term extraction technique using rapidly convergent series but it involved the computation of the generalized Riemann Zeta function and Gamma function for the computation of the coefficients which is time consuming although it converges quite fast. Also the convergence is slow by using very small number of basis functions.

The approximation of summation with a fast convergent series has been frequently used to speed up the solution of several problems in electromagnetics. But such convergent series exist only for specific cases and cannot be applied to speed up the summation in any general case. The Euler Maclaurin formula (EMF) [15]-[16] has been widely used for approximation of finite and infinite series summations for any general series [17]. The Shanks transformation has been used to accelerate the convergence of infinite series [18]. However, the problem with the Shanks transfor-

mation is that it can accelerate only certain type of series and it does not work well especially for the kinds of series which occur in the SDA. Also, an approach known as summation by parts has been reported for fast convergence of series in which one of the terms is easily integrable and the other one is convergent [19] but its efficiency decreases for small values of the argument. Another promising approach to approximate an infinite summation of series is the Richardson extrapolation [20] but again its convergence depends on the nature of series.

1.3.2 Equivalent Model

Although a unified dispersion model was developed by Verma and Hassani [21] for the shielded multilayer microstrip using the single layer reduction (SLR) formulation and a new unified dispersion model was developed by Verma and Kumar [22] but both approaches are based on the dispersion model of the effective dielectric constant for an open microstrip line over a single layer which makes the equivalent structure lose its inhomogeneity. In addition, it was restricted to lossless media.

1.3.3 Analysis of Multilayered Shielded Interconnects

Several approaches have been used for the modeling of multi layered on chip interconnect structures. Zhu and Jiao [23] have used the finite element method for the full wave analysis of on chip interconnect structures. Chew and Radhakrishnan [2] have used the finite difference method for the analysis of multilayered multi conductor shielded interconnects. Mosig et al. have used an approach based on the method of moments for the analysis multilayer planar boxed circuits [24]. The finite element approach and the finite difference approach are slow. Also to get an accurate solution the mesh size has to be very small which will lead to very large matrix sizes. But by using the spectral domain approach with a small number of basis functions it is possible to obtain a very accurate solution for the propagation constant or the effective medium. Also, it is possible to accelerate the slow convergence of spectral series using leading term extraction by several orders

of magnitude. Xu and Omar [25] have presented an improved formulation of the singular integral equation method for shielded multilayer microstrip lines. But this method is complicated compared to the SDA because of being multistage and requires a large number of basis functions and hence a large matrix size to obtain the propagation constant.

1.3.4 Approximation of Finite Thickness and Conductivity of Signal Strip

Another big obstacle in accurate modeling of multilayered interconnects is the modeling of metal lines with finite thickness and conductivity. In the newer technologies as the size of the chips is decreasing and more and more functionality it being packed into them the width of the on chip interconnects is decreasing. But in order to keep the resistance small the thickness of the metal layer is also increasing. So this puts forth a great challenge for accurate modeling of metal layers with finite conductivity and thickness in interconnect structures. In order to solve this problem several approaches like the perturbation approach, the quasi TEM method and full wave approaches like conformal mapping, hybrid-mode formulation, mode matching, method of lines (MOL), spectral domain approach (SDA), the finite element method (FEM), boundary integral equation method, transverse resonance technique, the extended spectral domain approach ([26]-[27]) have been proposed but all of them fail the test of accuracy or computation time. The perturbation approach [28] works well only when the strip thickness is comparable to the skin depth. The quasi TEM approach ([29]-[30]) can accurately model metal losses but it cannot handle multilayered structures. Also the current and field distribution as obtained using the full wave methods may be completely different from the quasi static case, especially for suspended substrate structure. The quasi-TEM approach fails when the conductivity of the substrate is greater than 0.1 S/mm. The mode matching method [31] and FEM [32] can take care of real metal but the computation becomes very time consuming if we have a large number of layer which is generally the case with interconnects. Thus the above mentioned full wave techniques cannot be used in all situations because of the approximation made or computation complexity. In the transverse resonance

method [33] and the extended spectral domain approach ([26]-[27]) the metal was first assumed to have infinite conductivity in order to calculate the effective dielectric constant and the electric and magnetic fields. The expression for the fields along with the power loss method [34] is used to determine the loss due to the real metal comprising the metal strip. Some researchers have used the skin depth approximation (thickness of strip is much larger than skin depth) and treated the real metal signal strip using surface impedance boundary condition (IBC) to determine propagation and attenuation constants at the same time ([9] and [10]). The IBC describes the relationship between the electric and magnetic fields on the boundary, which is defined as the surface impedance, when the metallization thickness is much thicker than the skin depth. This metallization layer attenuates transmitted waves and eventually becomes impenetrable. The impedance boundary condition and the power loss method are suitable for cases in which the skin depth is of the order of strip thickness. Krowne et al. [35] have used the resistive boundary condition (R-Card) to solve for the propagation constant assuming the strip thickness to be much smaller than skin depth which is not the case in many applications in MMICs and interconnects. However, the IBC and R-Card models neglect the dependence of surface impedance on TE/TM fields of the hybrid LSE/LSM modes inside the conductor, therefore Amari et al. [36] presented a LSE/LSM-mode impedance model. For large thickness (t), the model converges to a surface impedance as in the IBC approximation and for $t \rightarrow 0$ it converges to a shunt resistance as in the R-card model. In [37], all three components of strip currents were considered in the modified SDA. The rigorous integral equation formulation with dyadic Green's function was proposed for the skin effect of conductor strips [38]. A generalized transverse-resonance-diffraction approach was developed for the modeling of planar structures with thick lossy conductors [39]. In [40], a two-layer model was used to approximate the moderately thick conductors on the top and bottom surfaces with two PEC BCs. A N-layer model was applied to evaluate the conductor loss in [41].

CHAPTER 2. Numerical Acceleration of Spectral Domain Approach for Shielded Microstrip Lines by Approximating Summation with Mid-Point Summation and Super Convergent Series

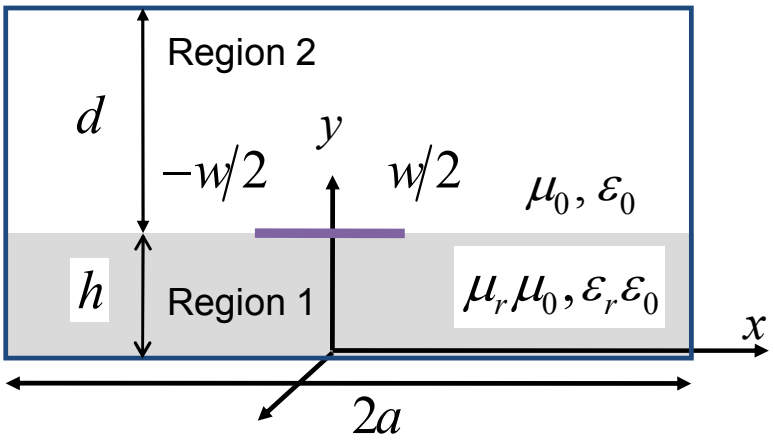

Figure 2.1 Single layer shielded interconnect with one signal strip

In this chapter, two novel techniques for numerical acceleration of the SDA for shielded microstrip by accelerating the convergence of series summation in the elements of the Galerkin matrix have been presented. The first approach uses Maclaurin series and theory of contour integrals to approximate the infinite summation of the leading term with a super convergent series (SCS). So there is neither a need for evaluation of complex coefficients using Gamma functions or Riemann Zeta functions nor for numerical integration. The second approach approximates the summation of the leading terms from $N_{\max}$ to infinity using a novel mid-point summation (MPS) formula. The

derivation of the mid-point summation formula is also included.

2.2 Shielded Microstrip

Figure 2.1 shows a cross section of a shielded microstrip. The region 2 consists of air. Region 1 is a dielectric material with relative permittivity and permeability ϵ_r and μ_r, respectively. The structure is uniform and infinite along the z axis. The thin metal casing and the thin metal strip are assumed to be perfect electric conductors (PECs). The width of the metal strip is w and that of the box is $2a$.

2.3 Spectral Domain Approach (SDA)

The microstrip structure cannot support pure transverse electromagnetic (TEM) waves. The solutions are hybrid modes which are superpositions of infinite TE^z and TM^z modes or TE^y and TM^y modes [42], [43]. For the solution of hybrid modes using infinite TE^y and TM^y please refer to Appendix B. For the TE^z and TM^z modes all the field components can be expressed as two z-components of vector potentials [34].

2.3.1 Vector Potentials

The z dependency of the electric and magnetic field has the form of $e^{-j\beta z}$. The vector potential for TM^z mode is

$$A_{zi}(x,y,z) = -\frac{\omega\epsilon_i\mu_i}{\beta}\Phi_i^{(e)}(x,y)e^{-j\beta z} \tag{2.1}$$

and the vector potential for TE^z mode is

$$F_{zi}(x,y,z) = -\frac{\omega\epsilon_i\mu_i}{\beta}\Phi_i^{(h)}(x,y)e^{-j\beta z} \tag{2.2}$$

They satisfy homogeneous Helmholtz equation in source free region ($y \neq h$),

$$\nabla_t^2\Phi_i^{(p)}(x,y) + (k_i^2 - \beta^2)\Phi_i^{(p)}(x,y) = 0 \tag{2.3}$$

where $k_i^2 = \omega^2 \epsilon_i \mu_i$, $i = 1, 2$, and $p = e, h$.

The z-components of transverse electric (TE) and transverse magnetic (TM) modes can be written in terms of $\Phi_i^{(p)}(x, y)$ as

$$E_{zi}(x, y, z) = j \frac{k_i^2 - \beta^2}{\beta} \Phi_i^{(e)}(x, y) e^{-j\beta z} \tag{2.4}$$

$$H_{zi}(x, y, z) = j \frac{k_i^2 - \beta^2}{\beta} \Phi_i^{(h)}(x, y) e^{-j\beta z} \tag{2.5}$$

The transverse components can be written in terms of $\nabla_t \Phi_i^{(p)}(x, y)$ as

$$\mathbf{E}_{ti}(x, y, z) = \nabla_t \Phi_i^{(e)}(x, y) e^{-j\beta z} - \frac{\omega \mu_i}{\beta} \hat{z} \times \nabla_t \Phi_i^{(h)}(x, y) e^{-j\beta z} \tag{2.6}$$

$$\mathbf{H}_{ti}(x, y, z) = \nabla_t \Phi_i^{(h)}(x, y) e^{-j\beta z} + \frac{\omega \epsilon_i}{\beta} \hat{z} \times \nabla_t \Phi_i^{(e)}(x, y) e^{-j\beta z} \tag{2.7}$$

or

$$E_{xi}(x, y) = \frac{\partial \Phi_i^{(e)}}{\partial x} + \frac{\omega \mu_i}{\beta} \frac{\partial \Phi_i^{(h)}}{\partial y} \tag{2.8}$$

$$E_{yi}(x, y) = \frac{\partial \Phi_i^{(e)}}{\partial y} - \frac{\omega \mu_i}{\beta} \frac{\partial \Phi_i^{(h)}}{\partial x} \tag{2.9}$$

$$H_{xi}(x, y) = \frac{\partial \Phi_i^{(h)}}{\partial x} - \frac{\omega \epsilon_i}{\beta} \frac{\partial \Phi_i^{(e)}}{\partial y} \tag{2.10}$$

$$H_{yi}(x, y) = \frac{\partial \Phi_i^{(h)}}{\partial y} + \frac{\omega \epsilon_i}{\beta} \frac{\partial \Phi_i^{(e)}}{\partial x} \tag{2.11}$$

All the fields and the potentials are defined from $x = -a$ to a and can be expanded as follows.

$$\tilde{f}(m) = \int_{-a}^{a} dx\, \tilde{f}(x) e^{j\alpha_m x} = \int_{-a}^{a} dx\, \tilde{f}(x) \left[\cos(\alpha_m x) + j \sin(\alpha_m x)\right] \tag{2.12}$$

$$f(x) = \frac{1}{2a} \sum_{m=-\infty}^{\infty} \tilde{f}(m) e^{-j\alpha_m x} = \frac{1}{2a} \sum_{m=-\infty}^{\infty} \tilde{f}(m) \left[(\cos \alpha_m x) - j \sin(\alpha_m x)\right] \tag{2.13}$$

where $\alpha_m = m\pi/a$. Using the boundary conditions and the properties of Fourier series [43] we can obtain that $m = (n - 1/2)$ for the even mode ($n = 1, 2, ...$).

2.3.2 Fourier Transform and General Solutions

By taking the Fourier transform of $\Phi_i^{(e)}(x,y)$ and $\Phi_i^{(h)}(x,y)$ with respect to x the partial differential equation (2.3) can be reduced to ordinary differential equation

$$\tilde{\Phi}_i^{(p)}(\alpha_n, y) = \int_{-a}^{a} dx\, \Phi_i^{(p)}(x,y) e^{j\alpha_n x} \tag{2.14}$$

$$\Phi_i^{(p)}(x,y) = \begin{cases} \frac{1}{a}\sum_{m=1}^{\infty} \tilde{\Phi}_i^{(p)}(\alpha_n, y)\cos(\alpha_n x) \\ -\frac{j}{a}\sum_{m=1}^{\infty} \tilde{\Phi}_i^{(p)}(\alpha_n, y)\sin(\alpha_n x) \end{cases} \tag{2.15}$$

where $i = 1, 2$, $p = e, h$ and $\alpha_n = (n - 1/2)\pi/a$.

The wave equation (2.3) now becomes

$$\left(\frac{d^2}{dy^2} - \gamma_i^2\right) \tilde{\Phi}_i^{(p)}(\alpha_n, y) = 0 \tag{2.16}$$

where $\gamma_i^2 = \alpha_n^2 + \beta^2 - k_i^2$.

The general solutions of the wave equation are of the form

$$\begin{aligned} \tilde{\Phi}_i^{(p)}(\alpha_n, y) &= A_i^{(p)}(\alpha_n) e^{\gamma_i y} + B_i^{(p)}(\alpha_n) e^{-\gamma_i y} \\ &= C_i^{(p)}(\alpha_n)\sinh(\gamma_i y) + D_i^{(p)}(\alpha_n)\cosh(\gamma_i y) \end{aligned} \tag{2.17}$$

The field components in the spectral domain can be written as

$$\tilde{E}_{zi}(\alpha_n, y) = j\frac{k_i^2 - \beta^2}{\beta}\tilde{\Phi}_i^{(e)}(\alpha_n, y) \tag{2.18}$$

$$\tilde{H}_{zi}(\alpha_n, y) = j\frac{k_i^2 - \beta^2}{\beta}\tilde{\Phi}_i^{(h)}(\alpha_n, y) \tag{2.19}$$

$$\tilde{E}_{xi}(\alpha_n, y) = -j\alpha_n\tilde{\Phi}_i^{(e)}(\alpha_n, y) + \frac{\omega\mu_i}{\beta}\frac{\partial}{\partial y}\tilde{\Phi}_i^{(h)}(\alpha_n, y) \tag{2.20}$$

$$\tilde{H}_{xi}(\alpha_n, y) = -j\alpha_n\tilde{\Phi}_i^{(h)}(\alpha_n, y) - \frac{\omega\epsilon_i}{\beta}\frac{\partial}{\partial y}\tilde{\Phi}_i^{(e)}(\alpha_n, y) \tag{2.21}$$

We can see that we do not need normal component $\tilde{E}_y$ and $\tilde{H}_y$ to solve the problem.

2.3.3 Boundary Conditions

Applying the boundary conditions to find the unknowns in (2.17). Considering PEC boundary conditions at $y = 0$ and $y = h + d$ we get

$$\begin{aligned} E_{z1}(x,0) = 0 &\implies \tilde{E}_{z1}(\alpha_n, 0) = 0 \implies \tilde{\Phi}_1^{(e)}(\alpha_n, 0) = 0 \\ &\implies \tilde{\Phi}_1^{(e)}(\alpha_n, y) = A(\alpha_n)\sinh(\gamma_1 y) \end{aligned} \tag{2.22}$$

$$\begin{aligned} E_{z2}(x,h+d) = 0 &\implies \tilde{E}_{z2}(\alpha_n, h+d) = 0 \implies \tilde{\Phi}_2^{(e)}(\alpha_n, h+d) = 0 \\ &\implies \tilde{\Phi}_2^{(e)}(\alpha_n, y) = B(\alpha_n)\frac{\sinh[\gamma_2(h+d-y)]}{\sinh(\gamma_2 d)} \end{aligned} \tag{2.23}$$

$$\begin{aligned} E_{x1}(x,0) = 0 &\implies \tilde{E}_{x1}(\alpha_n, 0) = 0 \implies \frac{\partial}{\partial y}\tilde{\Phi}_1^{(h)}(\alpha_n, y)\Big|_{y=0} = 0 \\ &\implies \tilde{\Phi}_1^{(h)}(\alpha_n, y) = C(\alpha_n)\cosh(\gamma_1 y) \end{aligned} \tag{2.24}$$

$$\begin{aligned} E_{x2}(x,h+d) = 0 &\implies \tilde{E}_{x2}(\alpha_n, h+d) = 0 \implies \frac{\partial}{\partial y}\tilde{\Phi}_2^{(h)}(\alpha_n, y)\Big|_{y=h+d} = 0 \\ &\implies \tilde{\Phi}_2^{(h)}(\alpha_n, y) = D(\alpha_n)\frac{\cosh[\gamma_2(h+d-y)]}{\cosh(\gamma_2 d)} \end{aligned} \tag{2.25}$$

We have four unknowns $A(\alpha_n)$, $B(\alpha_n)$, $C(\alpha_n)$, and $D(\alpha_n)$, so we need four more boundary conditions to solve for them. There is no surface magnetic current $\mathbf{M}_s$ on the interface, so tangential electric fields are continuous

$$\begin{aligned} \tilde{E}_{z1}(\alpha_n, h) = \tilde{E}_{z2}(\alpha_n, h) &\implies \frac{k_1^2 - \beta^2}{\beta}\tilde{\Phi}_1^{(e)}(\alpha_n, h) = \frac{k_2^2 - \beta^2}{\beta}\tilde{\Phi}_2^{(e)}(\alpha_n, h) \\ &\implies (k_1^2 - \beta^2)A(\alpha_n)\sinh(\gamma_1 h) = (k_2^2 - \beta^2)B(\alpha_n) \end{aligned} \tag{2.26}$$

$$\begin{aligned} &\tilde{E}_{x1}(\alpha_n, h) = \tilde{E}_{x2}(\alpha_n, h) \\ &\implies -j\alpha_n\tilde{\Phi}_1^{(e)}(\alpha_n, h) + \frac{\omega\mu_1}{\beta}\frac{\partial}{\partial y}\tilde{\Phi}_1^{(h)}(\alpha_n, y)\Big|_{y=h} = -j\alpha_n\tilde{\Phi}_2^{(e)}(\alpha_n, h) + \frac{\omega\mu_2}{\beta}\frac{\partial}{\partial y}\tilde{\Phi}_2^{(h)}(\alpha_n, y)\Big|_{y=h} \\ &\implies j\alpha_n[A(\alpha_n)\sinh(\gamma_1 h) - B(\alpha_n)] = \frac{\omega}{\beta}[\gamma_1\mu_1 C(\alpha_n)\sinh(\gamma_1 h) + \gamma_2\mu_2 D(\alpha_n)\tanh(\gamma_2 d)] \end{aligned} \tag{2.27}$$

Using the boundary condition for the magnetic field

$$\hat{y} \times (\mathbf{H}_2 - \mathbf{H}_1) = \mathbf{J}_s \tag{2.28}$$

Generally, the surface current $\mathbf{J}_s$ has both x- and z-components

$$\mathbf{J}_s(x, y = h, z) = \left[\hat{x} J_x(x) + \hat{z} J_z(x)\right] e^{-j\beta z} \tag{2.29}$$

In spectral domain, it can be written as:

$$\hat{y} \times \left[\tilde{\mathbf{H}}_2(\alpha_n, h) - \tilde{\mathbf{H}}_1(\alpha_n, h)\right] = \hat{x}\tilde{J}_x(\alpha_n) + \hat{z}\tilde{J}_z(\alpha_n) \tag{2.30}$$

$$\begin{aligned} \tilde{H}_{z2}(\alpha_n, h) - \tilde{H}_{z1}(\alpha_n, h) &= \tilde{J}_x(\alpha_n) \\ \implies j\frac{k_2^2 - \beta^2}{\beta} D(\alpha_n) - j\frac{k_1^2 - \beta^2}{\beta} C(\alpha_n)\cosh(\gamma_1 h) &= \tilde{J}_x(\alpha_n) \end{aligned} \tag{2.31}$$

and

$$\begin{aligned} &\tilde{H}_{x2}(\alpha_n, h) - \tilde{H}_{x1}(\alpha_n, h) = -\tilde{J}_z(\alpha_n) \\ &\implies -j\alpha_n\left[D(\alpha_n) - C(\alpha_n)\cosh(\gamma_1 h)\right] + \frac{\omega}{\beta}\left[\epsilon_1\gamma_1 A(\alpha_n)\cosh(\gamma_1 h) + \epsilon_2\gamma_2 B(\alpha_n)\right] = -\tilde{J}_z(\alpha_n) \end{aligned} \tag{2.32}$$

Now we have four equations (2.26), (2.27), (2.31) and (2.32) so we can solve for A, B, C and D.

$$\begin{aligned} \tilde{E}_{x2}(\alpha_n, h) &= -j\alpha_n \tilde{\Phi}_2^{(e)}(\alpha_n, h) + \frac{\omega\mu_2}{\beta}\frac{\partial}{\partial y}\tilde{\Phi}_2^{(h)}(\alpha_n, y)\Big|_{y=h} \\ &= -j\alpha_n B(\alpha_n) - \frac{\omega\mu_2}{\beta}\gamma_2 \tanh(\gamma_2 d) D(\alpha_n) \\ &= G_{xx}(\alpha_n, \beta)\tilde{J}_x(\alpha_n) + G_{xz}(\alpha_n, \beta)\tilde{J}_z(\alpha_n) \end{aligned}$$

$$\begin{aligned} \tilde{E}_{z2}(\alpha_n, h) = j\frac{k_2^2 - \beta^2}{\beta}\tilde{\Phi}_2^{(e)}(\alpha_n, h) &= j\frac{k_2^2 - \beta^2}{\beta} B(\alpha_n) \\ = G_{zx}(\alpha_n, \beta)\tilde{J}_x(\alpha_n) + G_{zz}(\alpha_n, \beta)\tilde{J}_z(\alpha_n) \end{aligned}$$

where

$$G_{xx}(\alpha_n,\beta)=\frac{j}{\omega\tilde{\Delta}}\Big[\mu_r\gamma_1(\alpha_n^2-k_2^2)\tanh(\gamma_1 h)+\gamma_2(\alpha_n^2-k_1^2)\tanh(\gamma_2 d)\Big] \tag{2.33}$$

$$G_{xz}(\alpha_n,\beta)=G_{zx}(\alpha_n,\beta)=\frac{j\alpha_n\beta}{\omega\tilde{\Delta}}\Big[\mu_r\gamma_1\tanh(\gamma_1 h)+\gamma_2\tanh(\gamma_2 d)\Big] \tag{2.34}$$

$$G_{zz}(\alpha_n,\beta)=\frac{j}{\omega\tilde{\Delta}}\Big[\mu_r\gamma_1(\beta^2-k_2^2)\tanh(\gamma_1 h)+\gamma_2(\beta^2-k_1^2)\tanh(\gamma_2 d)\Big] \tag{2.35}$$

$$\tilde{\Delta}=\big[\gamma_1\tanh(\gamma_1 h)+\epsilon_r\gamma_2\tanh(\gamma_2 d)\big]\big[\gamma_1\coth(\gamma_1 h)+\mu_r\gamma_2\coth(\gamma_2 d)\big] \tag{2.36}$$

where $\epsilon_r=\epsilon_1/\epsilon_2$ and $\mu_r=\mu_1/\mu_2$.

2.3.4 Method of Moments

Now we have two equations with two unknowns

$$G_{xx}(\alpha_n,\beta)\tilde{J}_x(\alpha_n)+G_{xz}(\alpha_n,\beta)\tilde{J}_z(\alpha_n)=\tilde{E}_{x1}(\alpha_n,h) \tag{2.37}$$

$$G_{zx}(\alpha_n,\beta)\tilde{J}_x(\alpha_n)+G_{zz}(\alpha_n,\beta)\tilde{J}_z(\alpha_n)=\tilde{E}_{z1}(\alpha_n,h) \tag{2.38}$$

Finally, let us look at electric fields and currents at the interface $y=h$. We have PEC boundary condition on strip

$$E_{x1}=E_{x2}=E_{z1}=E_{z2}=\begin{cases}0 & |x|<w/2\\ \text{unknown} & |x|>w/2\end{cases}$$

There is no current outside PEC strip

$$J_x(x)=J_z(x)=\begin{cases}\text{unknown} & |x|<w/2\\ 0 & |x|>w/2\end{cases}$$

Therefore their products are zero

$$E_{x1}(x)J_x(x)=0 \tag{2.39}$$

$$E_{z1}(x)J_z(x)=0 \tag{2.40}$$

The unknown current $\tilde{J}_x(\alpha_n)$ and $\tilde{J}_z(\alpha_n)$ are be expanded in terms of basis function $\tilde{J}_{xi}(\alpha_n)$ and $\tilde{J}_{zi}(\alpha_n)$ as follows

$$\tilde{J}_x(\alpha_n) = \sum_{i=1}^{M_x} a_i \tilde{J}_{xi}(\alpha_n) \tag{2.41}$$

$$\tilde{J}_z(\alpha_n) = \sum_{i=1}^{M_z} b_i \tilde{J}_{zi}(\alpha_n) \tag{2.42}$$

The basis currents are chosen such that $J_{xi}(x)$ and $J_{zi}(x)$ are nonzero only on the strip $|x| < w/2$, and $J_{xi}(x)$ is a real odd function, $J_{zi}(x)$ is a real even function for the dominant mode and other even modes. According to the properties of Fourier transform, $\tilde{J}_{xi}(\alpha_n)$ is a purely imaginary and odd function, $\tilde{J}_{zi}(\alpha_n)$ is a purely real and even function.

The Parseval's theorem says that

$$\sum_{n=1}^{\infty} \tilde{f}(n)\tilde{g}(n) = 2a \int_{-a}^{a} f(x)g(-x)dx \tag{2.43}$$

So we have

$$\sum_{n=1}^{\infty} \tilde{E}_{x2}(\alpha_n, h)\tilde{J}_{xm}(\alpha_n) = 2a \int_{-\infty}^{\infty} E_{x2}(-x, h)J_{xm}(x)dx = 0 \tag{2.44}$$

$$\sum_{n=1}^{\infty} \tilde{E}_{z2}(\alpha_n, h)\tilde{J}_{zm}(\alpha_n) = 2a \int_{-a}^{a} E_{z2}(-x, h)J_{zm}(x)dx = 0 \tag{2.45}$$

or

$$\sum_{n=1}^{\infty} \tilde{E}_{x2}(\alpha_n, h)\tilde{J}_{xm}(\alpha_n) = 0, m = 1, 2.....M_{\mathrm{x}} \tag{2.46}$$

$$\sum_{n=1}^{\infty} \tilde{E}_{z2}(\alpha_n, h)\tilde{J}_{zm}(\alpha_n) = 0, m = 1, 2.....M_{\mathrm{z}} \tag{2.47}$$

Equations (2.46) and (2.47) can be written it in matrix form as:

$$\begin{bmatrix} K^{xx} & K^{xz} \\ K^{zx} & K^{zz} \end{bmatrix} \begin{bmatrix} A \\ B \end{bmatrix} = \begin{bmatrix} 0 \\ 0 \end{bmatrix}$$

where

$$K_{ij}^{pq} = \sum_{n=1}^{\infty} \tilde{J}_{pi}(\alpha_n) G_{pq}(\alpha_n, \beta) \tilde{J}_{qj}(\alpha_n) = \sum_{n=1}^{\infty} F_{ij}^{pq} \tag{2.48}$$

where $F_{ij}^{pq} = \tilde{J}_{pi}(\alpha_n) G_{pq}(\alpha_n, \beta) \tilde{J}_{qj}(\alpha_n), \quad p = x, z$ and $q = x, z$. and

$$\begin{bmatrix} A \\ B \end{bmatrix} = \begin{bmatrix} a_1 \\ \vdots \\ a_{M_x} \\ b_1 \\ \vdots \\ b_{M_z} \end{bmatrix} \tag{2.49}$$

For a homogeneous system to have a non trivial solution determinant should be zero.

$$D(\beta, \omega) = \det \begin{bmatrix} K^{xx} & K^{xz} \\ K^{zx} & K^{zz} \end{bmatrix} = 0 \tag{2.50}$$

The propagation constant β, for each frequency point ω can be found by solving the above equation.

2.4 Basis Functions for Currents

There are multiple choices of current basis. The basis currents are chosen such that $J_{xi}(x)$ and $J_{zi}(x)$ are nonzero only on the strip $|x| < w/2$, and $J_{xi}(x)$ is a real odd function, $J_{zi}(x)$ is a real even function. So from the properties of Fourier transforms, $\tilde{J}_{xi}(\alpha_n)$ is a purely imaginary and odd function, $\tilde{J}_{zi}(\alpha_n)$ is a purely real and even function. Chebyshev polynomials of the first and second kind are chosen as the basis for $J_z(x)$ and $J_x(x)$, respectively [34]. This is because the Fourier transform for the Chebyshev polynomial along with the weighting function to take care of the edge singularity for the longitudinal current and the zero at the edges for the transverse current is the Bessel's function. We could also use weighted sine/cosine basis but its Fourier transform would be a sum of Bessel's functions which would complicate the formulation.

2.4.1 Chebyshev Polynomials

For the even mode $J_z(x)$ is an even function so it can be expanded using the even order Chebyshev polynomials of the first kind including a term to incorporate the edge singularities [34].

$$J_z(x) = \sum_{n=1}^{M_z} I_{zn} \frac{T_{2n-2}(2x/w)}{\sqrt{1-(2x/w)^2}} \tag{2.51}$$

where $T_{2n}(u)$ satisfies recursive relation [13]

$$\begin{aligned} T_0(u) &= 1 \\ T_1(u) &= u \\ T_2(u) &= 2u^2 - 1 \\ T_n(u) &= 2uT_{n-1}(u) - T_{n-2}(u) \end{aligned} \tag{2.52}$$

where $\delta_n = \alpha_n w/2$. The transverse current J_x is proportional to ω so as frequency decreases it will become very small compared to J_z therefore J_x has been normalized with $k_0 w$ [44]. $J_x(x)$ is an odd function so it is expanded using odd order Chebyshev polynomials of the second kind including a term to make sure that it vanishes at the edges.

$$J_x(x) = j\sqrt{1-(2x/w)^2} \sum_{n=1}^{M_x} I_{xn} U_{2n-1}(2x/w) \tag{2.53}$$

where U_{2n-1} satisfies

$$\begin{aligned} U_0(u) &= 1 \\ U_1(u) &= 2u \\ U_2(u) &= 4u^2 - 1 \\ U_n(u) &= 2uU_{n-1}(u) - U_{n-2}(u) \end{aligned} \tag{2.54}$$

The Fourier transforms of the unknown current $\tilde{J}_x(\alpha_n)$ and $\tilde{J}_z(\alpha_n)$ are expanded in terms of

basis functions $\tilde{J}_{xi}$ and $\tilde{J}_{zi}$ as follows:

$$\tilde{J}_x(\alpha_n) = \sum_{i=1}^{M_x} a_i \tilde{J}_{xi}(\alpha_n) k_0 w \tag{2.55}$$

$$\tilde{J}_z(\alpha_n) = \sum_{i=1}^{M_z} b_i \tilde{J}_{zi}(\alpha_n) \tag{2.56}$$

The Fourier transforms of the basis functions can be written as:

$$\tilde{J}_x(\alpha_n) = \frac{w\pi}{\delta_n} \sum_{i=1}^{M_x} I_{xi} i(-1)^i J_{2i}(\delta_n) k_0 w \tag{2.57}$$

$$\tilde{J}_z(\alpha_n) = \frac{w\pi}{2} \sum_{i=1}^{M_z} I_{z(i-1)}(-1)^{i-1} J_{2(i-1)}(\delta_n) \tag{2.58}$$

$J_n(z)$ is the Bessel function of the first kind.

2.5 Leading Term Extraction

2.5.1 Asymptotic Approximation to Green's Functions

As $\alpha_n \to \infty$, keeping the first two terms in Taylor expansion. We have

$$\gamma_1 = \sqrt{\alpha_n^2 + \beta^2 - k_1^2} \approx \alpha_n + \frac{\beta^2 - k_1^2}{2\alpha_n} \tag{2.59}$$

$$\gamma_2 = \sqrt{\alpha_n^2 + \beta^2 - k_2^2} \approx \alpha_n + \frac{\beta^2 - k_2^2}{2\alpha_n} \tag{2.60}$$

$$\begin{aligned}\tilde{\Delta} &\approx (\epsilon_r\gamma_2 + \gamma_2)(\mu_r\gamma_2 + \gamma_1) = \epsilon_r\mu_r\gamma_2^2 + (\epsilon_r + \mu_r)\gamma_1\gamma_2 + \gamma_1^2 \\ &\approx \alpha_n^2(1+\epsilon_r)(1+\mu_r) \\ &\quad + \frac{1}{2}(1+\epsilon_r)\Big[(\beta^2 - k_1^2) + \mu_r(\beta^2 - k_2^2)\Big] + \frac{1}{2}(1+\mu_r)\Big[(\beta^2 - k_1^2) + \epsilon_r(\beta^2 - k_2^2)\Big]\end{aligned} \tag{2.61}$$

Notice that higher order terms of α_n are thrown away and the Green's function can be approximated as:

$$G_{xx}(\alpha_n, \beta) \approx G_{xx0}\alpha_n w(1 - y_{1xx}/\alpha_n^2) \tag{2.62}$$

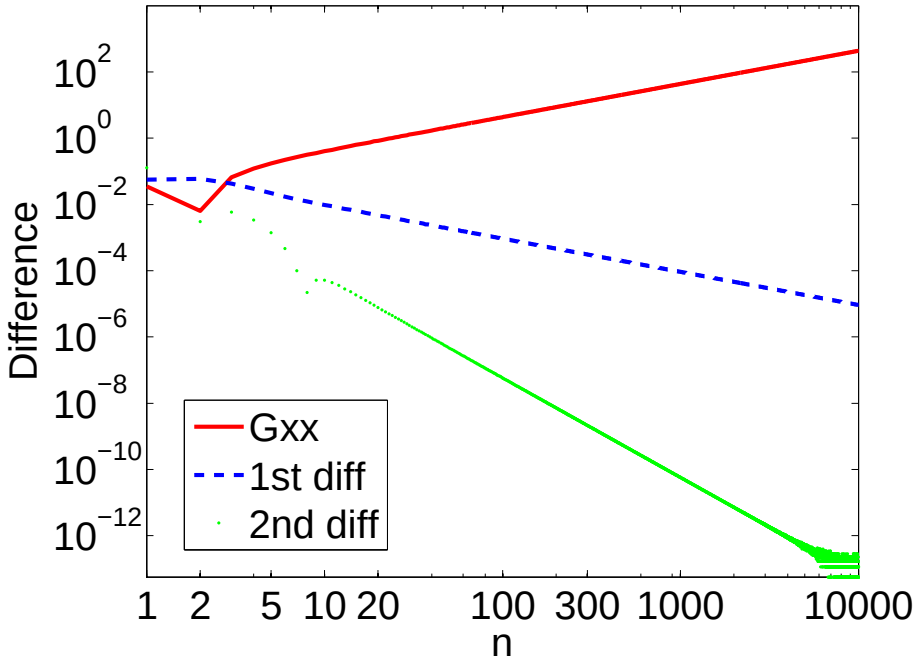

Figure 2.2 Convergence of G_{xx} using first and second leading terms for $\beta = 3k_0$

$$G_{xz}(\alpha_n, \beta) \approx G_{xz0}(1 - y_{1xz}/\alpha_n^2) \tag{2.63}$$

$$G_{zz}(\alpha_n, \beta) \approx \frac{G_{zz0}}{\alpha_n w}(1 - y_{1zz}/\alpha_n^2) \tag{2.64}$$

where

$$G_{xx0} = \frac{1}{1+\epsilon_r} \tag{2.65}$$

$$G_{xz0} = \frac{\beta}{(1+\epsilon_r)k_0} \tag{2.66}$$

$$G_{zz0} = \frac{(\beta^2 - k_1^2) + \mu_r(\beta^2 - k_2^2)}{k_0^2(1+\epsilon_r)(1+\mu_r)} \tag{2.67}$$

$$y_{1xx} = \frac{\beta^2}{2} + \frac{\epsilon_r k_1^2 + k_2^2}{2(1+\epsilon_r)} \tag{2.68}$$

$$y_{1xz} = \frac{\beta^2}{2} + \frac{(k_2^2 - k_1^2)(1-\mu_r)}{2(1+\mu_r)} - \frac{\epsilon_r k_2^2 + k_1^2}{2(1+\epsilon_r)} \tag{2.69}$$

$$y_{1zz} = \beta^2 - k_2^2 + \frac{1}{2}\Big[\Big(\frac{k_2^2 - k_1^2}{1+\mu_r} + \frac{k_2^2 - k_1^2}{1+\epsilon_r}\Big) - \frac{(\beta^2 - k_1^2)(\beta^2 - k_2^2)(1+\mu_r)}{(\beta^2 - k_1^2) + \mu_r(\beta^2 - k_2^2)}\Big] \tag{2.70}$$

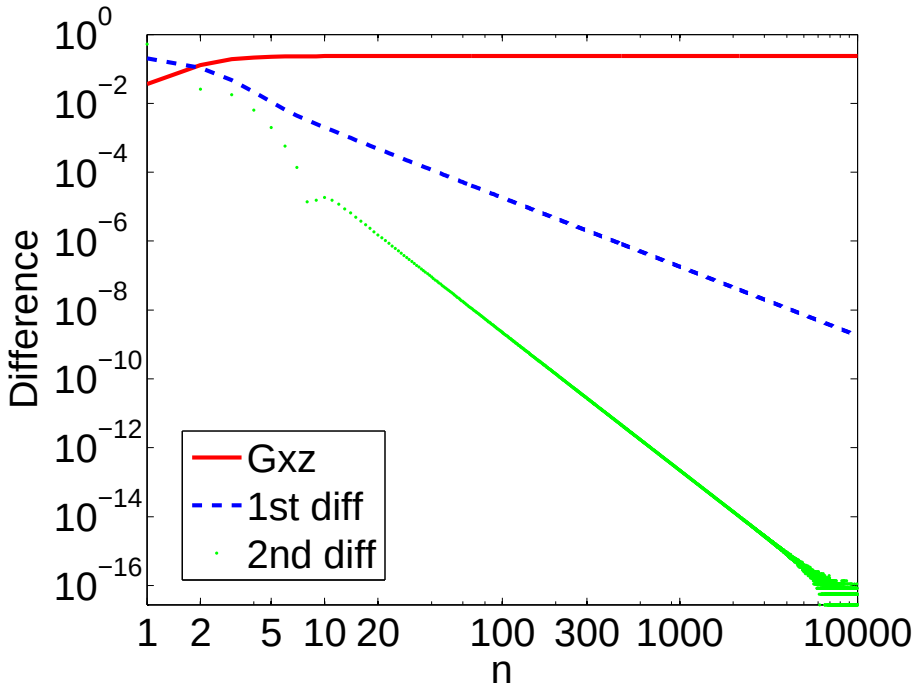

Figure 2.3 Convergence of G_{xz} using first and second leading terms for $\beta = 3k_0$

Consider a shielded microstrip with parameters $\epsilon_r = 11.7, \mu_r = 1, f = 4\text{GHz}, h = 3.17\text{mm}, w = 3.04\text{mm}, 2a = 34.74\text{mm}, d = 50\text{mm}$. Figure 2.2 shows that G_{xx} decreases as $1/n$, as $1/n^3$ after subtracting the first and as $1/n^5$ after subtracting the first two leading terms. Figure 2.3 shows that G_{xz} is nearly constant, it decreases as $1/n^2$ after subtracting the first and as $1/n^4$ after subtracting the first two leading terms. Also Figure 2.4 shows that G_{zz} increases as n, decreases as $1/n$ after subtracting the first and as $1/n^3$ after subtracting the first two leading terms. For derivation please refer to [13].

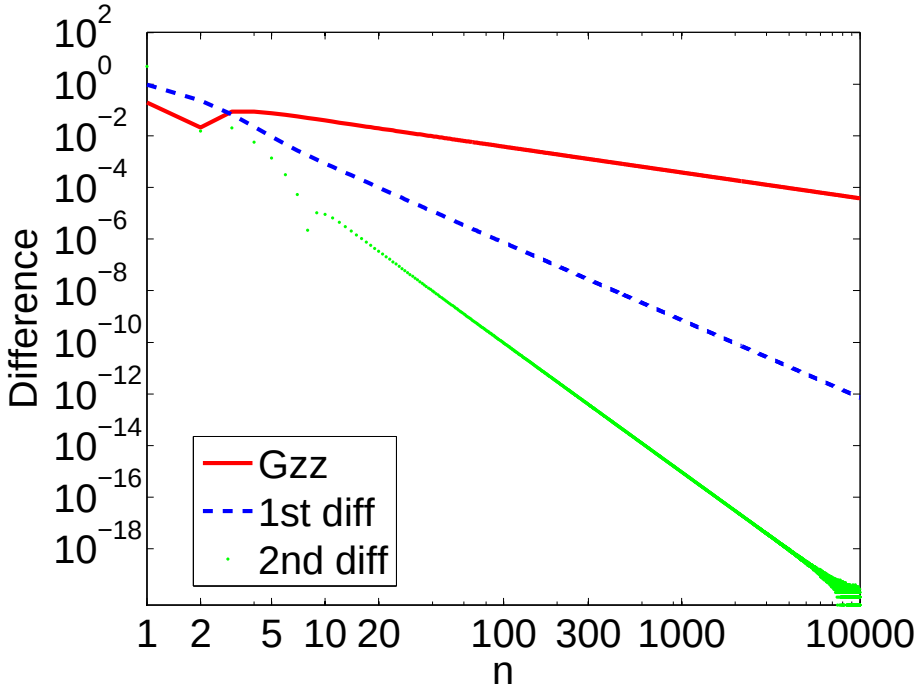

Figure 2.4 Convergence of G_{zz} using first and second leading terms for $\beta = 3k_0$

2.5.2 Approximating Summation with Super Convergent Series

2.5.2.1 Asymptotic Expansion for the Bessel Function

The series for the Bessel function [45], [46] is given by

$$J_n(z) = \left(\frac{2}{z\pi}\right)^{\frac{1}{2}}\left[\cos\left(z - \frac{n\pi}{2} - \frac{\pi}{4}\right)\left(1 - \frac{C_n^2}{(8z)^2} + ..\right) - \sin\left(z - \frac{n\pi}{2} - \frac{\pi}{4}\right)\left(\frac{C_n^1}{8z} - \frac{C_n^3}{(8z)^3} + ..\right)\right] \tag{2.71}$$

Therefore keeping terms up to $1/z^3$ and putting $z = \delta_n$ and $n = 2i$

$$J_{2i}(\delta_n) \approx \left(\frac{2}{\delta_n\pi}\right)^{\frac{1}{2}}(-1)^i\left[\cos\left(\delta_n - \frac{\pi}{4}\right)\left(1 - \frac{C_{2i}^2}{(8\delta_n)^2}\right) - \sin\left(\delta_n - \frac{\pi}{4}\right)\left(\frac{C_{2i}^1}{8\delta_n} - \frac{C_{2i}^3}{(8\delta_n)^3}\right)\right] \tag{2.72}$$

Putting $n = 2i - 1$

$$J_{2i-1}(\delta_n) \approx \left(\frac{2}{\delta_n\pi}\right)^{\frac{1}{2}}(-1)^{i+1}\left[\sin\left(\delta_n - \frac{\pi}{4}\right)\left(1 - \frac{C_{2i-1}^2}{(8\delta_n)^2}\right) + \cos\left(\delta_n - \frac{\pi}{4}\right)\left(\frac{C_{2i-1}^1}{8\delta_n} - \frac{C_{2i-1}^3}{(8\delta_n)^3}\right)\right] \tag{2.73}$$

where $n \in \{0, 1, 2, 3, ..\}$, $C_n^0 = 1$ and

$$C_n^k = \frac{1}{k!}\prod_{m=1}^{k}[4n^2 - (2m-1)^2] = \frac{4n^2 - (2k-1)^2}{k}C_n^{k-1} \tag{2.74}$$

Using (2.48), the leading term extraction for the Bessel's function and the Green's function and $\delta_n = \alpha_n w/2$, $K_{\text{ij}}^{\text{pq}}$ can be written as:

$$K_{ij}^{pq} \approx \sum_{n=1}^{N_{\max}}\left[F_{ij}^{pq} - \tilde{F}_{ij}^{pq}\right] + \sum_{n=1}^{\infty}\tilde{F}_{ij}^{pq} \tag{2.75}$$

Considering terms up to $1/\alpha_n^5$, $\tilde{F}_{ij}^{pq}$ can be written as:

$$\begin{aligned}\tilde{F}_{ij}^{pq}(-1)^{i+j} = \frac{G_{pq0}}{\alpha_n w}\Big(1 - \frac{y_{1pq}}{\alpha_n^2}\Big)J_{2i}(\delta_n)J_{2j}(\delta_n)(-1)^{i+j} = \frac{G_{pq0}}{(\alpha_n w)^2}\Big\{1 + \sin(\alpha_n w) \\ + (C_{2i}^1 + C_{2j}^1)\frac{\cos(\alpha_n w)}{4\alpha_n w} - \Big[16y_{1pq}w^2 + C_{2i}^2 + C_{2j}^2 - C_{2i}^1 C_{2j}^1 + (16y_{1pq}w^2 + C_{2i}^2 + C_{2j}^2 \\ + C_{2i}^1 C_{2j}^1)\sin(\alpha_n w)\Big]\frac{1}{(4\alpha_n w)^2} - \Big[C_{2i}^3 + C_{2j}^3 + C_{2i}^2 C_{2j}^1 + C_{2i}^1 C_{2j}^2 \\ + 16y_{1pq}w^2(C_{2i}^1 + C_{2j}^1)\Big]\frac{\cos(\alpha_n w)}{(4\alpha_n w)^3}\Big\}\end{aligned} \tag{2.76}$$

For any series of the form [34] $\sum_{n=1,3,5..}^{\infty} e^{jnz}/n^k$ where $k = 2, 3, 4, ...$:

$$\sum_{n=1,3,5..}^{\infty} e^{jnz}/n^k = j\sum_{n=1,3,5..}^{\infty}\int_0^z \left(e^{jnz}/n^{k-1}\right)dz + \sum_{n=1,3,5..}^{\infty} 1/n^k \tag{2.77}$$

Also we know that [34]

$$\sum_{n=1,3..}^{\infty} e^{jnz}/n = -(1/2)\ln[\tan(z/2)] + j\pi/4,\ |z| < \pi \tag{2.78}$$

From [47] the Maclaurin Series expansion of $\ln(\tan z)$ can be written as

$$\begin{aligned}\ln(\tan z) = \ln z + z^2/3 + 7z^4/90 + 62z^6/2835 + 127z^8/18900 + 146z^{10}/66825 \\ + 1414477z^{12}/1915538625 + 32764z^{14}/127702575 + O[z]^{16},\ |z| < \pi\end{aligned} \tag{2.79}$$

So the first term in right hand side of (2.77) is evaluated using (2.78) and (2.79) and the second term is calculated using the Riemann Zeta function [48].

$$\sum_{n=1,3,5,..}^{\infty} \sin(nz)/n^2 = -\left[(z/2)\ln(z/2) - z/2 + z^3/72 + 7z^5/14400 + 31z^7/1270080 + 127z^9/87091200 + 73z^{11}/752716800 + ..\right] \tag{2.80}$$

Similarly for any series of the form $\sum_{n=1}^{\infty} e^{jnz}/n^k$ where $k = 2, 3, 4, ...$ [34]:

$$\sum_{n=1}^{\infty} e^{jnz}/n^k = j\sum_{n=1}^{\infty}\int_0^z \left(e^{jnz}/n^{k-1}\right)dz + \sum_{n=1}^{\infty} 1/n^k \tag{2.81}$$

Also we know that [34]

$$\sum_{n=1}^{\infty} e^{jnz}/n = -\ln[2\sin(z/2)] + j(\pi - z)/2, 0 < z < 2\pi \tag{2.82}$$

From [47] the Maclaurin Series expansion of $\ln(\sin z)$ can be written as

$$\ln(\sin z) = \ln z - z^2/6 - z^4/180 - z^6/2835 - z^8/37800 - z^{10}/467775...., -\pi < z < \pi \tag{2.83}$$

So the first term in right hand side of (2.81) is evaluated using (2.82) and (2.83) and the second term is calculated using the Riemann Zeta function.

$$\sum_{n=1}^{\infty} \sin(nz)/n^2 = -\left(z\ln z - z - z^3/72 - z^5/14400 - z^7/1270080 - z^9/87091200 - z^{11}/5269017600 - ..\right) \tag{2.84}$$

In the second term on the right hand side in (2.75), as given in (2.76), terms involving infinite summation of sinusoidal functions divided by α_n^k can be approximated using super convergent series as in (2.78) and (2.82) and those of the form $1/\alpha_n^k$ can be evaluated using the Riemann Zeta function [48]. The expression for the SCS for higher orders are given in Appendix A.

2.5.3 Approximation of Summation to Integral with Mid-point Summation (MPS)

This section presents a new formula involving integral and derivatives of the function, to approximate the summation of a series to an integral with mid-point summation (MPS) [49]. In addition, a simple recursive relation to evaluate the coefficient has been derived. The error in approximating the summation with MPS, using the same number of terms, converges one order faster than the EMF. Also, a general expression for the special case involving a summation of a product of a sinusoidal function and another function which goes to zero as the argument approaches infinity has been developed. A recursive relation to obtain the coefficients for the special case has also been presented. This new formula has been used in accelerating the infinite summation of series occurring in SDA for shielded microstrips to obtain very accurate and quick results for the propagation constant.

2.5.3.1 Euler Maclaurin Formula (EMF)

According to the Euler Maclaurin formula [15]

$$\sum_{n=a}^{b} f(n) = \int_a^b f(x)dx + \frac{1}{2}\Big[f(a)+f(b)\Big] + \frac{1}{12}\Big[f^{'}(a)-f^{'}(b)\Big] - \frac{1}{720}\Big[f^{'''}(a)-f^{'''}(b)\Big] + ... + \frac{B_{2p}}{(2p)!}\Big[f^{(2p-1)}(a)-f^{(2p-1)}(b)\Big] + ... \tag{2.85}$$

where B_{2p} are Bernoulli numbers. $B_0 = 1$, $B_1 = -1/2$, $B_2 = 1/6$, $B_4 = -1/30$, $B_6 = 1/42$, $B_8 = -1/30$,... $B_{2n+1} = 0$ for $n > 1$ [50]. The Bernoulli numbers are defined as follows:

$$z/(e^z - 1) = \sum_{n=0}^{\infty} B_n z^n/n!, \quad |z| < 2\pi \tag{2.86}$$

For $F(x) = \int f(x)dx \to 0,\ f^{(n)}(x) \to 0$ as $x \to \infty$ using (2.85) we can write

$$\sum_{n=N}^{\infty} f(n) = -F(N) + \frac{1}{2}f(N) - \frac{1}{12}f^{'}(N) + \frac{1}{720}f^{'''}(N) - \frac{1}{30240}f^{(v)}(N) + ... \tag{2.87}$$

2.5.3.2 Mid-point Summation

Now we will approximate the summation with an integral. Using Taylor series we can write

$$f(x-N) = f(N) + \sum_{n=1}^{\infty} \frac{1}{n!} f^{(n)}(N)(x-N)^n \tag{2.88}$$

Integrating x from $N-1/2$ to $N+1/2$ using the mid-point rule we get

$$f(N) = \int_{N-\frac{1}{2}}^{N+\frac{1}{2}} f(x)dx - \sum_{n=1}^{\infty} \frac{2^{-2n}}{(2n+1)!} f^{(2n)}(N) \tag{2.89}$$

The general form is written as:

$$f(N) = F(x)\Big|_{N-\frac{1}{2}}^{N+\frac{1}{2}} + \sum_{n=1}^{\infty} c_n f^{(2n-1)}(x)\Big|_{N-\frac{1}{2}}^{N+\frac{1}{2}} \tag{2.90}$$

where a recursive relation for c_n is derived by substituting (2.90) into (2.89). Using (2.90) we can write:

$$f^{(2m)}(N) = f^{(2m-1)}(x)\Big|_{N-\frac{1}{2}}^{N+\frac{1}{2}} + \sum_{n=1}^{\infty} c_n f^{(2n+2m-1)}(x)\Big|_{N-\frac{1}{2}}^{N+\frac{1}{2}} \tag{2.91}$$

Substituting $f^{(2n)}(N)$ using (2.91) in (2.89) we get

$$f(N) = F(x)\Big|_{N-\frac{1}{2}}^{N+\frac{1}{2}} - \sum_{n=1}^{\infty} \frac{2^{-2n}}{(2n+1)!} \left[f^{(2n-1)}(x)\Big|_{N-\frac{1}{2}}^{N+\frac{1}{2}} + \sum_{m=1}^{\infty} c_m f^{(2m+2n-1)}(x)\Big|_{N-\frac{1}{2}}^{N+\frac{1}{2}} \right] \tag{2.92}$$

Changing the summation variable

$$\left\{ \begin{array}{c} n = 1 \to \infty \\ m = 1 \to \infty \end{array} \right\} \Rightarrow \left\{ \begin{array}{c} l = n + m = 2 \to \infty \\ n = 1 \to l - 1 \end{array} \right\}$$

we get:

$$f(N) = F(x)\Big|_{N-\frac{1}{2}}^{N+\frac{1}{2}} - \sum_{n=1}^{\infty} \frac{2^{-2n}}{(2n+1)!} f^{(2n-1)}(x)\Big|_{N-\frac{1}{2}}^{N+\frac{1}{2}} - \sum_{l=2}^{\infty} \sum_{n=1}^{l-1} c_{l-n} \frac{2^{-2n}}{(2n+1)!} f^{(2l-1)}(x)\Big|_{N-\frac{1}{2}}^{N+\frac{1}{2}} \tag{2.93}$$

$$= F(x)\Big|_{N-\frac{1}{2}}^{N+\frac{1}{2}} + \sum_{n=1}^{\infty} c_n f^{(2n-1)}(x)\Big|_{N-\frac{1}{2}}^{N+\frac{1}{2}} \tag{2.94}$$

Using (2.93) c_n can be obtained as:

$$c_n = -\frac{2^{-2n}}{(2n+1)!} - \sum_{m=1}^{n-1} \frac{2^{-2m} c_{n-m}}{(2m+1)!} \tag{2.95}$$

Some of the c_i's have been calculated to be:

$$c_1 = -\frac{1}{2^2 \cdot 3!}, \quad c_2 = \frac{2^3-1}{2^4 \cdot 3 \cdot 5!}, \quad c_3 = -\frac{2^5-1}{2^6 \cdot 3 \cdot 7!}, \quad c_4 = \frac{3(2^7-1)}{2^8 \cdot 5 \cdot 9!}, \quad c_5 = -\frac{5(2^9-1)}{2^{10} \cdot 3 \cdot 11!},$$
$$c_6 = \frac{691(2^{11}-1)}{2^{12} \cdot 105 \cdot 13!}, \quad c_7 = -\frac{35(2^{13}-1)}{2^{14} \cdot 15!} \tag{2.96}$$

Therefore

$$\sum_{n=a}^{b} f(n) = \int_{a-\frac{1}{2}}^{b+\frac{1}{2}} f(x)dx + \sum_{n=1}^{\infty} c_n f^{(2n-1)}(x)\Big|_{a-\frac{1}{2}}^{b+\frac{1}{2}} \tag{2.97}$$

This new formulation using MPS needs one term less than the EMF given in (2.85).

For $F(x) = \int f(x)dx \to 0,\ f^{(n)}(x) \to 0$ as $x \to \infty$ using (2.97) we can write

$$\sum_{n=N}^{\infty} f(n) = -F(N-\frac{1}{2}) + \frac{1}{24} f'(N-\frac{1}{2}) \tag{2.98}$$
$$- \frac{7}{5760} f'''(N-\frac{1}{2}) + \frac{31}{967680} f^{(v)}(N-\frac{1}{2}) + ...$$

Let us apply both the EMF (2.87) and the MPS formula (2.98) to the following example which has a closed form.

$$\sum_{n=1}^{\infty} \frac{1}{(n-\frac{1}{2})^2} = \sum_{n=1}^{N_{\max}} \frac{1}{(n-\frac{1}{2})^2} + \sum_{n=N_{\max}+1}^{\infty} \frac{1}{(n-\frac{1}{2})^2} \tag{2.99}$$

Figure 2.5 shows the comparison of the relative error in approximating $\sum_{n=1}^{\infty} 1/(n-1/2)^2$ using EMF and the MPS formula. The exact value of this expression is known to be $\pi^2/2$ [48]. *Direct* refers to considering only first term on the right hand side of (2.99), $n$th_ EMS refers to using up to n terms of the EMF and nth MPS refers to using first n terms of the MPS formula to approximate the second term on the right hand side of (2.99). The figure shows that the MPS requires one term less than the EMF in order to obtain similar order of accuracy. Therefore, EMF converges as $1/N_{\max}^n$ if we use the first n terms but the MPS formula converges as $1/N_{\max}^{n+1}$.

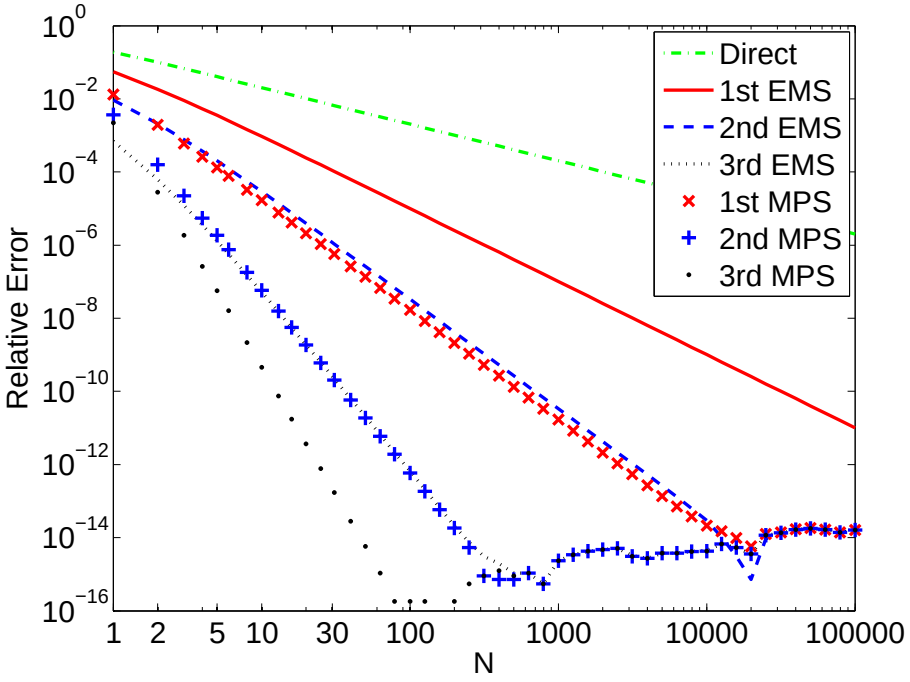

Figure 2.5 Comparison of MPS and EMF for evaluating $\sum_{n=1}^{\infty} 1/(n-1/2)^2$

2.5.3.3 Special Case

Let $f(x) = h(x)g(x)$ where $g(x) = \sin(zx+\alpha)$. Denote

$$\tilde{g}(x) = z\int g(x)dx = -\cos(zx+\alpha) \tag{2.100}$$

Then we have

$$g'(x) = z\cos(zx+\alpha) = -z\tilde{g}(x) \tag{2.101}$$

$$g''(x) = -z^2 g(x) \tag{2.102}$$

$$g^{(2n)}(x) = (-1)^n z^{2n} g(x) \tag{2.103}$$

$$g^{(2n-1)}(x) = (-1)^n z^{2n-1}\tilde{g}(x) \tag{2.104}$$

Define n times integral of $g(x)$ as

$$\tilde{g}^{(n)}(x) \equiv \begin{cases} (-1)^{n-1}\tilde{g}(x) & n = \text{odd} \\ (-1)^n g(x) & n = \text{even} \end{cases}$$

Therefore

$$g^{(n)}(x) = (-1)^n z^n \tilde{g}^{(n)}(x) \tag{2.105}$$

Using integral by part, we have

$$\int dx h(x) g(x) = \sum_{n=1}^{\infty} \frac{1}{z^n} (-1)^{n-1} h^{(n-1)}(x) \tilde{g}^{(n)}(x) \tag{2.106}$$

The $(2n)^{th}$ order derivative in (2.89) is written as:

$$f^{(2n)}(x) = \Big[h(x)g(x)\Big]^{(2n)} = \sum_{i=1}^{2n} \frac{(2n)!}{i!(2n-i)!} h^{(i)}(x) g^{(2n-i)}(x) \tag{2.107}$$

Now, the second term in (2.89) can be written as:

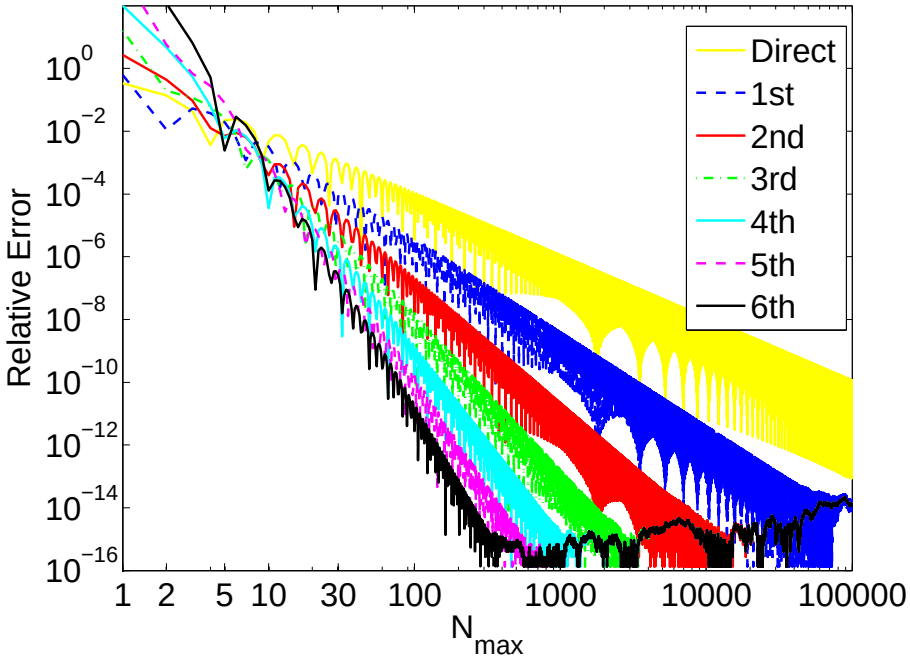

Figure 2.6 Convergence of Mid-point Summation for evaluating $\sum_{n=1}^{\infty} \sin[(n-1/2)z]/(n-1/2)^2$, $z = \pi w/a = .55$

$$\sum_{n=1}^{\infty} \frac{2^{-2n}}{(2n+1)!} f^{(2n)}(N) = \sum_{n=1}^{\infty} \frac{2^{-2n}}{(2n+1)} \sum_{i=0}^{2n} \frac{1}{i!(2n-i)!} h^{(i)}(N) g^{(2n-i)}(N) \tag{2.108}$$

For the $i = 0$ term on the right hand side of (2.108)

$$h(N)\sum_{n=1}^{\infty}\frac{2^{-2n}}{(2n+1)!}g^{(2n)}(N) = h(N)g(N)\sum_{n=1}^{\infty}\frac{(-1)^n}{(2n+1)!}(z/2)^{2n}$$
$$= h(N)g(N)\Big[\frac{\sin(z/2)}{z/2} - 1\Big] \tag{2.109}$$

For the $i = 2m-1$ term on the right hand side of (2.108)

$$h^{(2m-1)}(N)\frac{1}{(2m-1)!}\sum_{n=m}^{\infty}\frac{2^{-2n}}{(2n+1)(2n-2m+1)!}g^{(2n-2m+1)}(N) \tag{2.110}$$
$$= h^{(2m-1)}(N)\tilde{g}(N)\frac{1}{2^{2m-1}(2m-1)!}\sum_{n=m}^{\infty}\frac{(-1)^{n-m-1}}{(2n+1)(2n-2m+1)!}(z/2)^{2n-2m+1}$$
$$= h^{(2m-1)}(N)\tilde{g}(N)\frac{(-1)^{m-1}}{2^{2m-1}(2m-1)!}\text{sinc}^{(2m-1)}(z/2)$$

where

$$\text{sinc}^{(n)}(z/2) = \frac{d^n}{dx^n}\frac{\sin(x)}{x}\Big|_{x=z/2} \tag{2.111}$$

For the $i = 2m$ term on the right hand side of (2.108)

$$h^{(2m)}(N)\frac{1}{(2m)!}\sum_{n=m}^{\infty}\frac{2^{-2n}}{(2n+1)(2n-2m)!}g^{(2n-2m)}(N) \tag{2.112}$$
$$= h^{(2m)}(N)g(N)\frac{1}{2^{2m}(2m)!}\sum_{n=m}^{\infty}\frac{(-1)^{n-m}}{(2n+1)(2n-2m)!}(z/2)^{2n-2m}$$
$$= h^{(2m)}(N)g(N)\frac{(-1)^m}{2^{2m}(2m)!}\text{sinc}^{(2m)}(z/2)$$

Combining the above results we have

$$\sum_{n=1}^{\infty}\frac{2^{-2n}}{(2n+1)!}f^{(2n)}(N) = \sum_{n=1}^{\infty}\frac{2^{-2n}}{2n+1}\sum_{i=0}^{2n}\frac{1}{i!(2n-i)!}h^{(i)}(N)g^{(2n-i)}(N) \tag{2.113}$$
$$= \sum_{i=1}^{\infty}\frac{1}{i!}h^{(i)}(N)\sum_{n=[i/2]}^{\infty}\frac{2^{-2n}}{(2n+1)(2n-i)!}g^{(2n-2[i/2])}(N)$$
$$= h(N)g(N)\Big[\text{sinc}(z/2) - 1\Big] + \sum_{i=1}^{\infty}h^{(i)}(N)\tilde{g}^{(i)}(N)\frac{1}{2^i i!}\text{sinc}^{(i)}(z/2)$$

where $[i/2]$ is the integer part of $i/2$.

Using (2.89) and (2.106) we can write

$$\sum_{n=1}^{\infty}\frac{1}{z^n}(-1)^{n-1}h^{(n-1)}(x)\tilde{g}^{(n)}(x)\Big|_{N-\frac{1}{2}}^{N+\frac{1}{2}}=h(N)g(N)\text{sinc}(z/2)+\sum_{i=1}^{\infty}h^{(i)}(N)\tilde{g}^{(i)}(N)\frac{1}{2^i i!}\text{sinc}^{(i)}(z/2) \tag{2.114}$$

Substituting (2.108) in (2.89) yields the result in general form:

$$h(N)g(N)=\sum_{n=1}^{\infty}\frac{c_n}{z^n}(-1)^{n-1}h^{(n-1)}(x)\tilde{g}^{(n)}(x)\Big|_{N-\frac{1}{2}}^{N+\frac{1}{2}} \tag{2.115}$$

Deriving a recursive relation to find c_i's

$$h^{(i)}(N)\tilde{g}^{(i)}(N)=\sum_{n=1}^{\infty}\frac{c_n}{z^n}(-1)^{n-1}h^{(i+n-1)}(x)\tilde{g}^{(i+n)}(x)\Big|_{N-\frac{1}{2}}^{N+\frac{1}{2}} \tag{2.116}$$

$c_1=1/\text{sinc}(z/2)$. Substituting (2.118) in (2.117) we get:

$$\begin{aligned}\frac{1}{c_1}h(N)g(N)=&\sum_{n=1}^{\infty}\frac{1}{z^n}(-1)^{n-1}h^{(n-1)}(x)\tilde{g}^{(n)}(x)\Big|_{N-\frac{1}{2}}^{N+\frac{1}{2}}\\&+\sum_{i=1}^{\infty}\frac{(-1)^{[i/2]}}{2^i i!}\text{sinc}^{(i)}(z/2)\sum_{n=1}^{\infty}\frac{c_n}{z^n}(-1)^{n-1}h^{(i+n-1)}(x)\tilde{g}^{(i+n)}(x)\Big|_{N-\frac{1}{2}}^{N+\frac{1}{2}}\end{aligned} \tag{2.117}$$

Changing the summation variable

$$\left\{\begin{array}{c}n=1\to\infty\\ i=1\to\infty\end{array}\right\}\Rightarrow\left\{\begin{array}{c}m=n+i=2\to\infty\\ i=1\to m-1\end{array}\right\}$$

we get:

$$\begin{aligned}\frac{1}{c_1}h(N)g(N)=&\sum_{n=1}^{\infty}\frac{1}{z^n}(-1)^{n-1}h^{(n-1)}(x)\tilde{g}^{(n)}(x)\Big|_{N-\frac{1}{2}}^{N+\frac{1}{2}}\\&-\sum_{m=2}^{\infty}\frac{1}{z^m}(-1)^{m-1}h^{(m-1)}(x)\tilde{g}^{(m)}(x)\Big|_{N-\frac{1}{2}}^{N+\frac{1}{2}}\sum_{i=1}^{m-1}\frac{(-1)^i c_{m-i}}{i!}\left(\frac{z}{2}\right)^i\text{sinc}^{(i)}(z/2)\\=&\frac{1}{z}h(x)\tilde{g}(x)\Big|_{N-\frac{1}{2}}^{N+\frac{1}{2}}\\&+\sum_{m=2}^{\infty}\frac{1}{z^m}\left[1-\sum_{i=1}^{m-1}\frac{(-1)^i c_{m-i}}{i!}\left(\frac{z}{2}\right)^i\text{sinc}^{(i)}(z/2)\right](-1)^{m-1}h^{(m-1)}(x)\tilde{g}^{(m)}(x)\Big|_{N-\frac{1}{2}}^{N+\frac{1}{2}}\end{aligned} \tag{2.118}$$

Therefore

$$h(N)g(N) = \sum_{n=1}^{\infty} \frac{c_n(z/2)}{z^n}(-1)^{n-1}h^{(n-1)}(x)\tilde{g}^{(n)}(x)\Big|_{N-\frac{1}{2}}^{N+\frac{1}{2}} \tag{2.119}$$

where the coefficients c_n are derived in a recursive form using

$$c_1(x) = 1/\text{sinc}(x) \tag{2.120}$$

$$\frac{c_n(x)}{c_1(x)} = 1 - \sum_{m=1}^{n-1} \frac{c_{n-m}(x)}{m!}(-1)^m x^m \text{sinc}^{(m)}x, \quad \text{n} \geq 2 \tag{2.121}$$

where

$$\text{sinc}^{(n)}x = \frac{d^n}{dx^n}\text{sinc}x = \frac{d^n}{dx^n}\frac{\sin x}{x} \tag{2.122}$$

Using this relation we can derive

$$c_2 = \frac{\cos x}{\text{sinc}^2 x}, \quad c_3 = \frac{3+\cos(2x)}{4\text{sinc}^3 x}, \quad c_4 = \frac{23\cos x + \cos(3x)}{24\text{sinc}^4 x}, \quad c_5 = \frac{115 + 76\cos(2x) + \cos(4x)}{192\text{sinc}^5 x},$$
$$c_6 = \frac{1682\cos x + 237\cos(3x) + \cos(5x)}{1920\text{sinc}^6 x} \tag{2.123}$$

Thus, for $h(x) \to 0$, $h^{(n)}(x) \to 0$ as $x \to \infty$.

$$\sum_{n=N}^{\infty} h(n)g(n) = -\frac{c_1}{z}h(N-\frac{1}{2})\tilde{g}(N-\frac{1}{2}) - \frac{c_2}{z^2}h'(N-\frac{1}{2})g(N-\frac{1}{2}) + \frac{c_3}{z^3}h''(N-\frac{1}{2})\tilde{g}(N-\frac{1}{2}) + \ldots \tag{2.124}$$

Figure 2.6 shows the convergence of the MPS formula for approximating $\sum_{n=1}^{\infty}\sin[(n-1/2)z]/(n-1/2)^2$, $z = \pi w/a = .55$ using different number of terms of (2.124). The summation can be written in a form similar to (2.99). The reference value is calculated using the super convergent series [51]. *Direct* refers to considering sum of terms up to N_{max}, nth refers to using first n terms of the MPS formula to approximate the summation from $N_{\text{max}}+1$ to ∞. The figure shows that the rate of convergence using n terms of the series is $1/N_{\text{max}}^{n+2}$. The formulation for the SDA and the leading term extraction will be the same as the previous case. But the summation of the matrix elements can be written in the following form.

$$K_{ij}^{pq} \approx \sum_{n=1}^{N_{\text{max}}} F_{ij}^{pq} + \sum_{n=N_{\text{max}}+1}^{\infty} \tilde{F}_{ij}^{pq} \tag{2.125}$$

$\sum_{n=N_{\max}}^{\infty} \tilde{F}_{ij}^{pq}$ consists of terms of the form sinusoidal functions divided by α_n^k which are approximated using (2.124) with $g(x)$ equal to constant or sinusoidal function and $h(x)$ equal to $1/\alpha_n^k$ as it satisfies the condition $h(x) \to 0$, $h^{(n)}(x) \to 0$ as $x \to \infty$. Terms of the form $1/\alpha_n^k$ are approximated using (2.98).

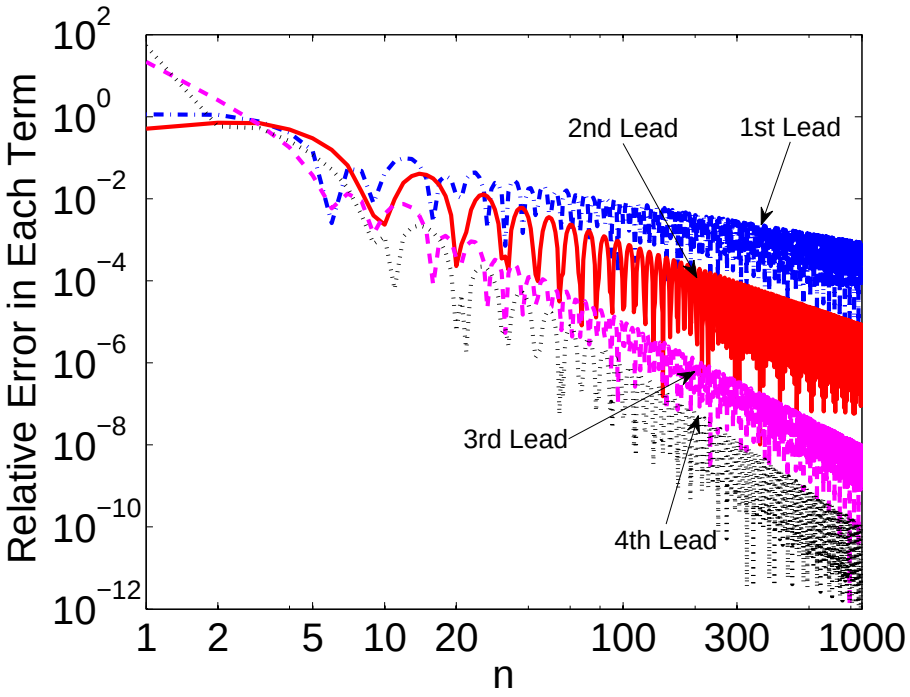

Figure 2.7 Convergence of $(F_{11}^{zz} - \tilde{F}_{11}^{zz})\alpha_n^2$ as function of n for $\beta = 3k_0$ for different number of leading terms.

2.6 Numerical Results

Both the approach were numerically validated using a shielded microstrip with parameters $\epsilon_r = 11.7, \mu_r = 1, f = 4\text{GHz}, h = 3.17\text{mm}, w = 3.04\text{mm}, 2a = 34.74\text{mm}, d = 50\text{mm}$ [3].

The results for the first approach or the convergent series approach are as follows. Figure 2.7 shows that if we use k leading terms the difference $F_{11}^{zz} - \tilde{F}_{11}^{zz}$ converges as $1/n^{k+2}$. From Figures 2.8(a) and 2.8(b) it is observed that the convergence of K_{11}^{zz} and determinant of K matrix changes from $1/N_{\max}$ using the direct summation to $1/N_{\max}^3$ using up to second leading term and

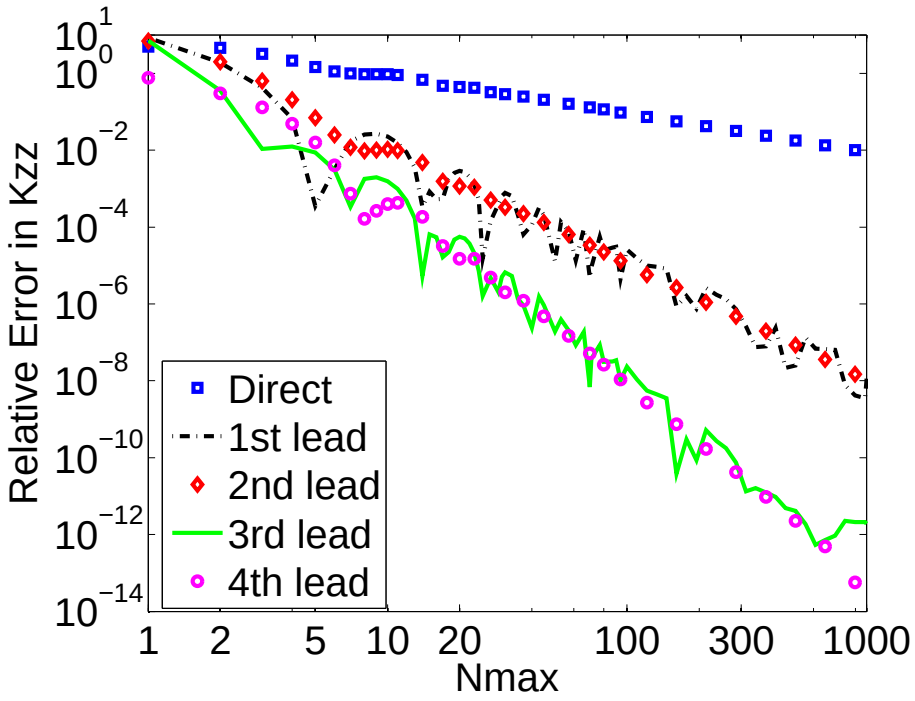

(a) Convergence of K_{11}^{zz}

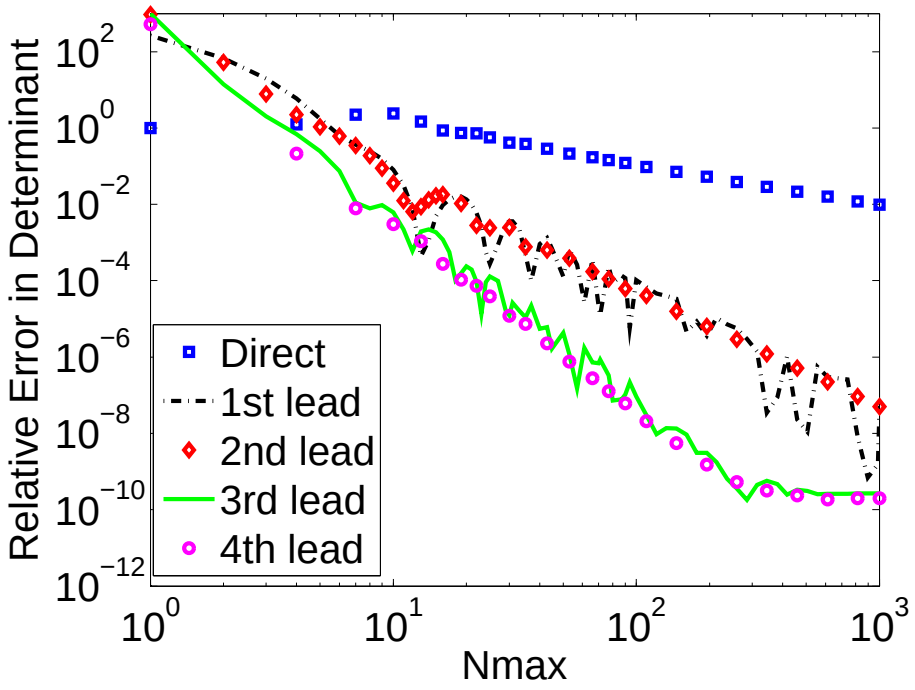

(b) Determinant of K matrix

Figure 2.8 Convergence of (a)K_{11}^{zz} and (b)determinant of K matrix for M_z=1, M_x=1 and $\beta = 3k_0$ using different number of leading terms.

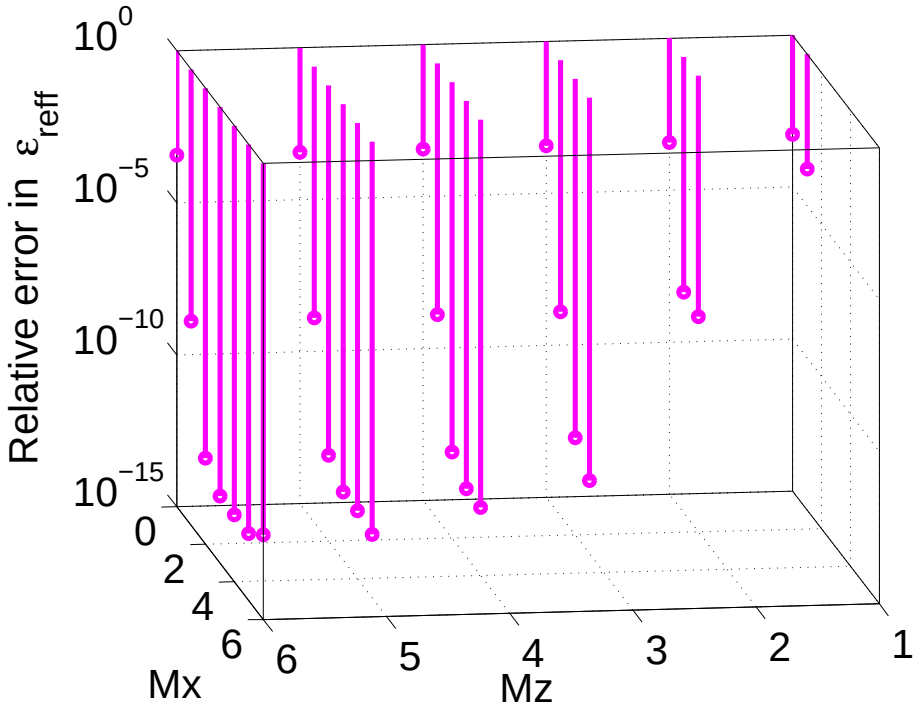

Figure 2.9 3D plot for Relative error in ϵ_{reff} with different number of basis functions using four leading terms

finally to $1/N_{\text{max}}^5$ using up to fourth leading term. Here, the result using four leading terms with $N_{\text{max}} = 1000000$ is used as reference. Also Figures 2.8(a), 2.8(b), 2.10(a) and 2.10(b) show that the results are similar if we use odd number of leading terms or the next even number of leading terms. This can be explained by the fact that the even leading terms do not have a constant term but only have sinusoidal functions which converge faster than the constant term.

Figure 2.12 shows the relative error in ϵ_{reff} as a function of different combinations of the basis function and it can be observed that the result become more and more accurate if we fix the basis function in one direction and increase the number of basis in the other direction. Also it is seen that if M_{z} is fixed the optimal value of M_{x} will be $M_{\text{z}} - 1$ or M_{z} keeping in mind the speed of computation and the accuracy.

As shown in Table 2.1 using $N_{\text{max}} = 18$ for $M_{\text{z}} = 2$, $M_{\text{x}} = 1$ results accurate within 7 significant digits and $N_{\text{max}} = 232$ for $M_{\text{z}} = 4, M_{\text{x}} = 3$ results accurate within 12 significant digits

Table 2.1 ϵ_{reff} for different basis functions

$M_{\mathbf{z}}$	$M_{\mathbf{x}}$	ϵ_{reff}	$N_{\mathbf{max}(SCS)}$	$N_{\mathbf{max}(MPS)}$
1	1	8.81	4	11
2	1	8.810041	18	42
2	2	8.8100416	52	61
3	2	8.810041567	130	140
3	2	8.8100415677	210	210
3	3	8.81004156779	243	255
4	3	8.81004156779	232	243

can be obtained ($\epsilon_{\text{reff}} = 8.81004156779$). Also by using $M_{\text{z}} = 2, M_{\text{x}} = 2$ and $N_{\text{max}} = 52$, an $\epsilon_{\text{reff}} = 8.8100416$ is obtained which is the same as [3]. The result highly depends on the value of ϵ_0 so results differ in the last four digits from [12]. We have used $c = 299792458$m/s[52] which is slightly different from [53]. The approach can be further accelerated to any extent by using more number of leading terms.

Figure 2.10(a) shows that rate of convergence decreases as we increase the number of basis functions for small N_{max} but by using higher order basis functions and more number of terms we get even more accurate results. Figure 2.10(b) shows that the rate of convergence increases as we use more number of leading terms.

The results for the MPS approach are as follows. Table 2.1 shows a combination of minimum number of basis functions and minimum number of terms using which we can obtain the required number of significant digits using our approach. As the table shows, using $N_{\text{max}} = 42$ for $M_{\text{z}} = 2$, $M_{\text{x}} = 1$ results accurate within 7 significant digits and $N_{\text{max}} = 255$ for $M_{\text{z}} = 3, M_{\text{x}} = 3$ results accurate within 12 significant digits can be obtained ($\epsilon_{\text{reff}} = 8.81004156779$). Also by using $M_{\text{z}} = 2, M_{\text{x}} = 2$ and $N_{\text{max}} = 61$, an $\epsilon_{\text{reff}} = 8.8100416$ is obtained which is the same as [3]. With $M_{\text{z}} = 4$ and $M_{\text{x}} = 3$, ϵ_{reff} correct up to 12 significant digits ($\epsilon_{\text{reff}} = 8.81004156779$) can be obtained by truncating the summation at $N_{\text{max}} = 243$ using the MPS formula. The result slightly depends on

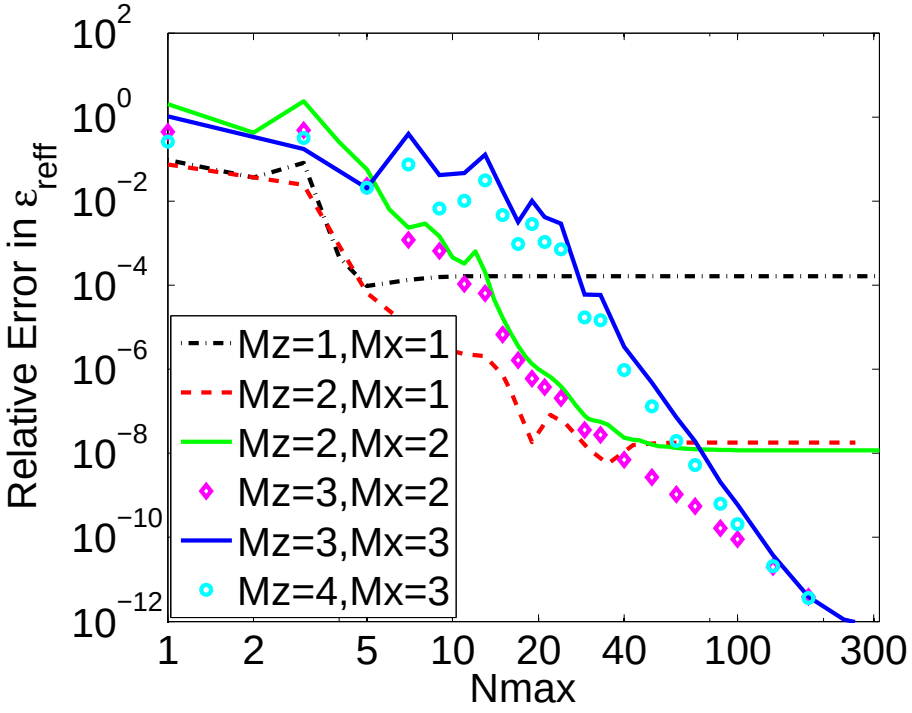

(a) Convergence of ϵ_{reff} using different number of basis

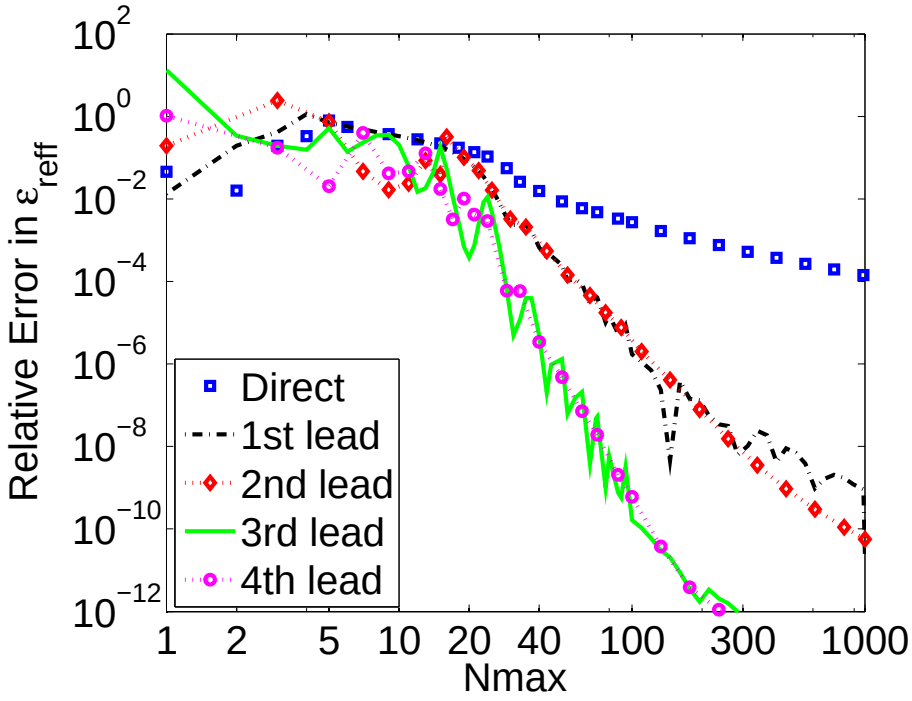

(b) Convergence of ϵ_{reff} using different number of leading terms

Figure 2.10 The convergence of ϵ_{reff} for different basis using four leading terms and different number of leading terms.

the value of ϵ_0, so it differs from [12] in the last four digits. We have used $c = 299792458$m/s[52] which is slightly different from [53]. The approach can be further accelerated to any extent by using more number of leading terms.

From Figure 2.11(b) it is observed that the convergence of determinant of K matrix changes from $1/N_{\text{max}}$ using the direct summation to $1/N_{\text{max}}^3$ using up to second leading term and finally to $1/N_{\text{max}}^5$ using up to fourth leading term. Here, the result using four leading terms with $N_{\text{max}} = 10^6$ is used as reference. Figure 2.13 shows that the rate of convergence of ϵ_{reff} increases as we use more number of leading terms. Also Figures 2.11(b) and 2.13 show that the results are similar if we use odd number of leading terms or the next even number of leading terms. This is because the even leading terms have only sinusoidal functions and no constant terms and sinusoidal functions converge faster than the constant terms using the special case which we have derived. Figure 2.12 clearly shows that the error in ϵ_{reff} decreases very rapidly when we consider more number of basis functions for the longitudinal and the transverse current. But after a while it appears to saturate because of the limits of double precision.

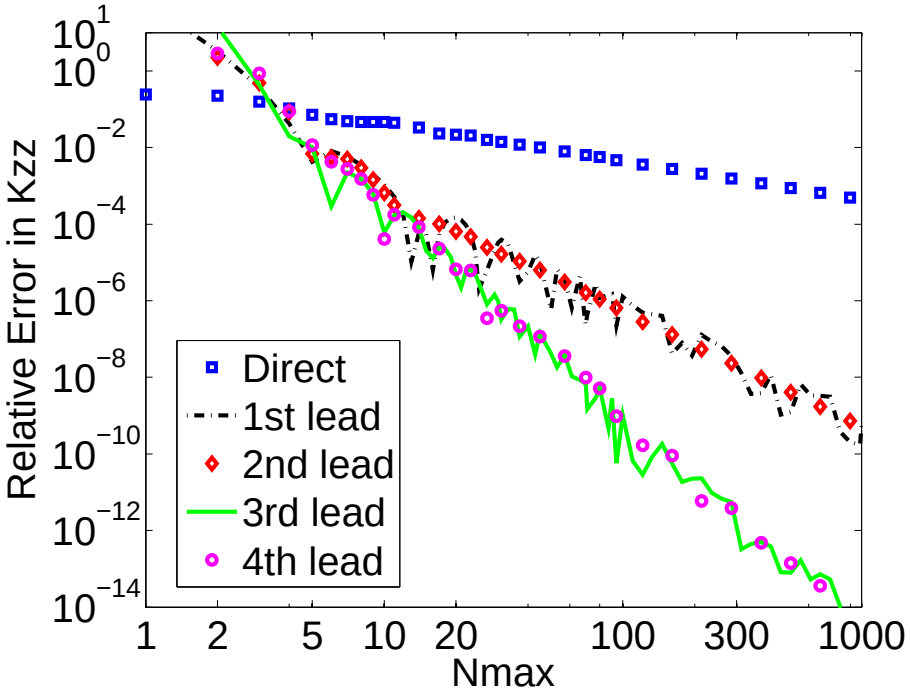

(a) Convergence of K_{11}^{zz}

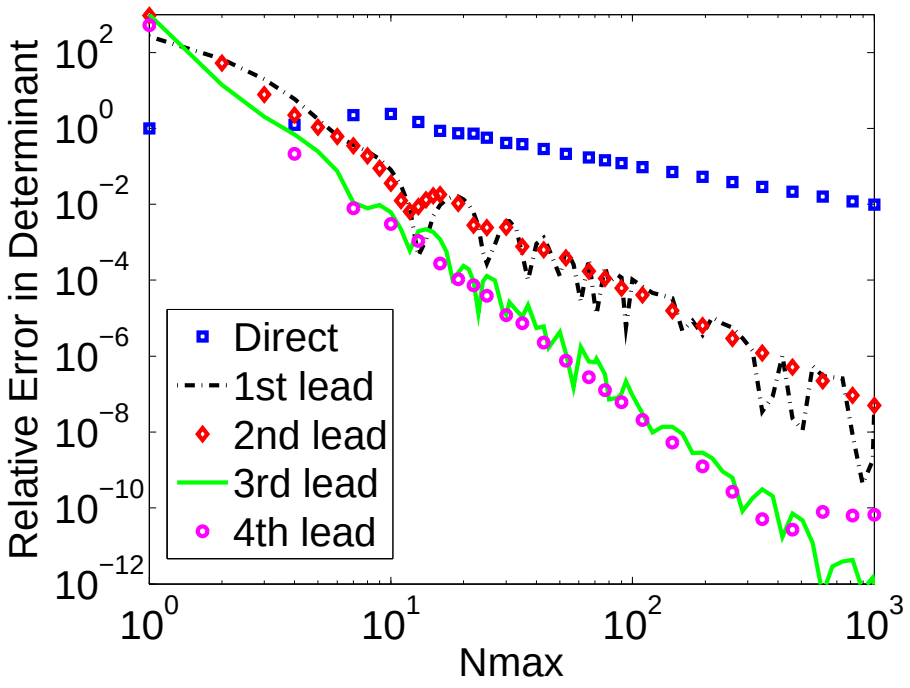

(b) Determinant of K matrix

Figure 2.11 Convergence of (a)K_{11}^{zz} and (b)determinant of K matrix for M_z=1, M_x=1 and $\beta = 3k_0$ using different number of leading terms.

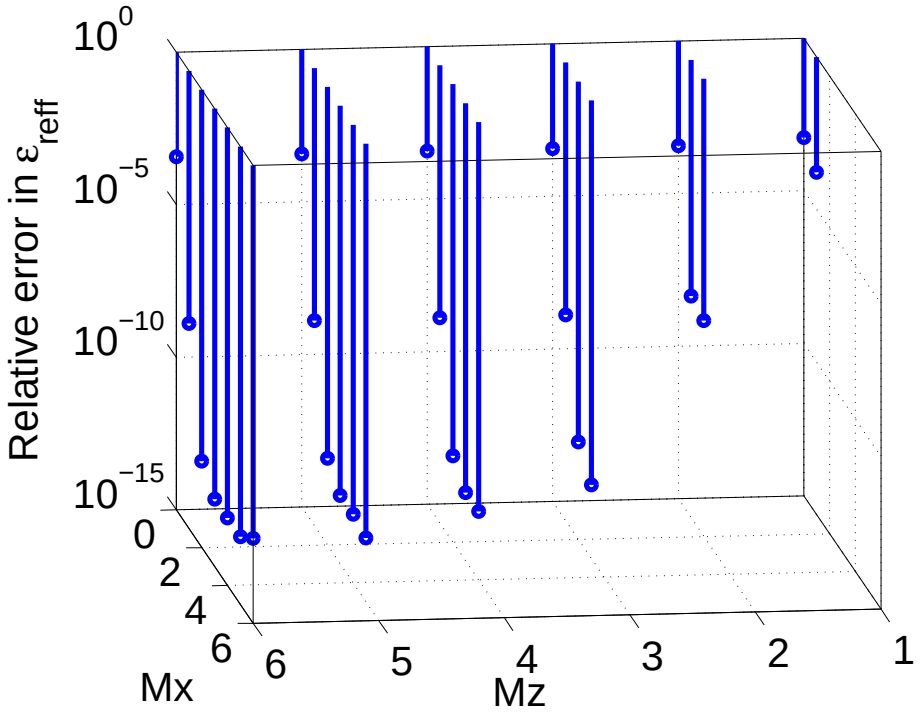

Figure 2.12 3D plot for Relative error in ϵ_{reff} with different number of basis functions using four leading terms

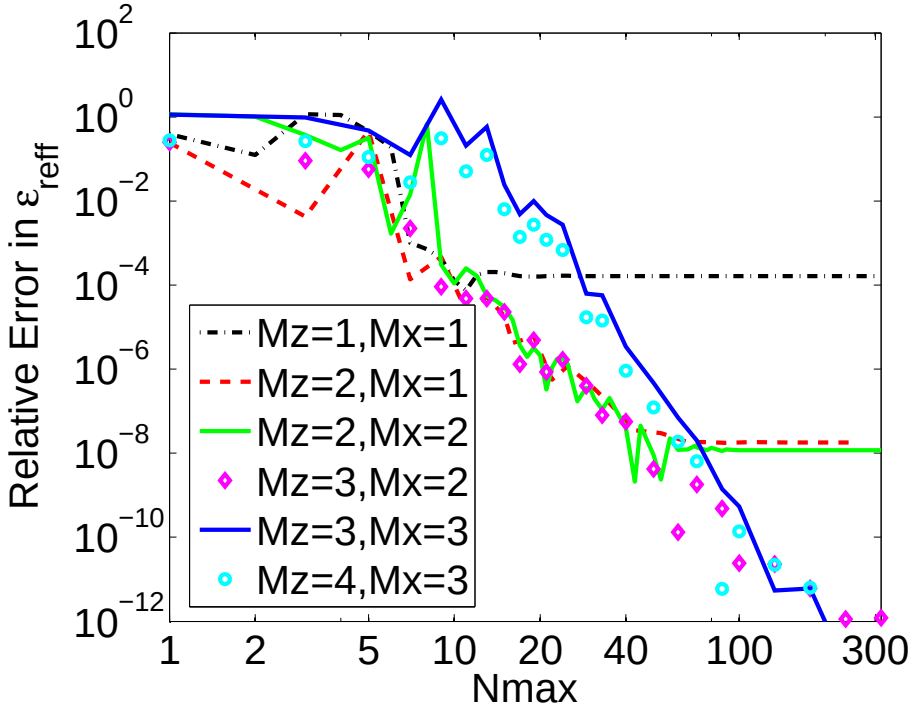

(a) Convergence of ϵ_{reff} using different number of basis

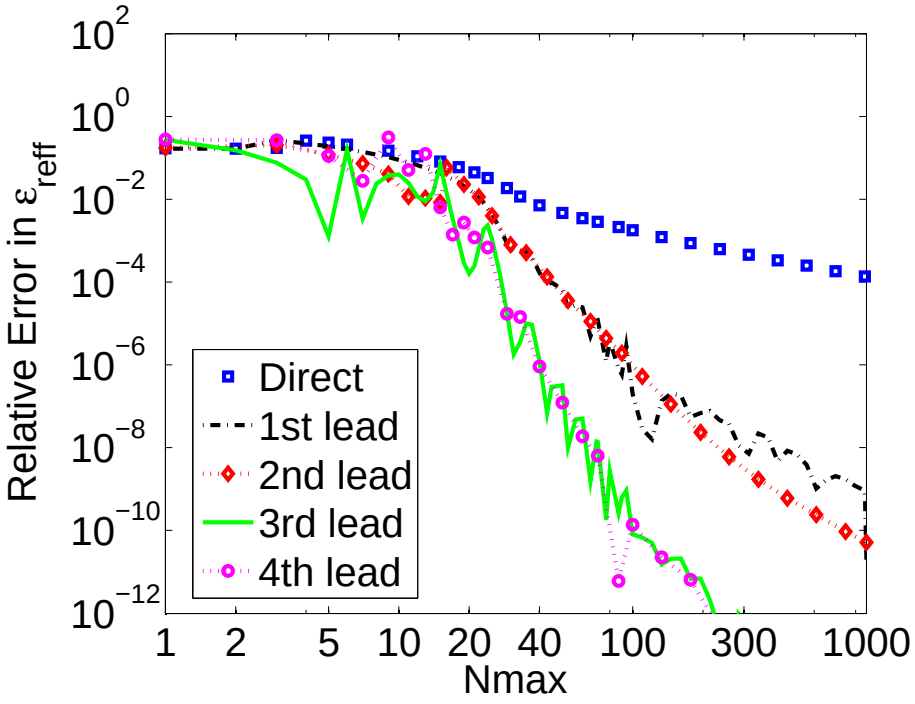

(b) Convergence of ϵ_{reff} using different number of leading terms with $M_{\text{z}} = 4, M_{\text{x}} = 3$

Figure 2.13 Convergence of ϵ_{reff} using different number of leading terms with $M_{\text{z}} = 4, M_{\text{x}} = 3$

CHAPTER 3. Acceleration of Spectral Domain Approach for Generalized Multilayered Shielded Microstrip using Two Super Convergent Series

3.1 Introduction

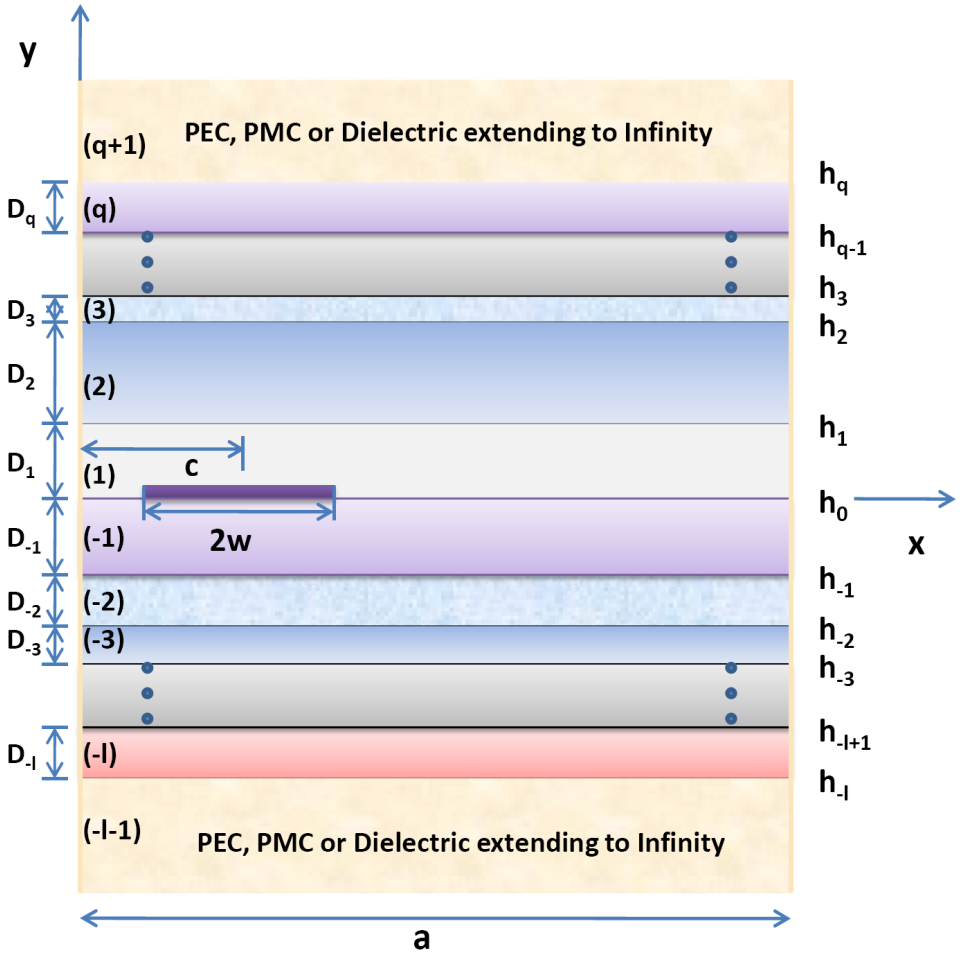

Figure 3.1 Shielded microstrip

In the previous chapter two techniques named mid point summation formula and the super convergent series have been applied to get fast convergence of infinite sine cosine series. The convergence of the mid point summation decreases when the value of the argument is very small and the super convergent series used in the previous chapter is converges fast for small values of the argument. So these techniques individually will not be sufficient for the multilayered case as the arguments of some terms are very small. We could use a combination of these techniques but here we introduce a second type of super convergent series which has a faster convergence than the MPS.

In this chapter, we propose an approach to speed up the SDA for the computation of the propagation constant for any mode of a generalized shielded microstrip. We use an asymptotic approximation to the Greens function and the Bessel's function and two different super convergent sine cosine series to accelerate the summation of the leading terms depending on the value of the argument. The higher order super convergent series (SCS) can be evaluated from the lower order ones by using integration by parts. As a result we can obtain very accurate results for the propagation constant of all the modes in a multilayered shielded microstrip in which the signal strip is at a distance c from the side wall of the box as shown in Figure 3.1. In addition to this, closed form expressions have been developed to dynamically choose the number of terms and the value of the parameter p as a function of the argument, to adaptively obtain the best convergence of the second type of super convergent series for a given accuracy and argument.

3.2 Multilayered Shielded Microstrip Line

The Figure 3.1 shows a multilayered shielded microstrip structure. The side walls are perfect electric conductor (PEC) or perfect magnetic conductor (PMC). The m^{th} layer is defined by ϵ_m, μ_m, thickness D_m and $k_m = \omega\sqrt{\epsilon_m \mu_m}$. A PEC metal strip of zero thickness and width $2w$ is located at $y = 0$ plane with its center at $x = c$ and extending infinitely in the z direction. The layers

above the signal metal strip are numbered from 1 to $q+1$ and the layers below are numbered from -1 to $-l-1$. The top and bottom cover layers can be PEC, PMC or dielectric extending up to infinity. Assuming the wave is propagating along the $-z$ direction. The spectral domain immitance approach (SDIA) is used to compute the Green's function [54]. Using the SDIA and the boundary conditions the *x* and *z* components of electric field on the metal interface can be written as [12]:

$$\tilde{E}_x(\alpha_n, h_0) = G_{xx}(\alpha_n, \beta)\tilde{J}_x(\alpha_n) + G_{xz}(\alpha_n, \beta)\tilde{J}_z(\alpha_n), \tag{3.1}$$

$$\tilde{E}_z(\alpha_n, h_0) = G_{zx}(\alpha_n, \beta)\tilde{J}_x(\alpha_n) + G_{zz}(\alpha_n, \beta)\tilde{J}_z(\alpha_n), \tag{3.2}$$

where $\alpha_n = n\pi/a$, $n = 1, 2, 3, ...$, and

$$G_{zz}(\alpha_n, \beta) = \frac{-1}{\alpha_n^2 + \beta^2}\left(\alpha_n^2 Z^{\text{TE}} + \beta^2 Z^{\text{TM}}\right) \tag{3.3}$$

$$\begin{aligned} G_{xz}(\alpha_n, \beta) &= G_{zx}(\alpha_n, \beta) \\ &= \frac{-\alpha_n\beta}{\alpha_n^2 + \beta^2}\left(Z^{\text{TM}} - Z^{\text{TE}}\right) \end{aligned} \tag{3.4}$$

$$G_{xx}(\alpha_n, \beta) = \frac{-1}{\alpha_n^2 + \beta^2}\left(\beta^2 Z^{\text{TE}} + \alpha_n^2 Z^{\text{TM}}\right) \tag{3.5}$$

$$Z^s = 1/[Y^s_{\text{up}}(h_0) + Y^s_{\text{down}}(h_0)], s = \text{TM}, \text{TE}. \tag{3.6}$$

where $Y^s_{\text{up}}(h_0)$ and $Y^s_{\text{down}}(h_0)$ are calculated recursively by going down from the topmost layer and going up from the bottommost layer using (3.7) and initial values $Y^s_{\text{up}}(h_q) = y^s_{q+1}$ and $Y^s_{\text{down}}(h_{-l}) = y^s_{-l-1}$ [12], respectively.

$$Y^s(h_{i\mp1}) = y^s_i \frac{Y^s(h_i) + y^s_i \tanh(\gamma_i D_i)}{y^s_i + Y^s(h_i)\tanh(\gamma_i D_i)} \tag{3.7}$$

where the '$-$' sign is used while calculating $Y^s_{\text{up}}, i = q, q-1, ..., 2, 1$ and the '$+$' sign is used while evaluating $Y^s_{\text{down}}, i = -l, -l+1, ..., -2, -1$.

$$y_i^{\text{TM}} = \frac{j\omega\epsilon_i}{\gamma_i}, \quad y_i^{\text{TE}} = \frac{\gamma_i}{j\omega\mu_i} \tag{3.8}$$

$$\gamma_i^2 = \beta^2 + \alpha_n^2 - k_i^2 \tag{3.9}$$

Entire domain basis like Chebyshev polynomials centered around $x = c$ are used as basis functions to expand the currents in the z and x direction, J_z and J_x, respectively [55],[44].

$$J_z(x) = (1/\sqrt{1-r^2}) \sum_{i=0}^{M_z-1} a_i T_i(r) \tag{3.10}$$

$$J_x(x) = \sqrt{1-r^2} \sum_{i=0}^{M_x-1} b_i U_i(r) \tag{3.11}$$

where $x = c + wr, |r| < 1$, T_i and U_i are the Chebyshev polynomials of the first and second kind, respectively.

The Fourier transforms of the basis functions can be written as:

$$\begin{aligned}\tilde{J}_x(\alpha_n) &= \int_0^a dx J_x(x)\cos(\alpha_n x) = \frac{w\pi}{\delta_n} \sum_{i=0}^{M_x-1} b_i(i+1) J_{i+1}(\delta_n) \mathrm{Re}\{(-j)^i e^{-j\alpha_n c}\} \\ &= \frac{w\pi}{\delta_n} \sum_{i=0}^{M_x-1} b_i(i+1) j^i \tilde{J}_{i+1}(\delta_n)\end{aligned} \tag{3.12}$$

$$\begin{aligned}\tilde{J}_z(\alpha_n) &= \int_0^a dx J_z(x)\sin(\alpha_n x) = -w\pi \sum_{i=0}^{M_z-1} a_i J_i(\delta_n) \mathrm{Im}\{(-j)^i e^{-j\alpha_n c}\} \\ &= w\pi \sum_{i=0}^{M_z-1} a_i j^{i-1} \tilde{J}_i(\delta_n)\end{aligned} \tag{3.13}$$

where $\delta_n = \alpha w$ and

$$\tilde{J}_u(\alpha_n) = J_u(\alpha_n w) \cdot \begin{cases} \cos(\alpha_n c), & u \text{ odd} \\ j\sin(\alpha_n c), & u \text{ even} \end{cases} \tag{3.14}$$

where J_u is the u^{th} order Bessel function. Further, using the Galerkin method and taking the inner product of (3.1) with the Fourier transform of the bases for the transverse current and of (3.2) with the Fourier transform of the bases for the longitudinal current the following matrix equation is obtained:

$$\begin{bmatrix} K^{xx} & K^{xz} \\ K^{zx} & K^{zz} \end{bmatrix} \begin{bmatrix} A \\ B \end{bmatrix} = \begin{bmatrix} 0 \\ 0 \end{bmatrix}$$

where A and B are vectors which are proportional to the coefficients a_i and b_i, respectively.

$$A_k = \pi w k j^{k-1} a_{k-1} \tag{3.15}$$

$$B_l = -\pi w j^l b_{l-1} \tag{3.16}$$

The elements of the K matrix can be written as:

$$K_{kl}^{ef} = -\frac{1}{4}\delta_{ex}\delta_{fx}\delta_{k1}\delta_{l1} Z^{\text{TE}}\Big|_{n=0} + \sum_{n=1}^{\infty} \frac{G_{ef}(\alpha_n, \beta)}{\delta_n^{\delta_{ex}+\delta_{fx}}} \tilde{J}_{k-\delta_{pz}}(\alpha_n)\tilde{J}_{l-\delta_{qz}}(\alpha_n) \tag{3.17}$$

$$= -\frac{1}{4}\delta_{ex}\delta_{fx}\delta_{k1}\delta_{l1} Z^{\text{TE}}\Big|_{n=0} + \sum_{n=1}^{\infty} F_{kl}^{ef}(\alpha_n) \tag{3.18}$$

where $e, f \in x, z$, $k = 1, .., M_e$, $l = 1, .., M_f$, and

$$\delta_{pq} = \begin{cases} 1 & p = q \\ 0 & p \neq q \end{cases} \tag{3.19}$$

The $n = 0$ term in (3.17) is taken care separately [12]. Finally, the propagation constant β can be obtained by solving $\det[K] = 0$.

3.3 Extraction of Asymptotic Terms

3.3.1 Asymptotic Approximation of the Green's Function

The difference between the Green's function for different structures with the same set of layers just above and below the signal strip lies in smaller values of α_n [56]. Because for large n, $\tanh(\gamma_i D_i) \approx 1$. Let $\gamma_i D_{\text{min}} = L$ where L depends on the accuracy required. e.g. for $L = 20$, $\tanh(L) \approx 1$ with double precision accuracy and for $L = 10$ with single precision. For large n, $\gamma_i \approx \alpha_n$. Therefore,

$$\alpha_n D_{\text{min}} \approx L$$

$$\Rightarrow N_{\text{min}} = La/(D_{\text{min}}\pi) \tag{3.20}$$

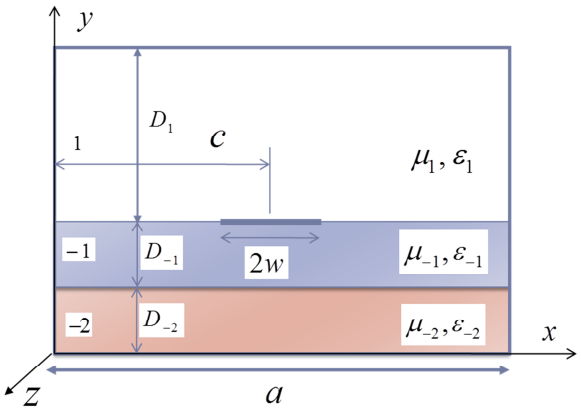

Figure 3.2 Three layered shielded microstrip with parameters $\epsilon_{r_{-2}} = 1,\ ,\epsilon_{r_{-1}} = 10.2,\ ,\epsilon_{r_1} = 1,\ \mu_{r_i} = 1,\ D_{-2} = 6.35\text{mm},\ D_{-1} = .635\text{mm},$ $D_1 = .635\text{mm},\ 2w = .635\text{mm},\ a = 7.62\text{mm},\ c = a/2.$

D_{min} is $\min(D_{-1}, D_1)$. In most cases the box width is about 10 times the thickness of layers so N_{min} will be a two digit number. Therefore for large n, $Y^s_{\text{up}}(h_0) \approx y^s_1$ and $Y^s_{\text{down}}(h_0) \approx y^s_{-1}$.

Also Figures 3.3(a) and 3.3(b) show that as the frequency increases beyond a few GHz the first two asymptotic terms of the Green's function as used in Chapter 2 are not good enough. Even the third asymptotic term has to be included. It is very complicated to obtain an analytical result for the third leading term. Therefore, a technique for numerical extraction of the higher order leading terms was developed which can be very handy when the Green's function becomes more complex as it is very difficult to obtain an analytical expression even for the first and second leading terms for the case with multiple metal lines in different layers.

As $\alpha_n \to \infty$ keeping the first three terms in Taylor expansion the Green's functions are approximated as [55], [13]:

$$G_{xx} \approx G_{xx0}\alpha_n w(1 - y_{1xx}/\alpha_n^2 - y_{2xx}/\alpha_n^4) \tag{3.21}$$

$$G_{xz} \approx G_{xz0}(1 - y_{1xz}/\alpha_n^2 - y_{2xz}/\alpha_n^4) \tag{3.22}$$

$$G_{zz} \approx \frac{G_{zz0}}{\alpha_n w}(1 - y_{1zz}/\alpha_n^2 - y_{2zz}/\alpha_n^4) \tag{3.23}$$

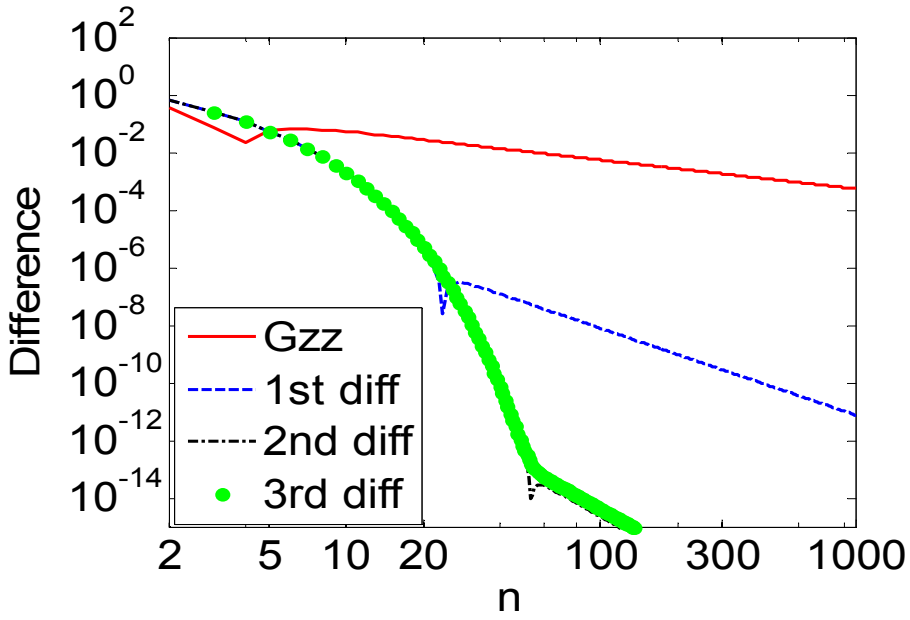

(a) Convergence of G_{zz} at 1 GHz

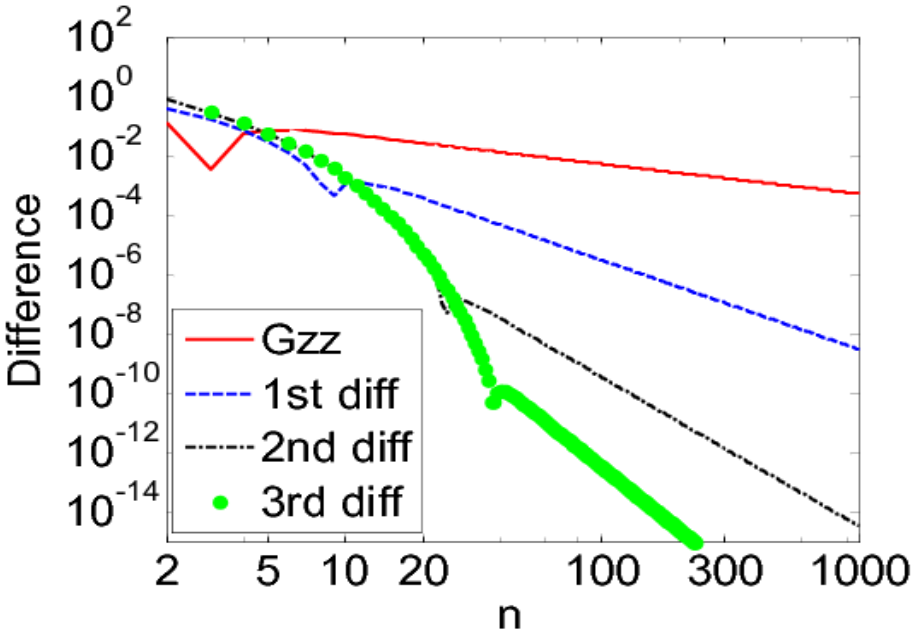

(b) Convergence of G_{zz} at 20 GHz

Figure 3.3 Convergence of G_{zz} using first, second and third leading terms for a three layered shielded microstrip with parameters as shown in Figure 3.2 at $\beta = 2k_0$ and a frequency of (a)1 GHz (b) 20 GHz.

The coefficients G_{ef0} and y_{1ef} can be determined analytically as given in Chapter 2 equations (2.65)-(2.70). But we need to replace k_1 by k_{-1} and k_2 by k_1 in these expressions to match the notation in this chapter. It is known that the Green's function is of the form:

$$G_{ef} = G_0(\alpha_n)[1 - y_{1ef}/\alpha_n^2 - y_{2ef}/\alpha_n^4 - y_{3ef}/\alpha_n^6 - ...] \tag{3.24}$$

The coefficients y_{2ef} and y_{3ef} are determined by solving the two linear equations obtained on substituting two different values of n in (3.24). But for this case only up to third leading term are needed so (3.24) is truncated keeping the first three leading terms. The values of n should be greater than N_{min} so that they lie in the region where G_{ef} depends only on the layers above and below the signal strip. Figure 3.3(b) shows the convergence of G_{zz} using up to first, second and third leading terms. Using first k leading terms G_{zz} converges as $1/n^{2k+1}$. This technique can be easily extended to extract the leading term even when the expression for the Green's function becomes very complex.

3.3.2 Asymptotic Approximation of the Bessel's Function

The series expansion for the Bessel's function [45] is given in (2.71).

$$\begin{aligned} J_u(z)J_v(z) =& \left(\frac{2}{\pi z}\right)\Big\{A + (-BC_v^1 - CC_u^1)/8z + (-AC_u^2 + DC_u^1C_v^1 - AC_v^2)/(8z)^2 \\ &+ \Big[B(C_v^3 + C_v^1C_u^2) + C(C_u^3 + C_u^1C_v^2)\Big]/(8z)^3 + [A(C_u^4 + C_v^4 \\ &+ C_u^2C_v^2) - DC_u^3C_v^1 - DC_u^1C_v^3]/(8z)^4\Big\} \end{aligned} \tag{3.25}$$

where the expression for A, B, C, D are given below:

$$A = \frac{1}{2}\Big\{\sin[2z - \frac{(u+v)\pi}{2}] + \cos[\frac{(u-v)\pi}{2}]\Big\} \tag{3.26}$$

$$B = \frac{1}{2}\Big\{-\cos[2z - \frac{(u+v)\pi}{2}] - \sin[\frac{(u-v)\pi}{2}]\Big\} \tag{3.27}$$

$$C = \frac{1}{2}\Big\{-\cos[2z - \frac{(u+v)\pi}{2}] + \sin[\frac{(u-v)\pi}{2}]\Big\} \tag{3.28}$$

$$D = \frac{1}{2}\Big\{ -\sin[2z - \frac{(u+v)\pi}{2}] + \cos[\frac{(u-v)\pi}{2}]\Big\} \tag{3.29}$$

Thus, using the asymptotic forms of the Bessel's function and the Green's function and keeping terms up to $1/\alpha_n^6$ one can get:

$$\begin{aligned}\tilde{F}_{kl}^{ef} = \frac{2G_{ef0}}{\pi(\alpha_n w)^2}\Big[A_g + (-B_g C_u^1 - C_g C_v^1)/(8\alpha_n w) + (-A_g C_v^2 + D_g C_v^1 C_u^1 - A_g C_u^2 \\ - 64 A_g y_{1ef} w^2)/(8\alpha_n w)^2 + \Big(B_g(C_u^3 + C_u^1 C_v^2) + C_g(C_v^3 + C_v^1 C_u^2) - 64 y_{1ef} w^2(-B_g C_u^1 \\ - C_g C_v^1)\Big)/(8\alpha_n w)^3 + \Big(A_g(C_v^4 + C_u^4 + C_v^2 C_u^2) - D_g C_v^3 C_u^1 - D_g C_v^1 C_u^3 - 64 y_{1ef} w^2(-A_g C_v^2 \\ + D_g C_v^1 C_u^1 - A_g C_u^2) - 4096 y_{2ef} w^4 A_g\Big)/(8\alpha_n w)^4\Big]\end{aligned} \tag{3.30}$$

where $g = o$ for $u+v$ odd, e for $u+v$ even. The expressions for A_g, B_g, C_g and D_g are given below:

$$A_e = \frac{1}{2}\Big[-(-1)^{\frac{3u+v}{2}} \sin\theta_1 - (-1)^{\frac{3u-v}{2}} + \frac{(-1)^{\frac{u+v}{2}}}{2}(\sin\theta_3 + \sin\theta_2) + (-1)^{\frac{u-v}{2}} \cos\theta_4\Big] \tag{3.31}$$

$$B_e = C_e = \frac{1}{2}\Big[-(-1)^{\frac{3u+v}{2}} \cos\theta_1 - (-1)^{\frac{u+v}{2}} + \frac{(-1)^{\frac{u+v}{2}}}{2}(\cos\theta_2 + \cos\theta_3)\Big] \tag{3.32}$$

$$D_e = \frac{1}{2}\Big[(-1)^{\frac{3u+v}{2}} \sin\theta_1 - (-1)^{\frac{3u-v}{2}} - \frac{(-1)^{\frac{u+v}{2}}}{2}(\sin\theta_3 + \sin\theta_2) + (-1)^{\frac{u-v}{2}} \cos\theta_4\Big] \tag{3.33}$$

$$A_o = -D_o = \frac{j}{4}(-1)^{\frac{u+v+1}{2}}(\sin\theta_3 - \sin\theta_2) \tag{3.34}$$

$$B_o = -\frac{j}{2}\Big[\frac{(-1)^{\frac{u+v-1}{2}}}{2}(\cos\theta_2 - \cos\theta_3) + (-1)^{\frac{u-v-1}{2}} \sin\theta_4\Big] \tag{3.35}$$

$$C_o = -\frac{j}{2}\Big[\frac{(-1)^{\frac{u+v-1}{2}}}{2}(\cos\theta_2 - \cos\theta_3) - (-1)^{\frac{u-v-1}{2}} \sin\theta_4\Big] \tag{3.36}$$

where $\theta_1 = 2\alpha_n w, \theta_2 = 2\alpha_n(w-c), \theta_3 = 2\alpha_n(w+c)$ and $\theta_4 = 2\alpha_n c$.

$$\sum_{n=1}^{\infty} F_{uv}^{ef} \approx \sum_{n=1}^{N_{\max}} \Big[F_{uv}^{ef} - \tilde{F}_{uv}^{ef}\Big] + \sum_{n=1}^{\infty} \tilde{F}_{uv}^{ef}. \tag{3.37}$$

The infinite summation of $\tilde{F}_{uv}^{ef}$ in (3.37) involves infinite summation of series of the form $\sum_{n=1}^{\infty} \frac{\sin(nz)}{n^k}$ and $\sum_{n=1}^{\infty} \frac{\cos(nz)}{n^k}$ $(k = 2, 3, 4, 5, 6...)$ which can be very accurately evaluated using two different types of fast convergent series derived in the following section. The first term on the right hand side of (3.37) can be evaluated directly. Thus the overall complexity for evaluation of the matrix elements is reduced to order N_{max}.

3.4 Fast Convergent Series

For any series of the form $\sum_{n=1}^{\infty} e^{jnz}/n^k$ where $k = 2, 3, 4, ...$ [34]:

$$\sum_{n=1}^{\infty} e^{jnz}/n^k = j \sum_{n=1}^{\infty} \int_0^z \left(e^{jnz}/n^{k-1} \right) dz + \sum_{n=1}^{\infty} 1/n^k \tag{3.38}$$

Also it is known that:

$$\sum_{n=1}^{\infty} e^{jnz}/n = -\ln[2\sin(z/2)] + j(\pi - z)/2, 0 < z < 2\pi \tag{3.39}$$

Using [47] the following expansion is obtained:

$$\ln(\sin z) = \ln z - z^2/6 - z^4/180 - z^6/2835 - z^8/37800$$
$$- z^{10}/479001600...., -\pi < z < \pi \tag{3.40}$$

The first term in right hand side of (3.38) is evaluated using the above expression and the second term is calculated using the Riemann Zeta function [48] to obtain:

$$\sum_{n=1}^{\infty} \frac{\sin(nz)}{n^2} = -z \ln z + \sum_{i=1}^{\infty} c_i z^{2i-1} \tag{3.41}$$

where $c_1 = 1$, $c_2 = 1/72$, $c_3 = 1/14400$, $c_4 = 1/1270080$, $c_5 = 1/87091200$. However, the above fast convergent series converges very fast only for small values of z as shown in Figure 3.4. When z is large enough the following fast convergent series [34] can be used.

$$\sum_{n=1}^{\infty} \frac{\sin(nz)}{n^2} = \sum_{n=1}^{\infty} \frac{\sin(nz)}{n^2} [1 - \tanh(np)] + \frac{p(\pi - z)}{2} \tag{3.42}$$
$$- \frac{\pi}{p} \sum_{n=1}^{\infty} \frac{\sinh[(2n-1)\pi(\pi - z)/(2p)]}{[(2n-1)\pi/(2p)]^2 \sinh[(2n-1)\pi^2/(2p)]}$$

In order of get faster convergence the value of the parameter p is chosen depending on the value of z so that when both summations in (3.42) are truncated they have similar order of errors. It can be derived from the asymptotic forms of the two summations. The asymptotic form for each term of the first summation can be written as $2e^{-2np}/n^2$ and for the second one can be written as $4p[e^{-b_n z/\pi} - e^{-b_n(2-z/\pi)}]/[(2n-1)^2\pi]$ where $b_n = (2n-1)\pi^2/(2p)$. Because this formula is used for $z < \pi$, therefore, for them to converge at the same rate the powers of the exponential terms should be same. Therefore,

$$2Np = (2N-1)\pi z/(2p) \tag{3.43}$$

where N is the number of terms at which the two infinite summations on the RHS in (3.42) are truncated. For large N, the parameter p is almost independent of N.

$$p \approx \sqrt{\pi z/2} \tag{3.44}$$

Figure 3.4 shows the relative error in the first and second types of FCS taking different number of terms for different values of z. The figure shows the convergence of first type of FCS using first $5, 7$ and 9 terms of the series and of the second type of fast convergent series for $N = 5, 7, 9$ and 11. From the figure it can be concluded that the first kind of fast convergent series converges faster for values of z/π closer to 0 and the second type of FCS converges faster for value of z/π closer to 1 and results accurate upto at least 8 significant digits can be obtained by using less than 5 terms. In order to obtain an accuracy of δ for a given z, p can be calculated using (3.44). Then using p and given accuracy δ a formula to calculate N is derived:

$$N = \text{ceil}\{[\log_{10}(1/\delta) - k]/p\} + 1 \tag{3.45}$$

where k is the power of n in the denominator in (3.38). Figure 3.5 shows the verification of the formula using summation of sine series for $k = 2$ and $k = 4$ for different values of accuracy δ. As a result when using (3.42) the rate of convergence can be further accelerated by choosing the value of p and N dynamically for a given z and δ. Similar, fast convergent series for higher values of k

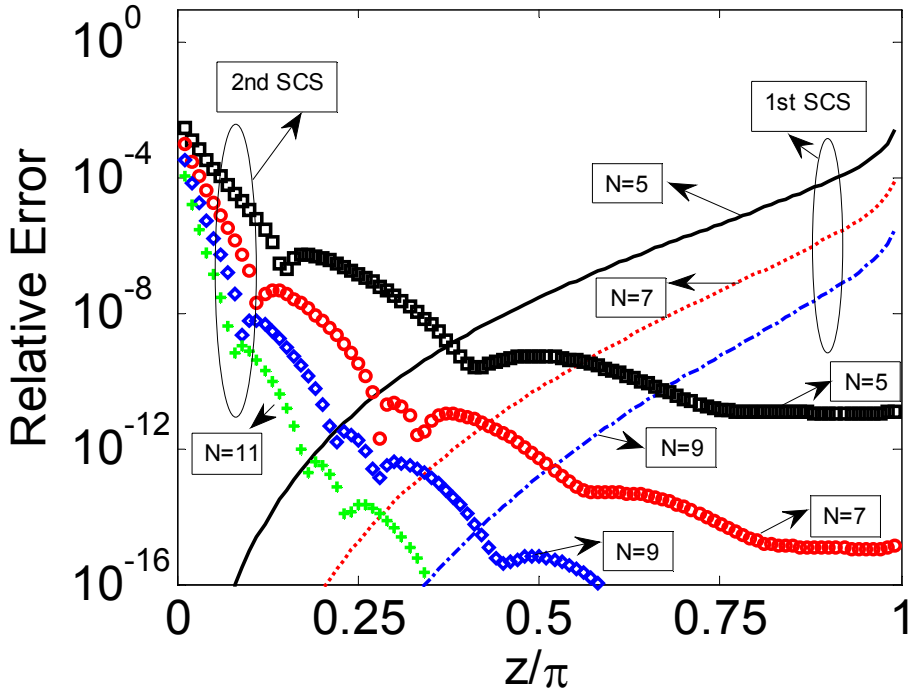

Figure 3.4 Relative error in first and second type of fast convergent series as a function of z/π for approximating $\sum_{n=1}^{\infty} \frac{\sin(nz)}{n^2}$ for different N using first and second type of FCS. Also (3.44) has been used to dynamically choose the value of p for the second type of FCS.

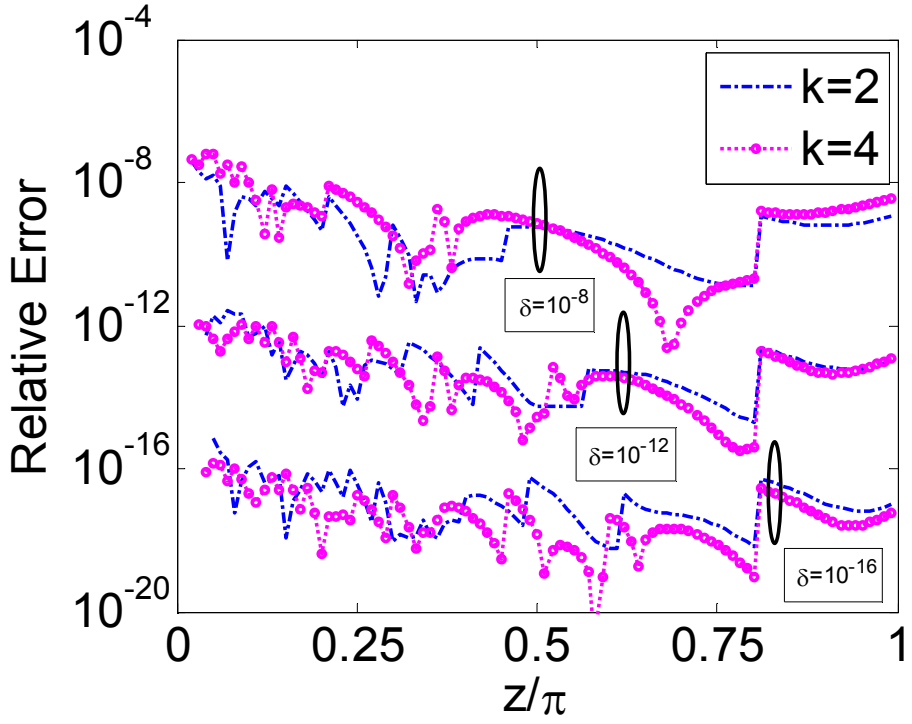

Figure 3.5 Proof of the formula (3.45) for calculating N for a given accuracy δ for approximating $\sum_{n=1}^{\infty} \frac{\sin(nz)}{n^k}$.

are derived using integration (3.38) and contour integration. So the expression for p will remain unchanged even for higher orders because the integration is done w.r.t. z and the expression for adaptively choosing the value of N in (3.45) has already been shown to work for higher values of k and the value of N will be even smaller as k increases. The code written to validate the results in the paper was made to switch from first kind of FCS to the second at $z = 1$.

Table 3.1 β/k_0 for the dominant mode in a two layered shielded microstrip for different c at 1 GHz and other parameters as given in Figure 3.2

	Normalized propagation constant			
$\mathbf{N_{max}}$	$\mathbf{c = a/2}$	$\mathbf{c = a/3}$	$\mathbf{c = a/5}$	$\mathbf{c = 2a/3}$
10	1.58812263	1.61882576	1.72652553	1.61882576
15	1.58814822	1.61872713	1.72656839	1.61872713
20	1.58814620	1.61871628	1.72656556	1.61871628
30	1.58818142	1.61874567	1.72659825	1.61874567
40	1.58818027	1.61874450	1.72659719	1.61874450
50	1.58818105	1.61874542	1.72659800	1.61874542
60	1.58818126	1.61874553	1.72659820	1.61874553
2000000	1.58818105	1.61874532	1.72659803	1.61874532

3.5 Numerical Results

A three layered shielded microstrip with parameters as shown in Figure 3.2 at 1 GHz was used to validate the results and demonstrate the convergence of the leading term extraction, the matrix elements, the ϵ_{reff} and the determinant. Figure 3.6 verifies the correctness of leading term extraction as when k leading terms are used the difference $F_{44}^{zz} - \tilde{F}_{44}^{zz}$ is of the order of $1/n^{k+2}$. From Figures 3.7(a) and 3.7(b) it is observed that the convergence of K_{44}^{zz} and determinant of K matrix changes from $1/N_{\text{max}}$ using the direct summation to $1/N_{\text{max}}^3$ using up to second leading term and finally to $1/N_{\text{max}}^7$ using up to fifth leading term.

Table 3.2 β/k_0 for different basis functions and $N_{\max}$=70 for first five modes of the shielded microstrip with parameters $\epsilon_{r_{-1}} = 8.875$, $\epsilon_{r_1} = 1$, $\mu_{r_i} = 1$, $f = 20$GHz, $D_{-1} = 1.27$mm, $D_1 = 11.43$mm, $2w = 1.27$mm, $a = 12.7$mm, $c = a/2$ at $\beta = 2k_0$.

		Normalized propagation constant				
M_z	M_x	**Mode 1**	**Mode 2**	**Mode 3**	**Mode 4**	**Mode 5**
2	2	2.7108347	1.2892179	1.1027109	0.9223126	0.7251113
3	3	2.7102057	1.2894955	1.1026366	0.9223134	0.7250996
4	4	2.7102058	1.2894526	1.1026366	0.9223133	0.7250996
5	5	2.7102057	1.2894526	1.1026366	0.9223133	0.7250996
5	5	2.7102057[12]	1.2894527[12]	1.1026366[12]	0.9223133[12]	0.7250996[12]

The results are similar if odd number of leading terms or the next even number of leading terms are used as seen from Figures 3.7(a), 3.7(b), 3.8(a) and 3.8(b). This is because the even leading terms do not have a constant term whose convergence is slow compared to the sinusoidal functions.

Figure 3.8(a) shows that using a larger number of basis functions decreases the convergence w.r.t $N_{\max}$. But by using higher order basis and higher $N_{\max}$ more accurate results are obtained. Figure 3.8(b) shows the convergence of ϵ_{reff} as a function of $N_{\max}$ for different leading terms using $M_z = 7$, $M_x = 7$. Also it is observed that ϵ_{reff} converges faster as more number of leading terms are used.

Table 3.1 shows a verification of the propagation constant obtained using the proposed approach for the same three layered shielded microstrip with different values of displacement of the signal metal from the edge c and $N_{\max}$ using $M_z = 5$, $M_x = 5$ and up to fifth leading terms. The correctness of the results is verified using the SDIA without acceleration using $M_z = 5$, $M_x = 5$ and $N_{\max} = 2 \times 10^6$ which results in β correct within 7 significant digits. The value of propagation constant obtained is correct within 9 significant digits using just 60 terms of the infinite summation using the proposed approach. In order to obtain the same accuracy using the SDIA without acceleration one will need to consider nearly 2×10^8 terms in the infinite

Table 3.3 β/k_0 for the dominant mode in a two layered shielded microstrip for different c

	Normalized propagation constant			
$\mathbf{N_{max}}$	$\mathbf{c = a/2}$	$\mathbf{c = a/3}$	$\mathbf{c = a/5}$	$\mathbf{c = 2a/3}$
5	1.5793	1.58	1.63	1.58
10	1.5793544	1.58	1.580	1.58
15	1.5793544	1.5797	1.5804	1.5797
20	1.5793544	1.57974	1.58041	1.57974
30	1.57935450	1.5797417	1.580414	1.5797417
40	1.57935450	1.57974176	1.58041436	1.57974176
50	1.57935450	1.57974176	1.580414362	1.57974176
60	1.579354501	1.579741762	1.580414362	1.579741762
2000000	1.57935450	1.57974176	1.58041436	1.57974176

summation. Also, it is observed that using just 10 terms the value of β obtained is correct up to 4 significant digits, respectively, which is enough for most practical applications. The proposed approach gives accurate results for the cases when the signal strip is displaced from the center. The result for the $c = a/3$ and $c = 2a/3$ should be same by symmetry and that is what is obtained using the proposed approach. Using more number of terms in the proposed approach even more accurate values of β are obtained. Also using higher order leading terms even faster convergence is obtained. The approach although seems to involve an approximation for the basis functions but it has been verified to give results accurate up to 11 significant digits $\epsilon_{\text{reff}} = 8.8100415749$ using $M_z = 5$, $M_x = 4$ and $N_{\text{max}} = 300$ for a shielded microstrip with parameters $\epsilon_r = 11.7$, $\mu_r = 1$, $f = 4$GHz, $h = 3.17$mm, $w = 3.04$mm, $2a = 34.74$mm, $d = 50$mm [12].

A shielded microstrip with parameters $\epsilon_{r_{-1}} = 8.875$, $\epsilon_{r_1} = 1$, $\mu_{r_i} = 1$, $f = 20$GHz, $D_{-1} = 1.27$mm, $D_1 = 11.43$mm, $2w = 1.27$mm, $a = 12.7$mm, $c = a/2$ [12] was also used to validate the results. Table 3.2 shows the numerical values of the normalized propagation constants for

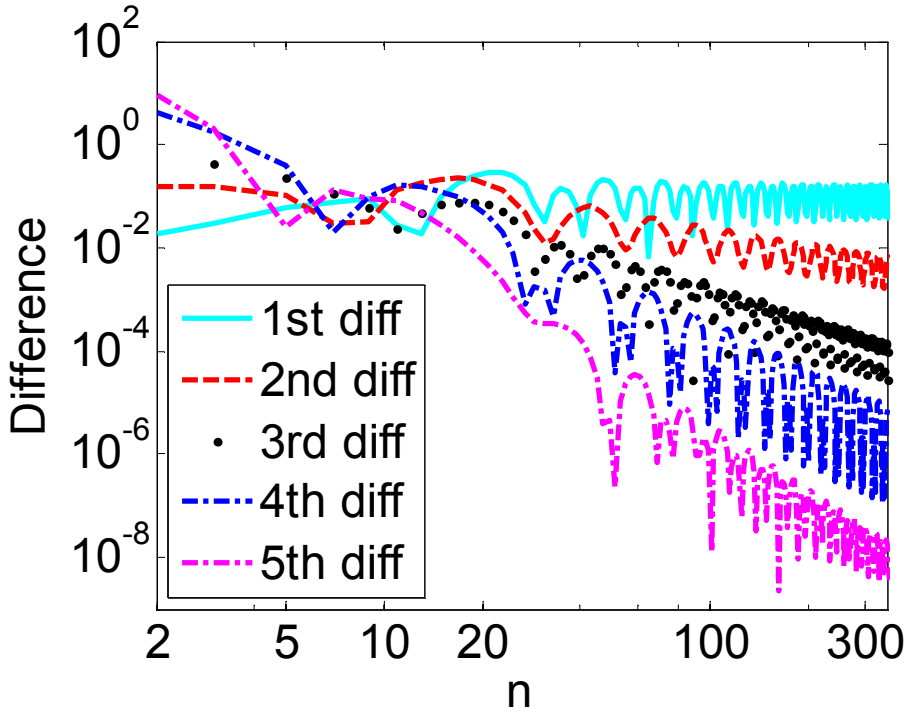

Figure 3.6 Convergence of $(F_{44}^{zz} - \tilde{F}_{44}^{zz})\alpha_n^3$ as function of n for $\beta = 2k_0$ for different number of leading terms.

the first five modes of a single layered shielded microstrip with above parameters using different number of basis functions for the currents in the longitudinal and the transverse directions. It also shows that using $M_z = 5$, $M_x = 5$ and $N_{max} = 70$ the propagation constant for the first five modes is obtained correct within 8 significant digits. In order to obtain this accuracy using the conventional SDA nearly $N_{max} = 2 \times 10^7$ terms of the infinite summation would be needed.

Table 3.3 shows the validity of the approach for a two layered shielded microstrip line with parameters $\epsilon_{r1} = 4$, $\epsilon_{r2} = 11.7$, $\mu_{r1} = \mu_{r2} = 1$, $h_1 = 5\mu$m, $h_2 = 500\mu$m, $w = 2\mu$m, $a = 50\mu$m, $d = 40\mu$m, $f = 1$ GHz for different values of displacement of the signal metal from the edge c and N_{max} using $M_z = 5$, $M_x = 5$ and up to fifth leading term. The correctness of the results is verified using the conventional SDIA without acceleration. The value of propagation constant obtained is correct within 9 significant digits using just 50 terms of the infinite summation using the proposed approach. In order to obtain the same accuracy using the conventional SDIA one will

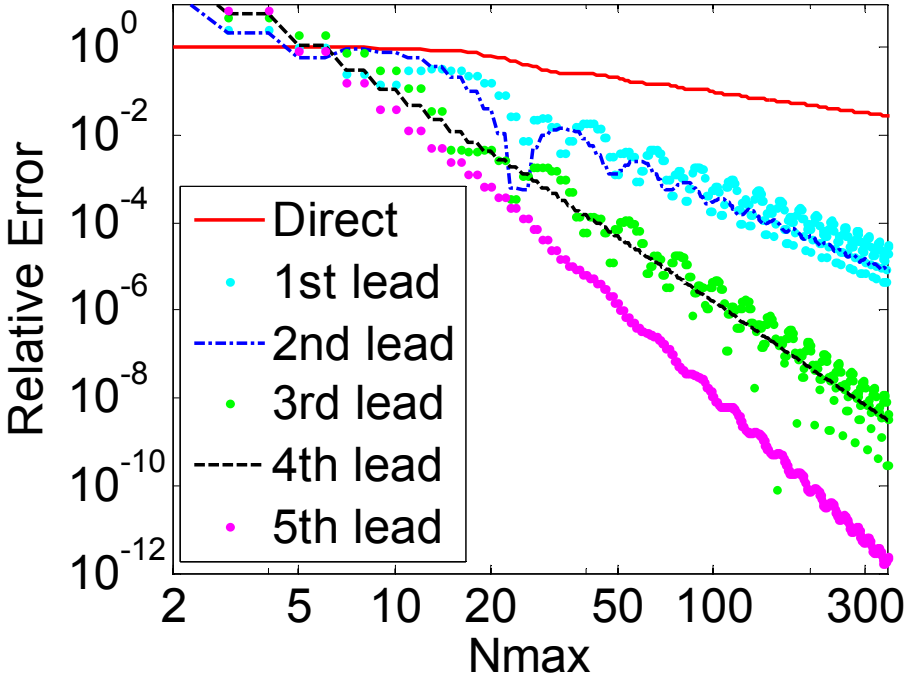

(a) Convergence of K_{44}^{zz}.

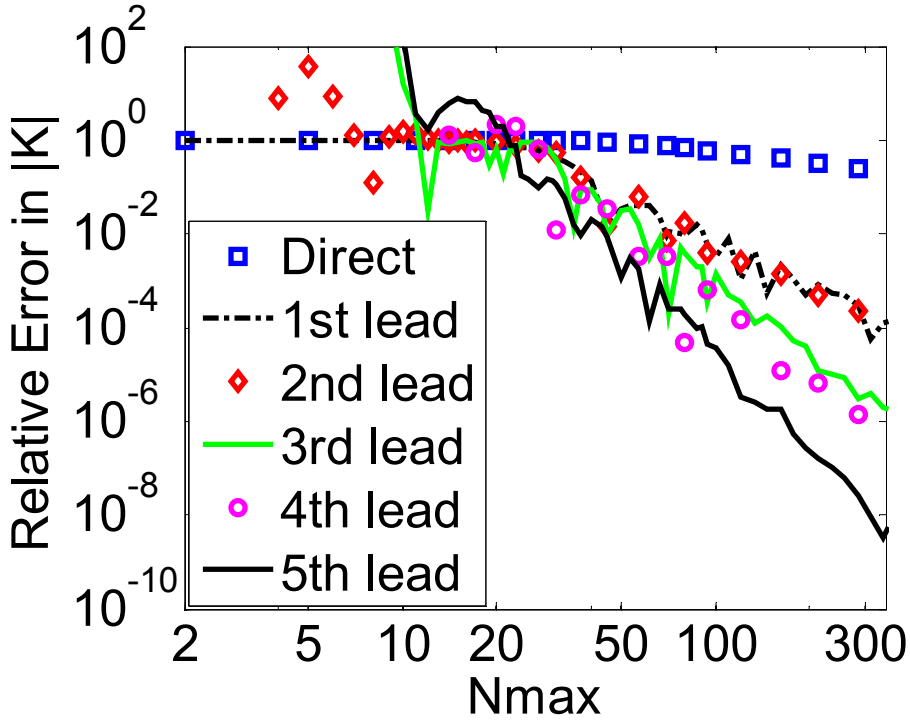

(b) Determinant of K matrix.

Figure 3.7 Convergence of (a) K_{44}^{zz} and (b) determinant of K matrix for M_z=4, M_x=4 and $\beta = 2k_0$ using different number of leading terms for the three layered shielded microstrip with parameters as given in Figure 3.2 at 1 GHz.

need to consider nearly 2×10^6 terms in the infinite summation. Also, it is observed that using just 5 terms and 15 terms, respectively, the value of β obtained is correct up to 5 and 7 significant digits, respectively, which is enough for most applications in semiconductors.

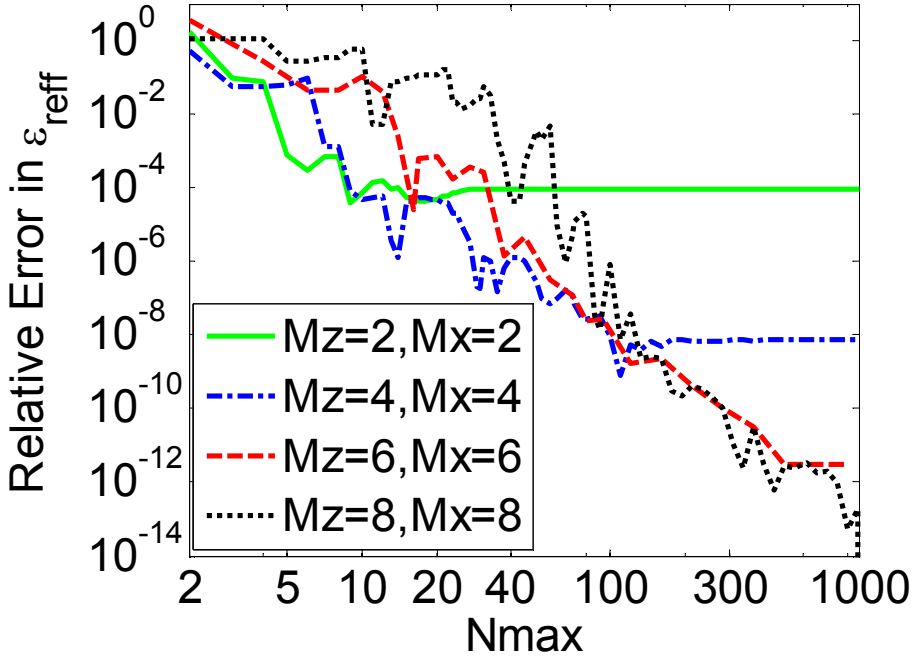

(a) Convergence of ϵ_{reff} using different number of basis functions using up to fifth leading term.

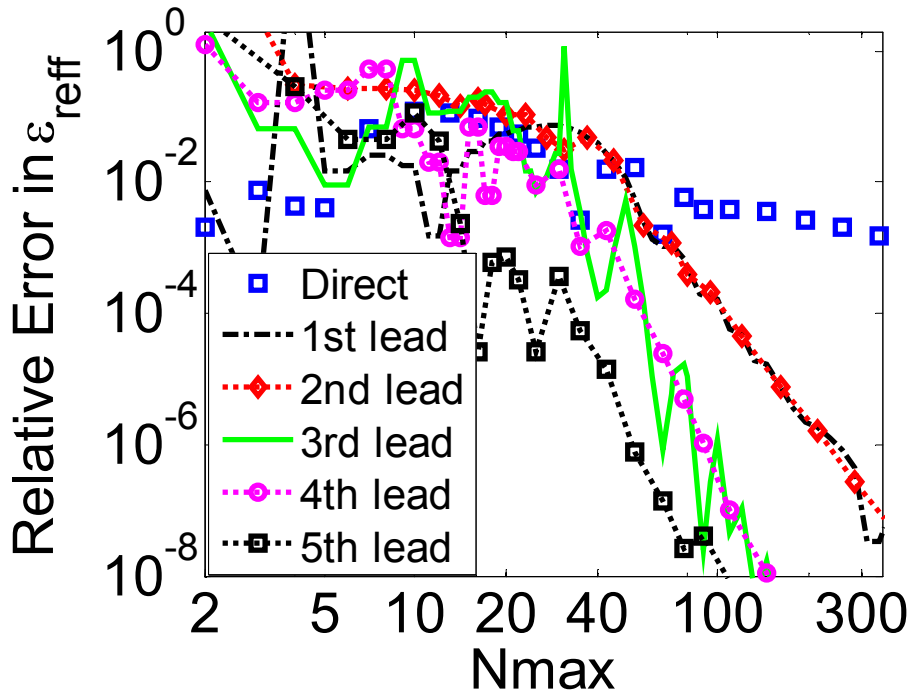

(b) Convergence of ϵ_{reff} using different number of leading terms for $M_{\text{z}} = 7$ and $M_{\text{x}} = 7$.

Figure 3.8 The convergence of ϵ_{reff} for different basis and different number of leading terms for the three layered shielded microstrip with parameters as given in Figure 3.2 at 1 GHz.

CHAPTER 4. Equivalent Model for Shielded Microstrip Transmission Lines over Lossy Layered Substrates

In the previous chapter we proposed a fast and accurate approach to obtain the effective medium parameters parameters for a multilayered shielded microstrip. In this chapter, we use this approach to develop an equivalent model for a multilayered lossy shielded microstrip transmission line by replacing the layered media below the signal strip with a single effective medium leaving the top part as it is there by retaining the inhomogeneity of the medium. The inhomogeneity is maintained by keeping the area above the transmission line intact. This is very helpful when analyzing the interaction between the devices and components located in different layers in an interconnect structure. Also, it can be integrated with the Agilent's Advanced Design Systems (ADS) Momentum module where a layered structure can be replaced with a single equivalent medium there by improving the mesh uniformity and hence reducing the computation time. The proposed equivalent model for the shielded microstrip transmission line on layered media is obtained by replacing the lossless, constant loss tangent or the layers with low finite conductivity with a single layer equivalent medium with parameters ϵ_{req}, equivalent loss tangent, σ_{req}, respectively. The results show that this model is frequency independent for layered structures when the given frequency and frequency of operation are less than the transition frequency (i.e. the frequency at which there is a sudden change in the equivalent dielectric constant (ϵ_{req})). For frequencies higher than the transition frequency the equivalent model is not frequency independent but it gives good results for the higher order mode although it is derived using the dominant mode. Also it is seen that at low frequency ϵ_{req} depends on the layers near to the signal metal but at higher frequencies it depends on the layer with the

highest value of ϵ_r irrespective of its location w.r.t to the metal strip.

4.1 Equivalent Model

The equivalent model consists of modeling the layered structure with a single layer such that the propagation constant for the two structures is the same for the dominant mode at the testing frequency (i.e. the frequency at which the model is evaluated). The thickness of equivalent layer is assumed to be equal to the sum of the thickness of each layer if all are lossless or the thickness of the layer with finite conductivities is much smaller than the skin depth. If the thickness of some layers is larger than the skin depth, the process of choosing the thickness is outlined later. A reverse process of root finding by Muller's method is used to evaluate the ϵ_{req} which gives the same value of the propagation constant for the dominant mode as the original layered structure. μ_{req} is assumed to be 1.

Figure 4.1(a) shows the cross section of a multi layered shielded microstrip which consists of a multi layer microstrip line enclosed in a perfect electric conductor (PEC) box of width a. Each layer has a thickness h_i complex dielectric constant ϵ_{ri}. Non zero imaginary part means the layer is lossy. It is infinitely long in the z-direction. The metal strip of width $2w$ located on top of the dielectric layers is also assumed to be a zero thickness PEC and can be located anywhere on the surface depending on the value of c. Figure 4.1(b) shows the equivalent model of this layered shielded microstrip where the layered structure is replaced with a single layer of thickness equal to the sum of thickness of all the layers and $\epsilon_r = \epsilon_{\text{req}}$ which is obtained using the method proposed above.

We have used the spectral domain immitance approach (SDIA) [54], [55] outlined and accelerated in the last chapter to evaluate the propagation constants. Chebyshev polynomial are used as the basis functions to expand the unknown currents in the transverse and longitudinal directions. Although the spectral domain approach (SDA) is computationally intensive but by using acceler-

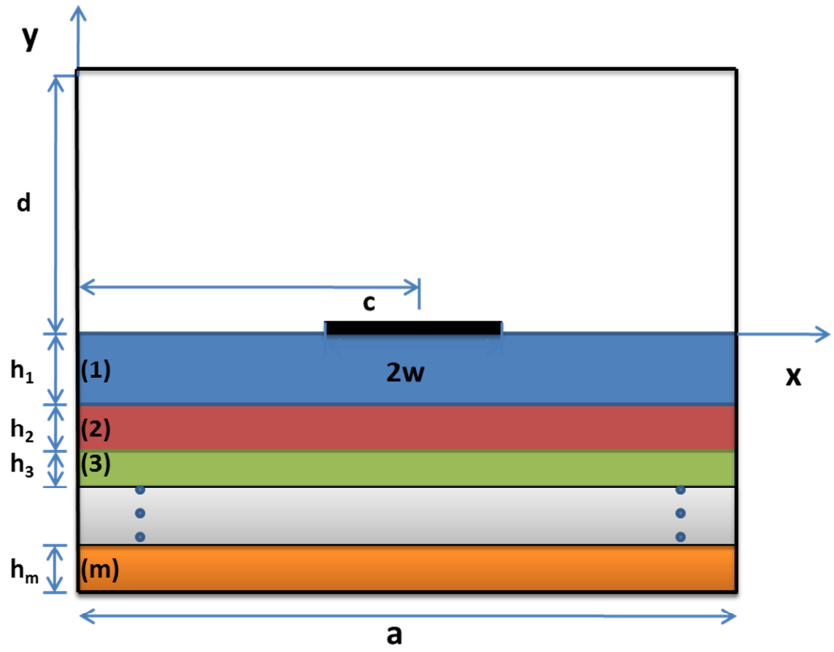

(a) Multilayered shielded microstrip

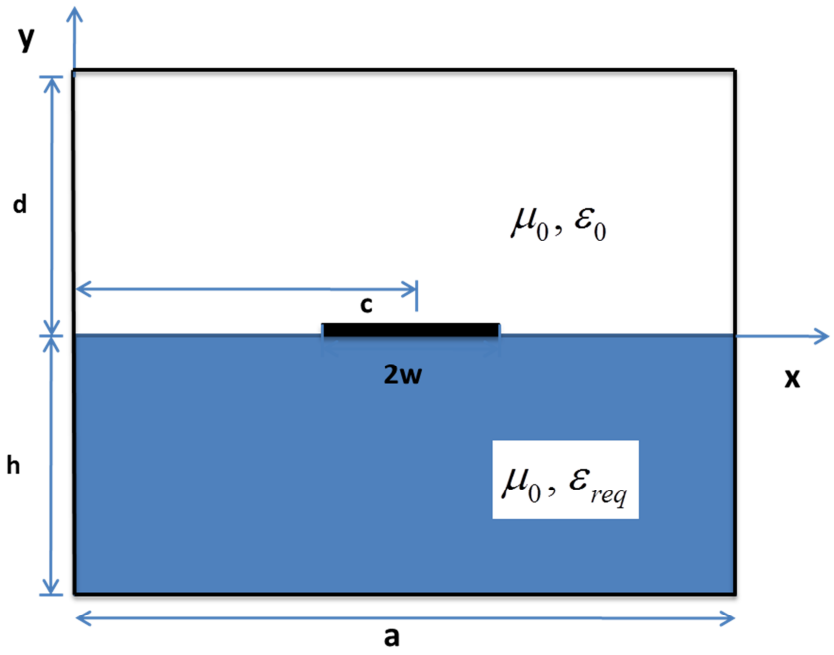

(b) Equivalent single layered shielded microstrip

Figure 4.1 (a) A multi layered shielded microstrip with air above the signal metal (b) Equivalent single layer model of the layered microstrip with air above the signal metal.

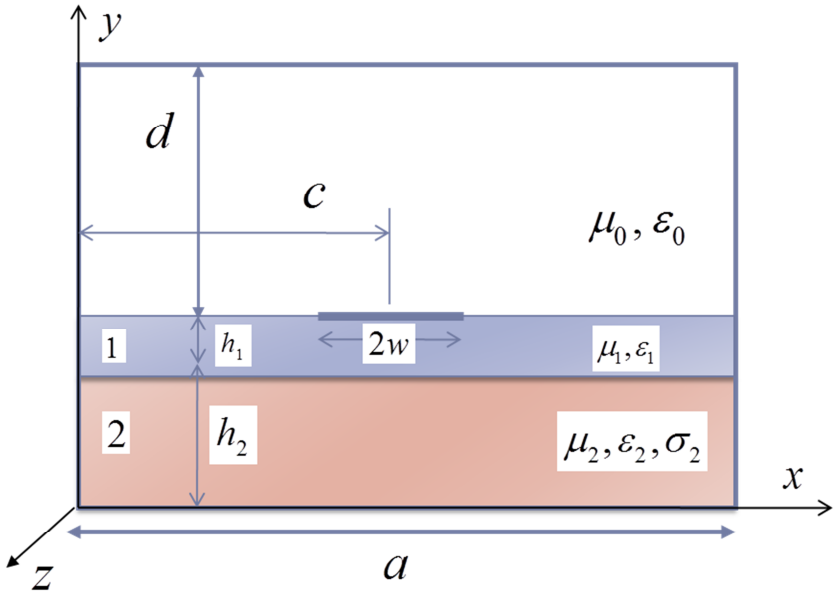

(a) MIS Structure

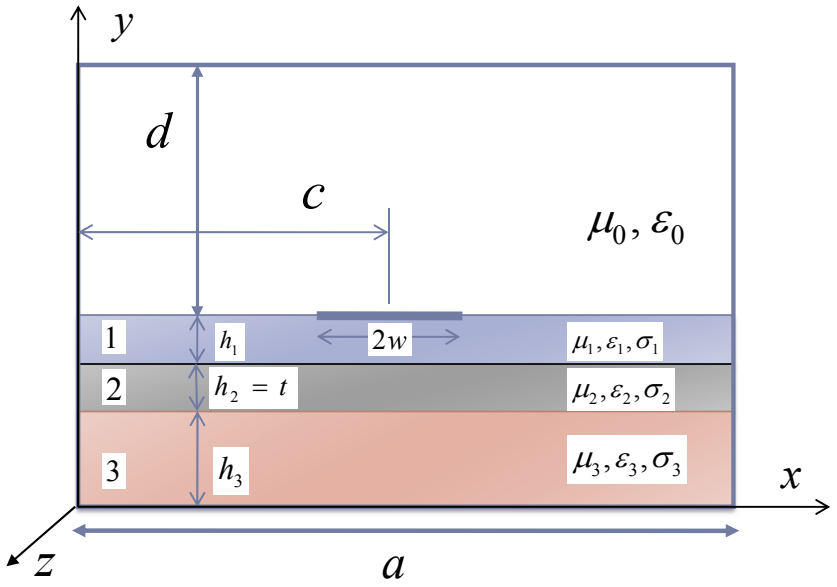

(b) MIMS Structure

Figure 4.2 A shielded microstrip with (a) MIS (Metal Insulator Semiconductor) Structure (b) MIMS (Metal Insulator Metal Semiconductor) Structure

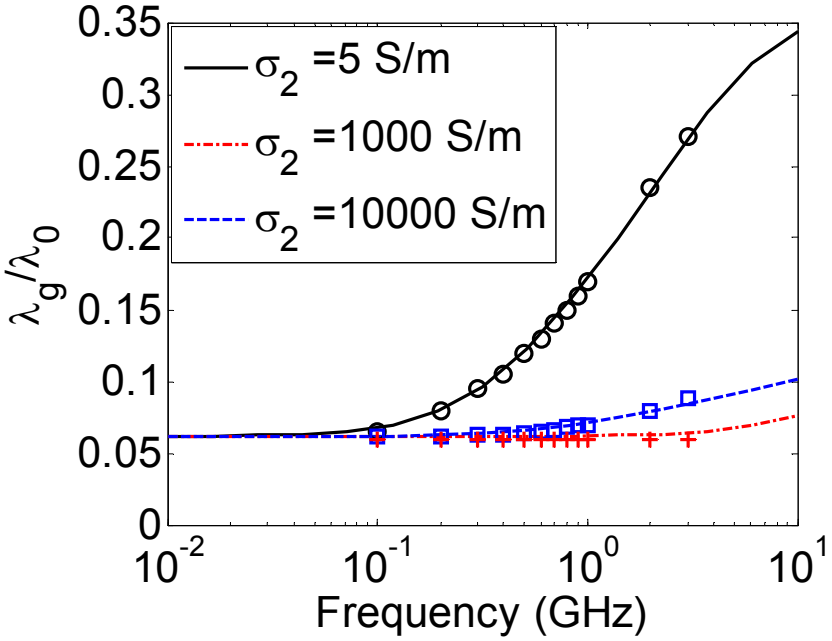

(a) λ_g/λ_0 vs frequency

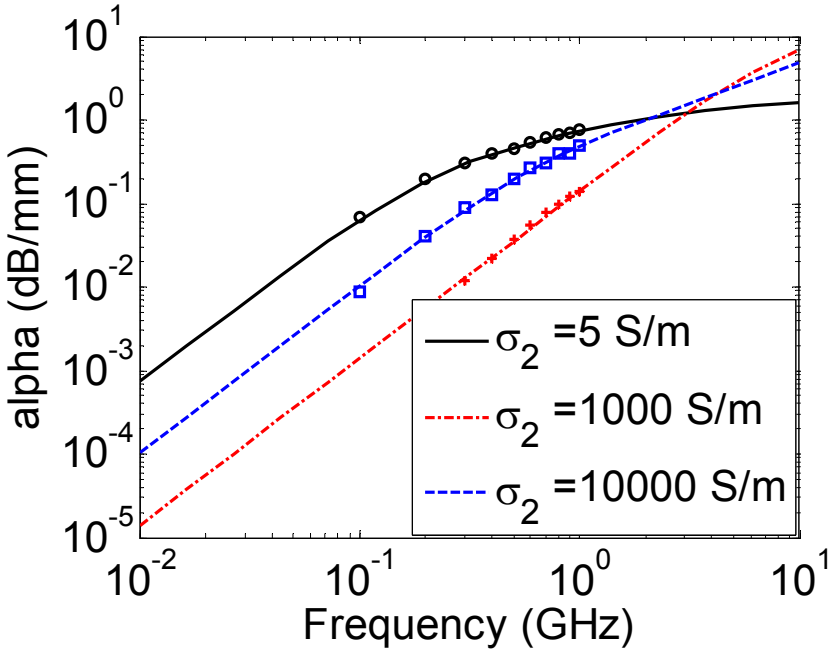

(b) α (dB/mm) vs frequency

Figure 4.3 (a) $\lambda g/\lambda_0$ (b) α (dB/mm) as a function of frequency for a shielded MIS transmission line with parameters $\mu_r = 1, h_1 = 1\mu$m, $h_2 = 250\mu$m, $w = 80\mu$m, $a = 1$cm, $d = 1.249$mm, $c = a/2, \epsilon_{r1} = 4, \epsilon_{r2} = 12, \sigma_1 = 0$ and $\sigma_2 = 5, 1000$ and 10000 S/m. The points are results from [1].

ated SDA the speed can be increased by nearly five orders of magnitude [49], [57] as shown in the last chapter. The SDIA was validated for metal insulator semiconductor (MIS) structure as shown in Figure 4.2(a) for different values of conductivity of the semiconductor as shown in Figure 4.3. Also it was validated for the metal insulator metal semiconductor (MIMS) structure as shown in Figure 4.2(b) for different thicknesses (t) of the metal layer as shown in Figure 4.4.

The effect of varying the conductivity of the semiconductor in a shielded MIS structure with parameters as in Figure 4.2(a) was studied using the SDIA. Figure 4.3(a) shows the normalized guided wavelength ($\lambda_g = 2\pi/\text{Re}(\beta)$). β is the complex propagation constant. Figure 4.3(b) shows the attenuation constant α (in dB/mm) as a function of frequency for σ_2=5, 1000 and 10000 S/m. The results show that as the conductivity of the semiconductor increases the guided wavelength will first decrease and then increase because of the transition from lossy dielectric to skin effect region (i.e. when the skin depth becomes less than the thickness of the layer). Also the attenuation first increases to a maximum and then again goes to zero as σ_2 approaches infinity i.e. the semiconductor layer acts as a perfect electric conductor, because of the same reason. Our results are in agreement with [1] as shown by the circles, squares and '+' signs. The effect of the thickness of the metal layer in a MIMS structure as shown in Figure 4.2(b) with parameters as in Figure 4.4 was also studied using the SDIA. Figures 4.4(a) and 4.4(b) show the normalized β and the attenuation constant α (in dB/mm), respectively. Higher the thickness of the metal layer the less penetrable it is for the field lines and so the contribution of the semiconductor layer below the metal layer becomes smaller and smaller. Also as the frequency increases the skin depth decreases so even very small thickness of metal become impenetrable and the effect of the layers below it is negligible and the result approaches that for a single layered shielded microstrip formed by replacing the metal layer with a PEC. Also, from Figure 4.4(b) it can be concluded that smaller the thickness of the strip higher is the attenuation constant and once the thickness becomes comparable to the skin depth the attenuation becomes nearly constant and approaches that for the case where thickness of metal layer in infinite.

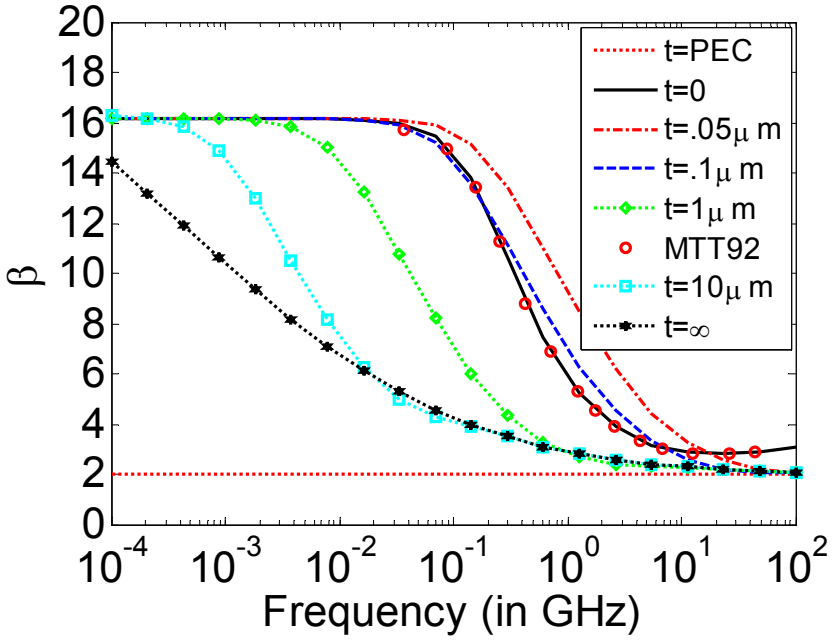

(a) β vs frequency

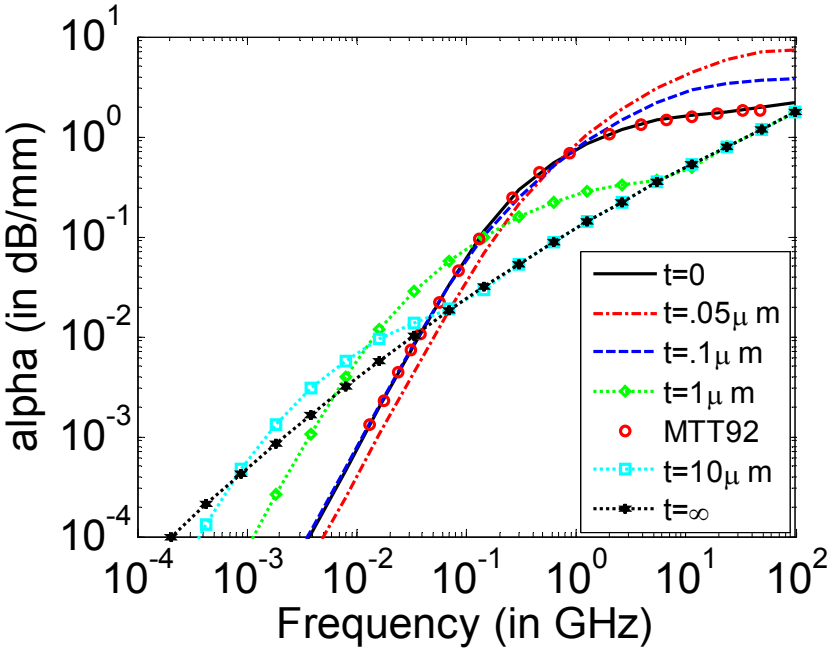

(b) α (dB/mm) vs frequency

Figure 4.4 (a)β (b)α (dB/mm) as a function of frequency for a shielded MIMS transmission line with parameters $\mu_r = 1, h_1 = 1\mu$m$, h_2 = t, h_3 = 250\mu$m$, w = 80\mu$m$, a = 1$cm$, d = 1.249$mm$, c = a/2, \epsilon_{r1} = 4, \epsilon_{r3} = 12, \sigma_1 = 0, \sigma_2 = 5.8 \times 10^7$, $\sigma_3 = 5$S/m and thickness $t = 0, .05\mu$m$, .1\mu$m$, 1\mu$m$, 10\mu$m$, \infty$.

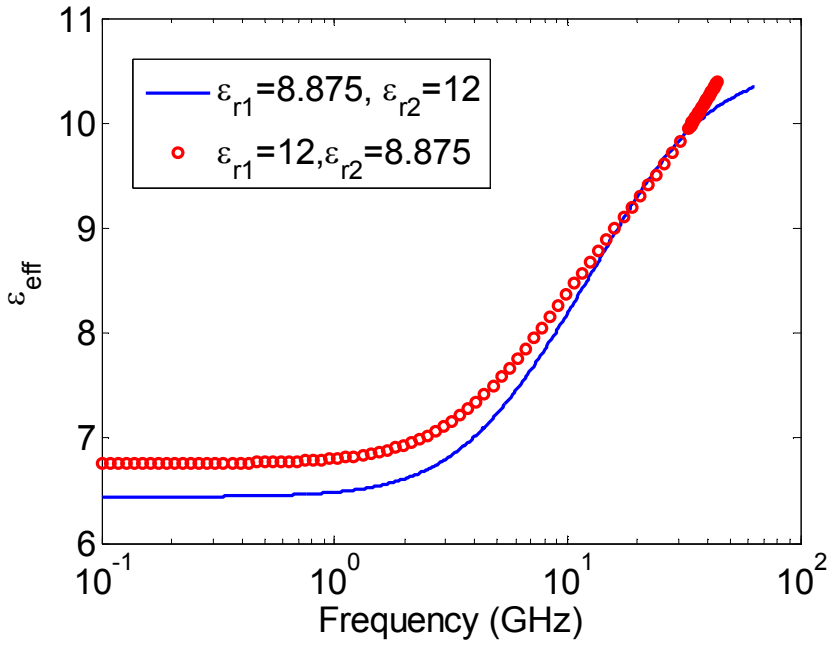

Figure 4.5 Comparison of ϵ_{reff} as a function of frequency on reordering the layers for a two layered shielded microstrip with parameters $\epsilon_{r1} = 8.875, \epsilon_{r2} = 12, \mu_r = 1, h_1 = h_2 = 1.27\text{mm}, w = 0.635\text{mm}, a = 12.7\text{mm}, d = 11.43\text{mm}, c = a/2$.

4.1.1 Extending the Equivalent Model for the Lossy Case

4.1.1.1 Constant Loss Tangent Case

In case some of the layers are dielectrics with constant loss tangents we can extend the same idea of the equivalent model by using complex dielectric constant. ($\epsilon_{ri} = \text{Re}(\epsilon_{ri})(1 - j\tan\delta_i)$ where $\tan\delta_i$ loss tangent of the particular layer). Then by using the same approach we can reduce the layered lossy structure into a single layer with thickness equal to the sum of all the layers and ϵ_{req} and equivalent loss tangent such that they result in the same value of complex ϵ_{reff} ($\beta^2 = \epsilon_{\text{reff}} k_0^2$) as the original layered structure at the testing frequency using the SDIA.

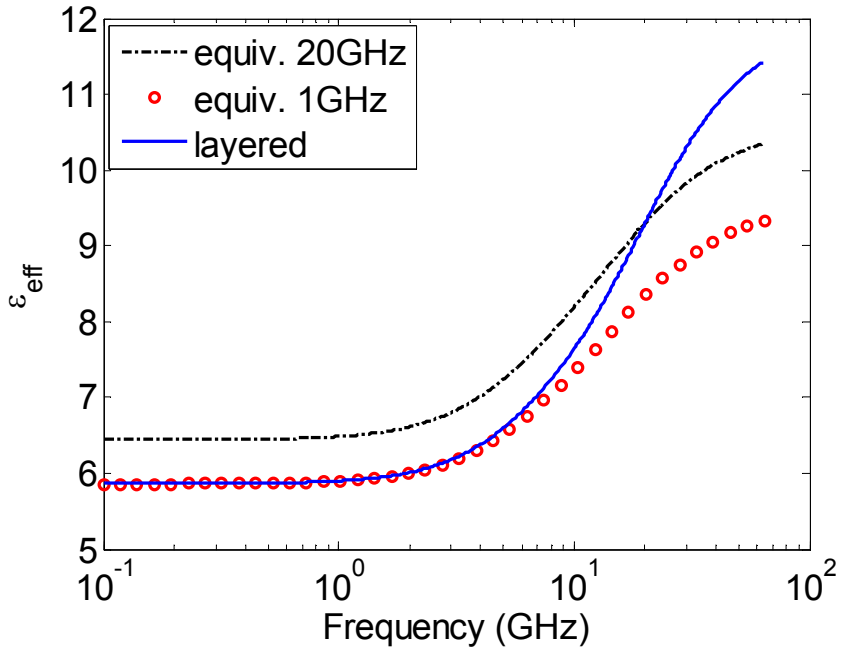

Figure 4.6 Comparison of ϵ_{reff} as a function of frequency for two layered shielded microstrip with air above the signal metal (solid line) and (circles, dotted line) the equivalent models at 1GHz and 20GHz (i.e. close to transition frequency) with $h = h_1 + h_2$, $\epsilon_{\text{req}} = 9.5057$ at 1GHz and $\epsilon_{\text{req}} = 10.5275$ at 20GHz, $\mu_{\text{req}} = 1$ for both. The parameters of the layered microstrip are same as in Figure 4.5.

4.1.1.2 Constant Conductivity Case

If some of the layers have a finite conductivity (σ_i) then we can extend our equivalent model by using complex dielectric constant ($\epsilon_{ri} = \text{Re}(\epsilon_{ri}) - j\sigma_i/(\omega\epsilon_0)$) where σ_{i} is the conductivity of the particular layer). It is worth to note that the imaginary part of the dielectric constant is inversely proportional to the testing frequency as opposed to the case with constant loss tangent where it was constant. If the thickness of the conductive layer is more than the skin depth then the contribution of this layer to the thickness of the single equivalent layer must be chosen as shown in the numerical results. Thus using the same approach as for the lossless case we can model a multilayered structure with a single layer with ϵ_{req} and σ_{eq} such that they give the same value of complex ϵ_{reff} at that frequency.

4.2 Numerical Results

4.2.1 Validation

Figures 4.5 and 4.7 show the normalized propagation constant squared, which is the same as the ϵ_{reff}, as a function of frequency for two layered shielded microstrip with dimensions of the order of few mm and two and three layered shielded microstrips with dimensions of the order of a few μm. From these figures we can come to the following three conclusions. Firstly, in the low frequency range the value of ϵ_{reff} and hence ϵ_{req} highly depends on the layers nearer to the signal metal and not on the layer with high value of ϵ_r because of the near field effect. Secondly, at very high frequency the ϵ_{reff} is close to the ϵ_r for the layer with the maximum value of ϵ_r irrespective of its location w.r.t. the signal metal. This is because most of the energy is confined to the layer with a high value of ϵ_{r} when the wavelength becomes comparable to the thickness of the layer. This result is further amplified by the results for the case in Figure 4.7(b) where the layer with the highest ϵ_r is the third one from the signal strip. Thirdly, the transition frequency i.e. the frequency at which there is a steep rise in the propagation constant highly depends on the thickness of the layers. The smaller the thickness of the layers, the higher is the transition frequency.

The concept of the equivalent model was numerically validated for three different layered shielded microstrips as shown in Figures 4.6, 4.8(a) and 4.8(b). In the SDIA the infinite series for the elements of the Galerkin matrix was truncated at $N = 2000$ and Chebyshev basis with two terms each were used to expand the current in the longitudinal and transverse direction. $\epsilon_0 = 8.854 \times 10^{-12}$ F/m was used and an ϵ_{req} of 9.5057 at 1GHz, 10.5275 at 20GHz for the case in Figure 4.6 and an ϵ_{req} of 4.8317 and 8.6485, respectively at 1GHz were obtained for the cases in Figures 4.8(a) and 4.8(b), respectively. Thus the equivalent model is very accurate for frequencies below the transition frequency if the testing frequency is much lower than the transition frequency. But if the testing frequency is close to the transition frequency this equivalent model is not frequency independent as shown in Figure 4.6 for the case when the testing frequency is 20GHz.

Table 4.1 Comparison of the normalized propagation constant for higher order modes in two layered shielded microstrip with the higher order modes of the equivalent model

	Mode 1	**Mode 2**	**Mode 3**
2 layer	3.0495	1.9396	.9967
1 layer Equiv.	3.0495	1.9294	.9856

Table 4.1 shows the normalized propagation constant for higher order modes calculated using a two-layer structure with parameters same as in Figure 4.6 and an equivalent single layer model at 20 GHz which has the same propagation constant for the dominant mode and $\epsilon_{\text{req}} = 10.5275$, $\mu_{\text{req}} = 1$ and $h = 2.54$mm. It is observed that the difference in the propagation constant for the higher order mode is less than 1% which is accurate enough for most practical applications. Therefore, for frequencies higher than the transition frequency, when the higher modes also start existing the equivalent model is not frequency independent but it gives accurate results for the propagation constant for the higher order modes.

Figures 4.9 and 4.10 show the validation of the equivalent model for different thickness of the layers and different widths of the metal strip. As as the thickness of the first layer approaches zero the ϵ_{req} approaches the ϵ_{r2} and vice versa. Also as the width of the strip increases the ϵ_{req} approaches that for a parallel plate capacitor model which is equal to 5.9618 for the cases in Figure 4.10.

The equivalent model was further validated by plotting the parameters of the equivalent medium such as ϵ_{req}, loss tangent $\tan\delta$ and the σ_{eq} as a function of testing frequency for the lossless, constant loss tangent and the constant conductivity cases.

4.2.1.1 Lossless Case

Figures 4.11(a) and 4.11(b) further validate that when the dimensions are in the range of microns the transition frequency is of the order of a few hundred GHz for the lossless case so the

equivalent model can be easily used to reduce several lossless dielectric layers into a single dielectric layer. The change in ϵ_{req} is found to be less than $.0015\%$ up to 100 GHz.

4.2.1.2 Constant Loss Tangent Case

Figures 4.12 and 4.13 show that for the constant loss tangent case the variation in ϵ_{req} and equivalent loss tangent is less than $.1\%$ with change in testing frequency up to 100 GHz. Also, at frequencies higher than the transition frequency the ϵ_{req} and equivalent loss tangent depend on the dielectric constant and the loss tangent of the layer with largest value of ϵ_{r}.

4.2.1.3 Constant Conductivity Case

Figure 4.14 show that higher values of conductivity of the layers nearer to signal metal results in a higher value ofϵ_{req} for lower frequencies but the effect decreases with increase in frequency. Figure 4.15 shows that at low frequencies the σ_{eq} highly depends on the conductivity of the layers nearer to the signal metal. The proposed equivalent model is almost frequency independent for frequencies up to few GHz.

For the case when the layers are lossy with finite conductivity we see a very interesting phenomena. In this case, we observe two transition frequencies. The first transition frequency depends on the layer with the largest $\sigma_{\text{i}}/\epsilon_{ri}$ ratio irrespective of where the layer is located with respect to the signal strip as can be observed from Figures 4.15-4.16. Also, this transition occurs the real and imaginary part of the ϵ_{reff} become equal i.e. when $\sigma_{\text{i}}/(\omega\epsilon_0\epsilon_{\text{ri}})$=1. The first transition frequency is also independent of the width of the different layers as seen by comparing Figures 4.20(b), 4.21(b) and 4.14(b), 4.15(b). The second transition frequency corresponds to the transition frequency in the lossless multilayered shielded microstrip which depends on the thickness of the layers. Between the first and second transition frequency region the near field effect dominates and the value of ϵ_{req} depends largely on the ϵ_r of the layers nearest to the signal metal due to near field effect. However, above the second transition frequency the ϵ_{req} depends only on the layer with the highest

value of ϵ_r. The second transition frequency (f_{T2}) highly depends on the thickness of the layer with the highest value of ϵ_r and the transition occurs when it becomes comparable to half of the wavelength [42]. From Figures 4.14, 4.20 and 4.16 we can easily conclude that f_{T1} just depends on the layer with the highest value of $\sigma_{\text{i}}/\epsilon_{ri}$ irrespective of its location w.r.t to the signal metal however the value of ϵ_{req} does depend on the parameters of the layer which is nearest to the signal metal. The first transition frequency (f_{T1}) can be obtained by the following expression:

$$f_{T1} = (\sigma_{ri}/\epsilon_{ri})_{\text{max}}/(2\pi\epsilon_0) \tag{4.1}$$

Therefore, the model can be used effectively in three distinct regions formed by the two transition frequencies where the value of the ϵ_{req} is almost constant. However, the model will have to be analyzed in more detail when the conductivity is very high or the layer with the highest value of ϵ_{ri} is very thick so that $f_{T1} > f_{T2}$. Figures 4.18(a) and 4.18(b) show the plot of the ϵ_{req} and ϵ_{reff} as a function of frequency for a two layered lossy shielded microstrip. Also, one can verify the formula for first transition frequency as for the parameters in Figure 4.18(a) it lies around 7.02 MHz and for the parameters in 4.18(b) it lies around 15.37 GHz. Also, Figures 4.19(a) and 4.19(b) show that the σ_{eq} and σ_{eff} will be frequency independent in these three regions and have the same transition frequencies as the ϵ_{reff}.

Therefore, the model is frequency independent three distinct regions between the two transition frequencies but it is frequency dependent for frequencies very close (nearly 5%) to the transition frequencies.

The transition in σ_{eq} and ϵ_{req} occur at nearly the same frequency as seen from Figures 4.16-4.20. Figure 4.14 show that higher values of conductivity of the layers nearer to signal metal results in a higher value of ϵ_{req} for lower frequencies but the effect decreases with increase in frequency. Figure 4.15 shows that at low frequencies the σ_{eq} highly depends on the conductivity of the layers nearer to the signal metal. Also the σ_{eff} at high frequency depends on the σ_{i} of the layer with the highest value of ϵ_{ri}.

4.2.2 Thickness

Table 4.2 ϵ_{reff} vs h_2/δ_2 for the MIS structure

$\mathbf{h}/\delta$	$\mathbf{Re}(\epsilon_{\text{reff}})$	$\mathbf{Im}(\epsilon_{\text{reff}})$	$\mathbf{Abs}(\epsilon_{\text{reff}})$
1	39.7503	-20.3706	44.6660
2	31.7358	-26.2836	41.2067
3	31.5750	-25.0388	40.2979
4	31.7346	-25.0803	40.4488
5	31.7213	-25.0978	40.4492
6	31.7198	-25.0953	40.4465
7	31.7202	-25.0953	40.4468
∞	31.7202	-25.0953	40.4468

Figure 4.22 and Table 4.2 show that using n skin depths we can obtain approximately $n-1$ significant digits in the value of the effective dielectric constant for a MIS structure. This can also be concluded from the fact that magnitude of current decreases by $1/e \approx .37$ for each skin depth. Also the layers below the semiconductor will have negligible effect on the effective medium if the semiconductor layer is thick enough (i.e. of the order of few skin depths) and can be neglected. Therefore, the equivalent thickness is assumed to be the sum of thickness of all the layers above the layer with finite conductivity and n times the skin depth of the conductive layer if we need $n-1$ significant digits in the equivalent medium parameters.

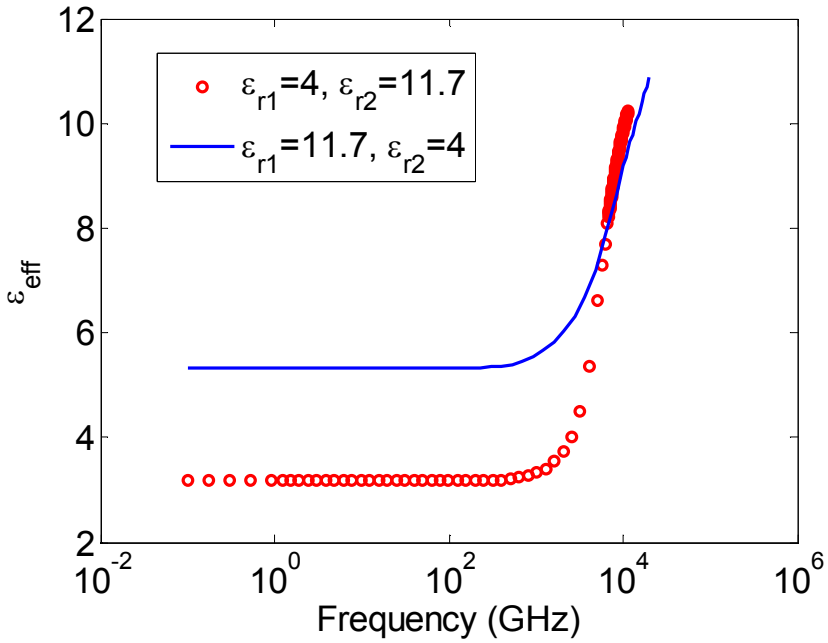

(a) Comparison of ϵ_{reff} on reordering the layers

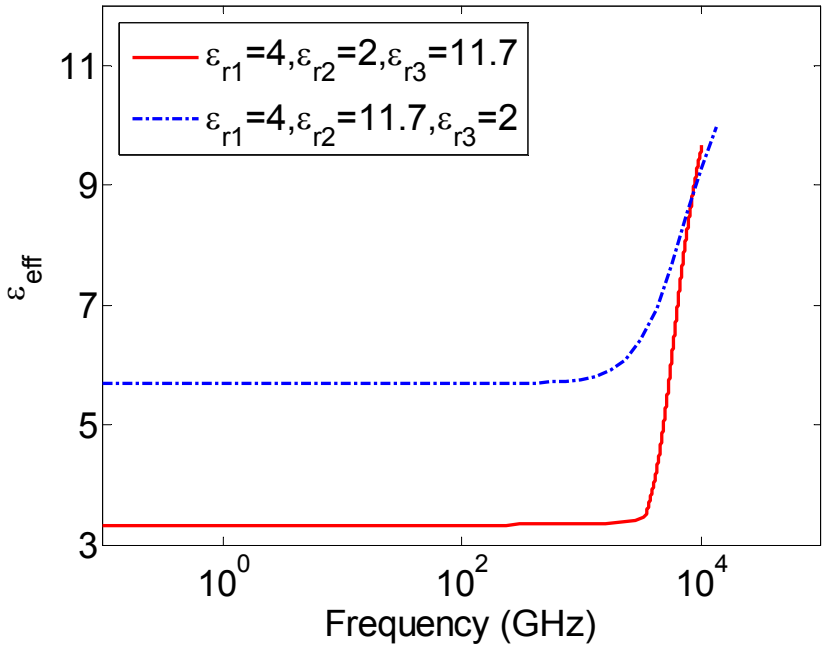

(b) Comparison of ϵ_{reff} on reordering the layers

Figure 4.7 Comparison of ϵ_{reff} as a function of frequency on reordering the layers for (a) two layered shielded microstrip with air on top and parameters $\mu_r = 1, h_1 = h_2 = 5\mu\text{m}, w = 2\mu\text{m}, a = 50\mu\text{m}, d = 40\mu\text{m}, c = a/2$ (b) three layered shielded microstrip with air on top and parameters $\mu_r = 1, h_1 = h_2 = h_3 = 5\mu\text{m}, w = 2\mu\text{m}, a = 55\mu\text{m}, d = 40\mu\text{m}$ and $\epsilon_{r1} = 4, \epsilon_{r2} = 11.7, \epsilon_{r3} = 2$.

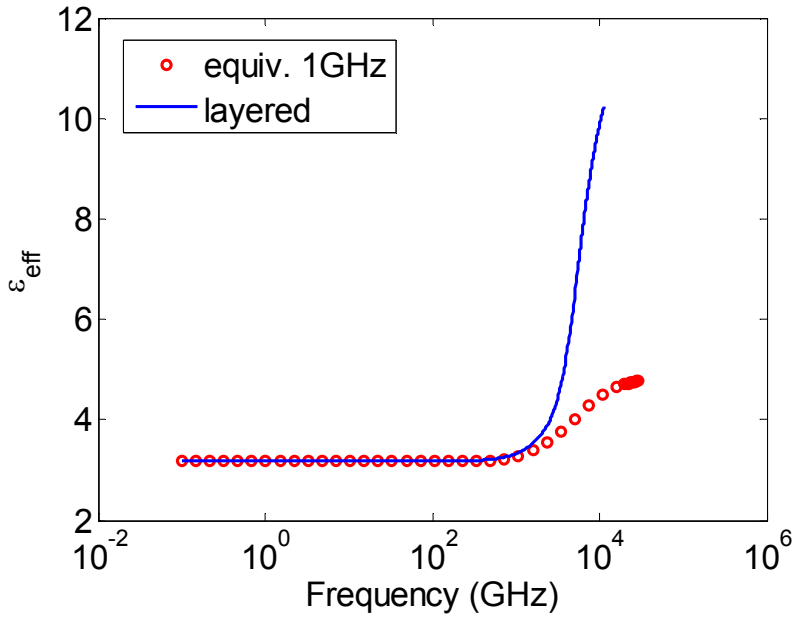

(a) Comparison of ϵ_{reff} with the equivalent model

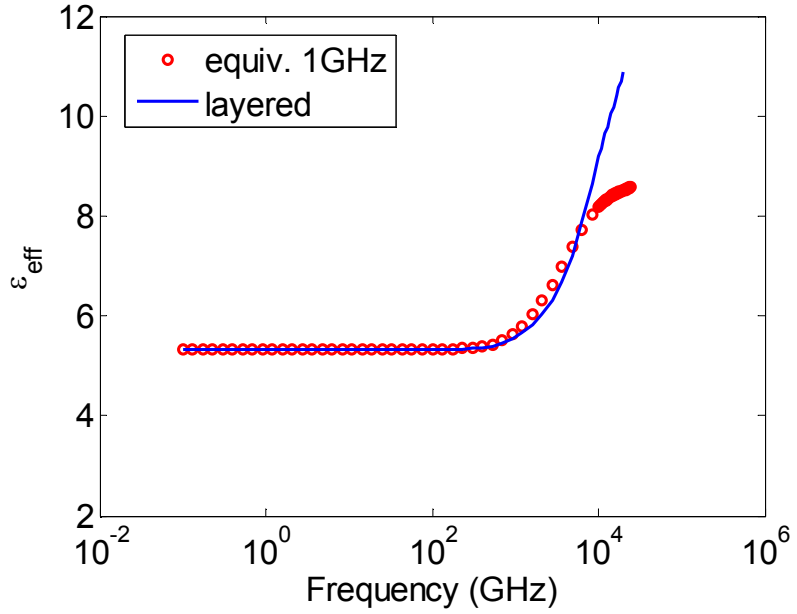

(b) Comparison of ϵ_{reff} with the equivalent model

Figure 4.8 Effective dielectric constant ϵ_{reff} as a function of frequency for (layered) two layered shielded microstrip with air above the signal metal and parameters $\mu_r = 1, h_1 = h_2 = 5\mu\text{m}, w = 2\mu\text{m}, a = 50\mu\text{m}, d = 40\mu\text{m}, c = a/2$ for the equivalent models at 1GHz with $h = h_1 + h_2$ for (a) $\epsilon_{r1} = 4, \epsilon_{r2} = 11.7, \epsilon_{\text{req}} = 4.8317$ (b) $\epsilon_{r1} = 11.7, \epsilon_{r2} = 4, \epsilon_{\text{req}} = 8.6485$.

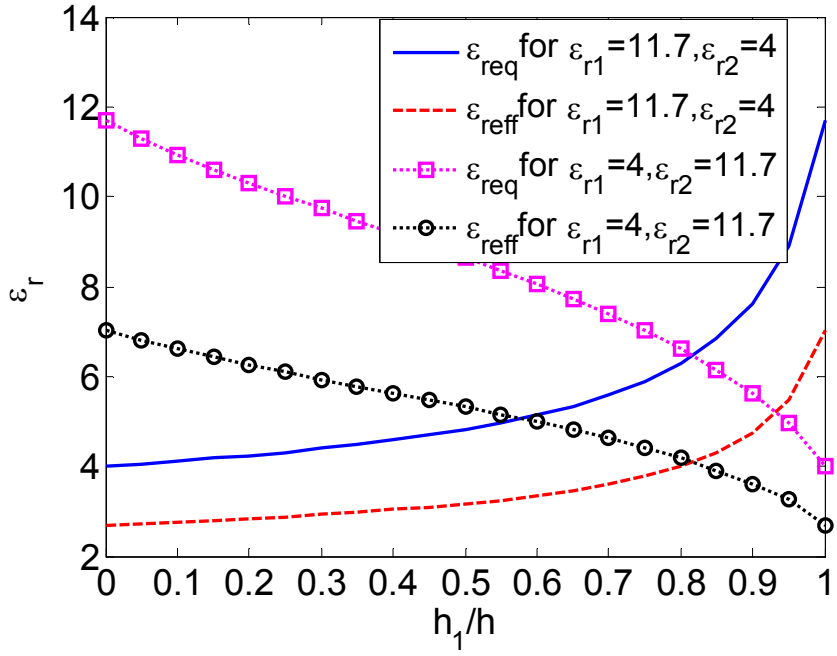

Figure 4.9 Variation of ϵ_{req}, ϵ_{reff} with $h1/h$ for two, two layered shielded microstrip with air above the signal metal and parameters $\mu_r = 1, w = 2\mu\text{m}, a = 50\mu\text{m}, d = 40\mu\text{m}, c = a/2$ for the equivalent models at 1GHz with $h = h_1 + h_2 = 10\mu\text{m}$, $\epsilon_{r1} = 4, \epsilon_{r2} = 11.7$ and $\epsilon_{r1} = 11.7, \epsilon_{r2} = 4$, respectively.

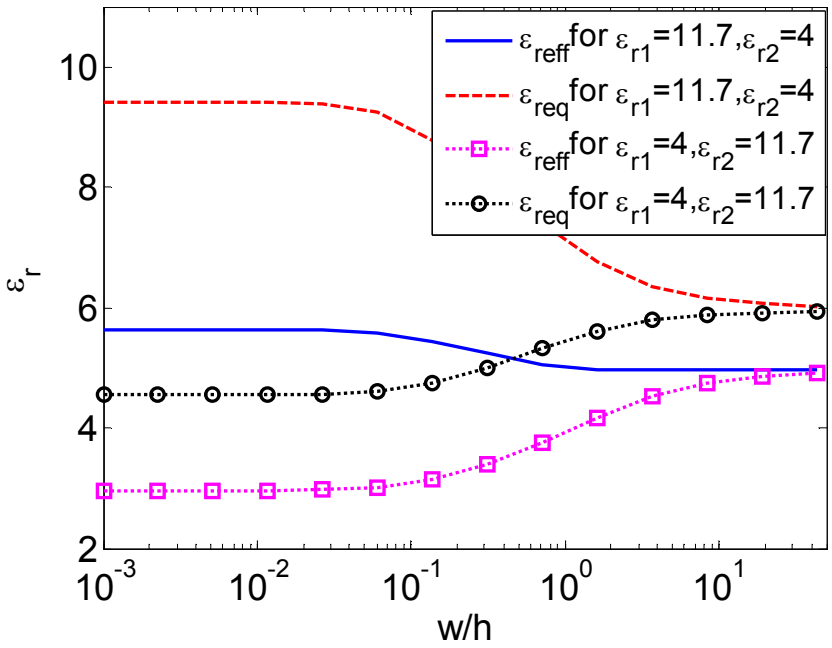

Figure 4.10 Variation of ϵ_{req}, ϵ_{reff} with width of signal metal for a two layered shielded microstrip with air above the signal metal and parameters $\mu_r = 1, h_1 = h_2 = 5\mu\text{m}, a = 1\text{mm}, d = 40\mu\text{m}, c = a/2$ for the equivalent models at 1GHz with $h = h_1 + h_2$ and $\epsilon_{r1} = 11.7, \epsilon_{r2} = 4$ and by reversing the layers.

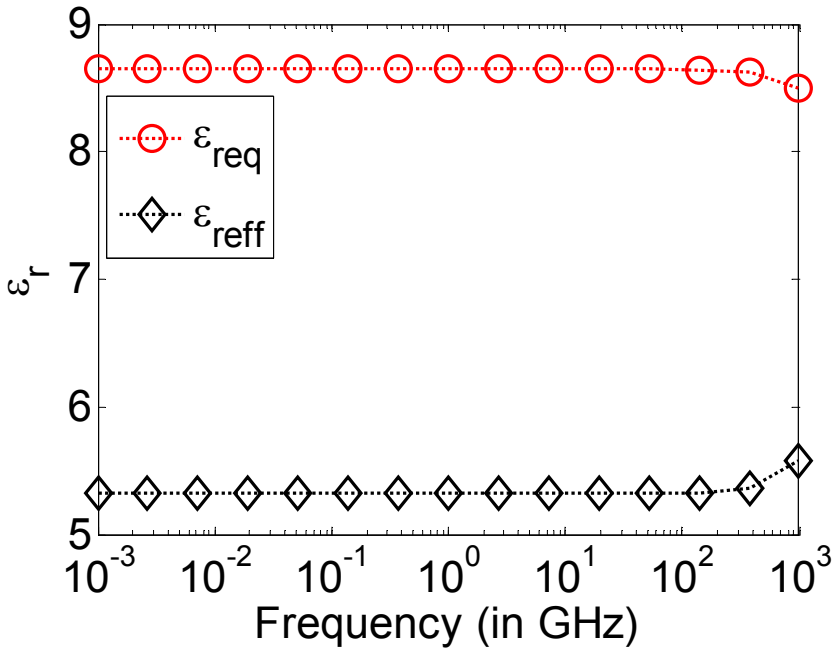

(a) ϵ_{reff} and ϵ_{req} vs testing frequency

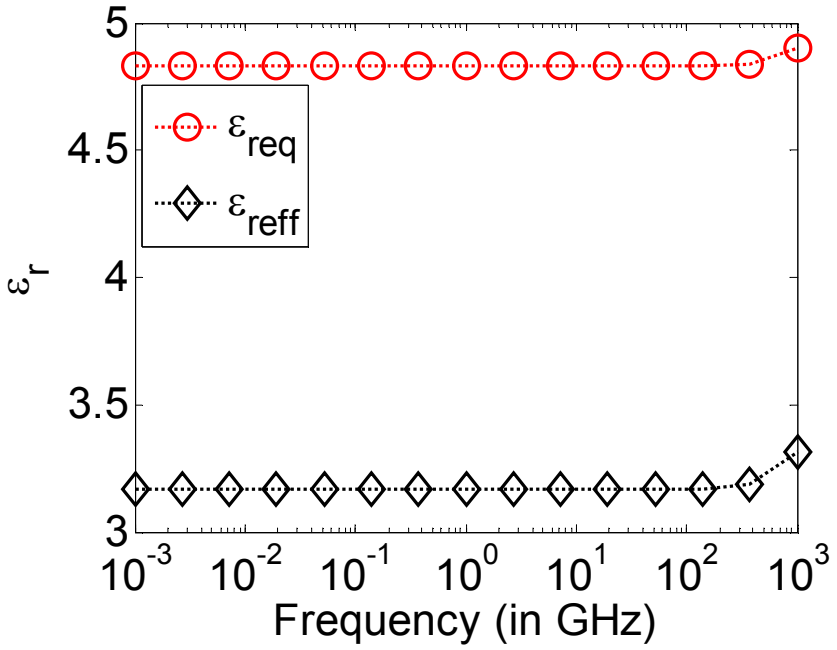

(b) ϵ_{reff} and ϵ_{req} vs testing frequency

Figure 4.11 ϵ_{reff} and ϵ_{req} as a function of testing frequency for two layered shielded microstrip with air above the signal metal and parameters $\mu_r = 1, h_1 = h_2 = 5\mu\text{m}, w = 2\mu\text{m}, a = 50\mu\text{m}, d = 40\mu\text{m}, c = a/2$ with $h = h_1 + h_2$ for (a) $\epsilon_{r1} = 11.7, \epsilon_{r2} = 4$ (b) $\epsilon_{r1} = 4, \epsilon_{r2} = 11.7$.

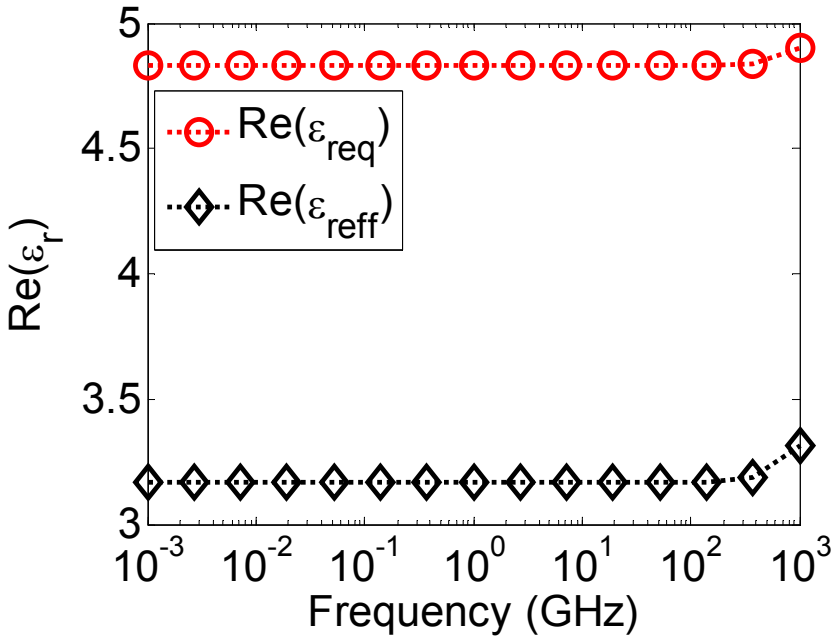

(a) ϵ_{reff} and ϵ_{req} vs testing frequency

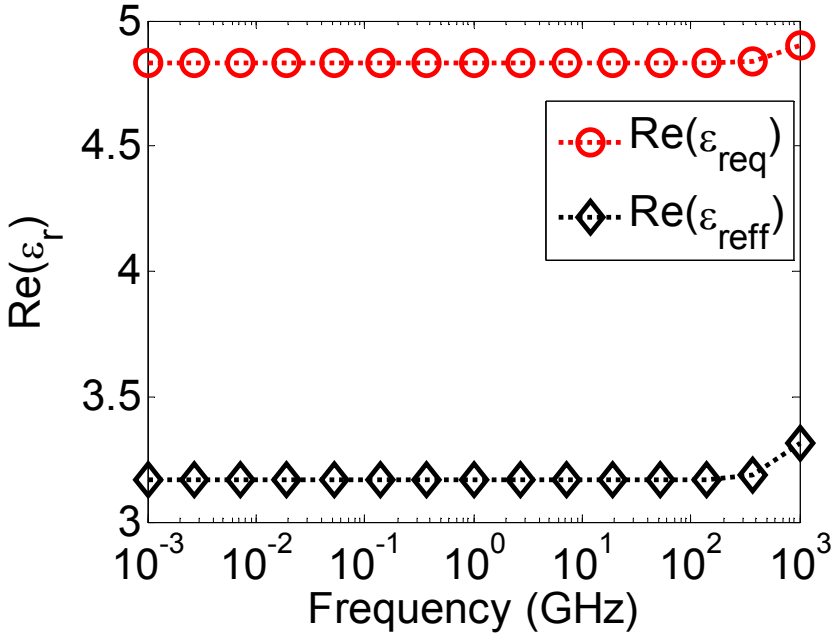

(b) ϵ_{reff} and ϵ_{req} vs testing frequency

Figure 4.12 ϵ_{reff} and ϵ_{req} as a function of testing frequency for two layered shielded microstrip with air above the signal metal and parameters $\mu_r = 1, h_1 = h_2 = 5\mu\text{m}, w = 2\mu\text{m}, a = 50\mu\text{m}, d = 40\mu\text{m}, c = a/2$ with $h = h_1 + h_2$, $\epsilon_{r1} = 4, \epsilon_{r2} = 11.7$ and loss tangents (a) tan(δ_1)=.005, tan(δ_2)=.05 (b) tan(δ_1)=.05, tan(δ_2)=.005.

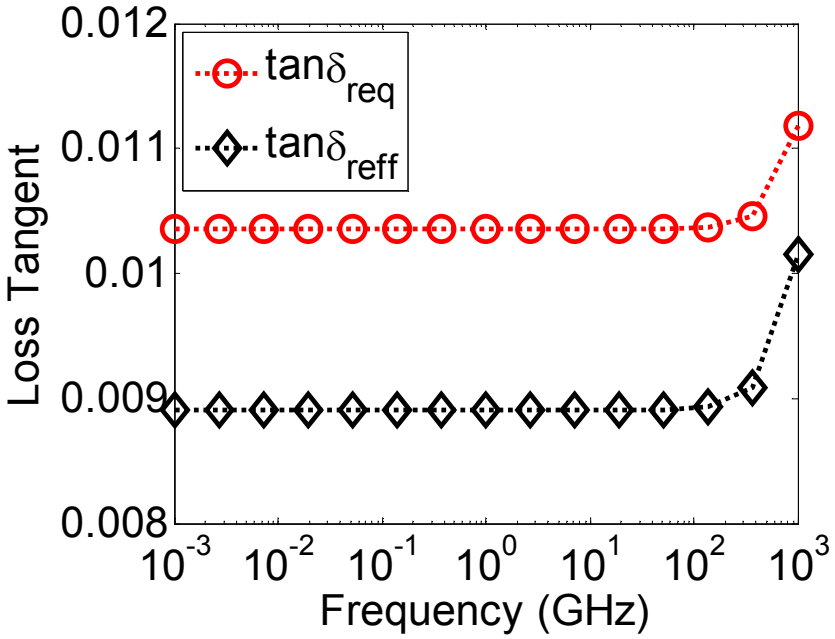

(a) Effective and Equivalent Loss tangent vs testing frequency

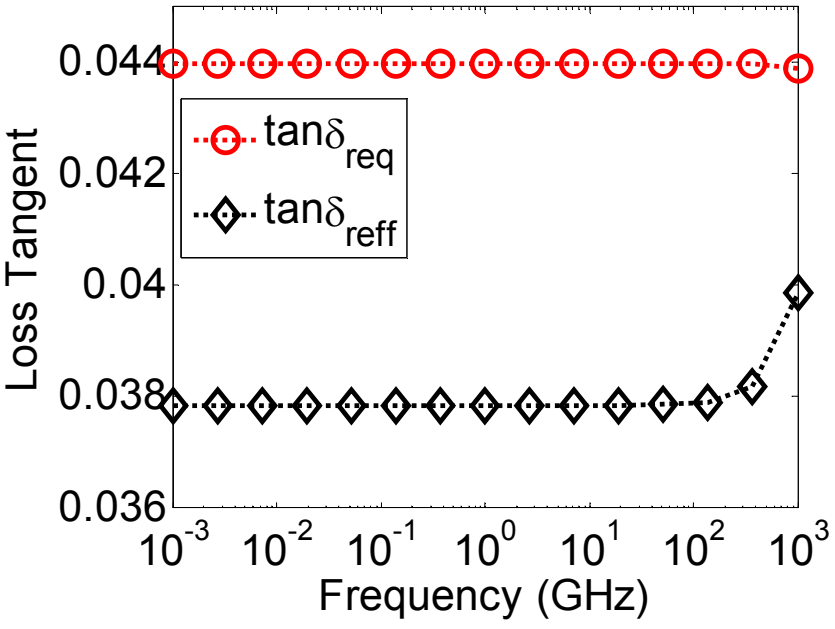

(b) Effective and Equivalent Loss tangent vs testing frequency

Figure 4.13 Same as Figure 4.12, imaginary parts are represented as loss tangent.

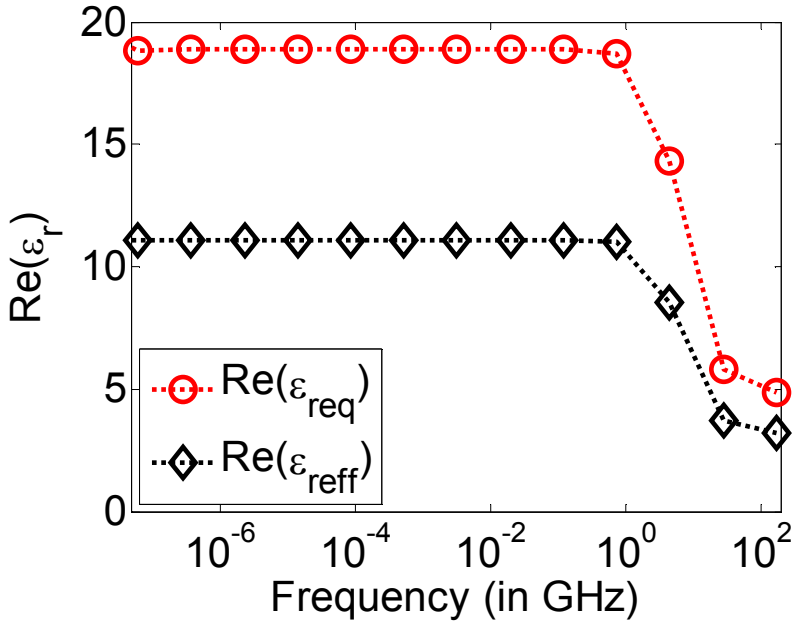

(a) ϵ_{reff} and ϵ_{req} vs testing frequency

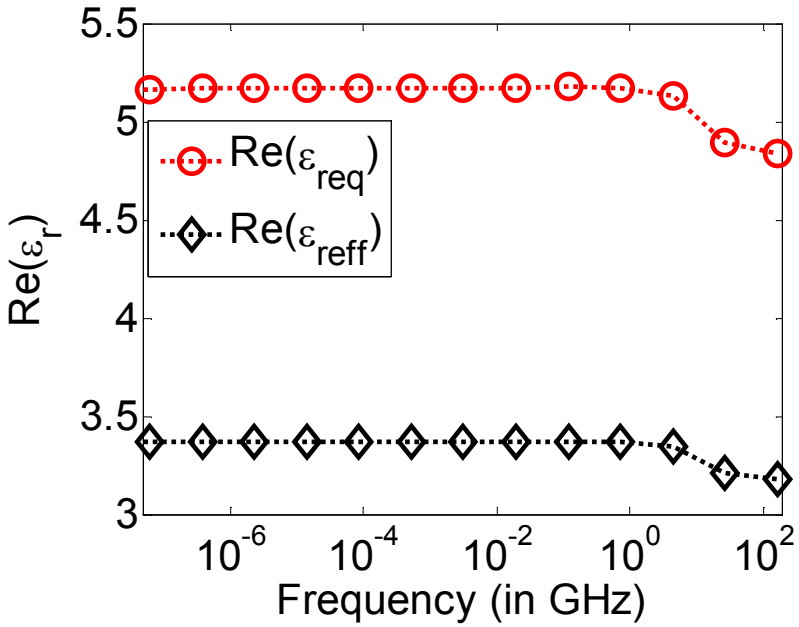

(b) ϵ_{reff} and ϵ_{req} vs testing frequency

Figure 4.14 Real parts of ϵ_{reff} and ϵ_{req} as a function of testing frequency for two layered shielded microstrip with air above the signal metal and parameters $\mu_r = 1, h_1 = h_2 = 5\mu$m$, w = 2\mu$m$, a = 50\mu$m$, d = 40\mu$m$, c = a/2$ with $h = h_1 + h_2$, $\epsilon_{r1} = 4, \epsilon_{r2} = 11.7$ and conductivities (a) σ_1=10 S/m, σ_2=1 S/m (b) σ_1=1 S/m, σ_2=10 S/m.

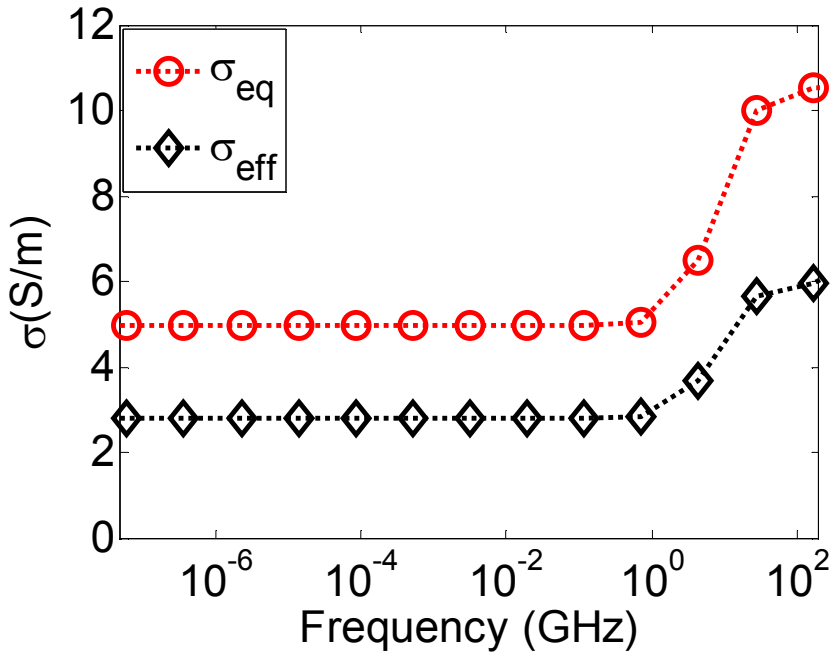

(a) σ_{reff} and σ_{req} vs testing frequency

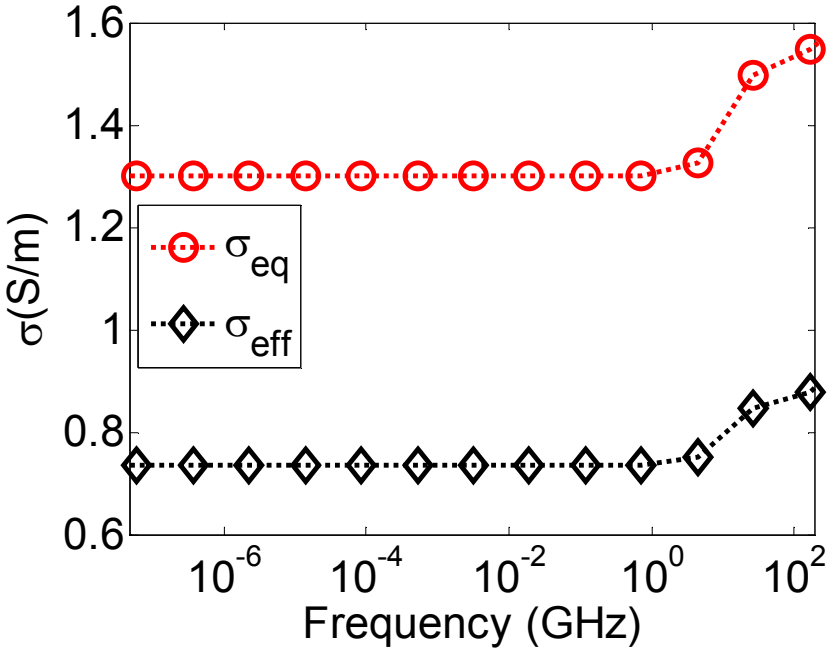

(b) σ_{reff} and σ_{req} vs testing frequency

Figure 4.15 Same as Figure 4.14, imaginary parts are represented as σ_{reff} and σ_{req}.

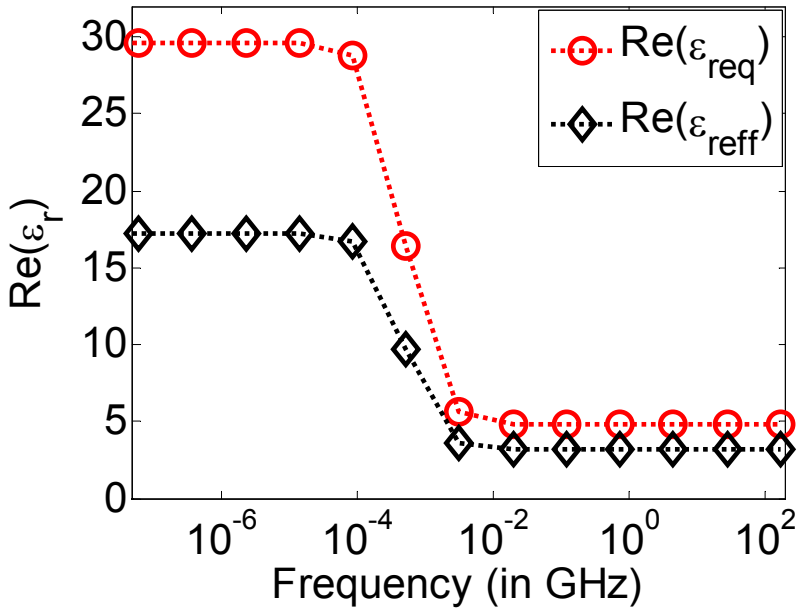

(a) ϵ_{reff} and ϵ_{req} vs testing frequency

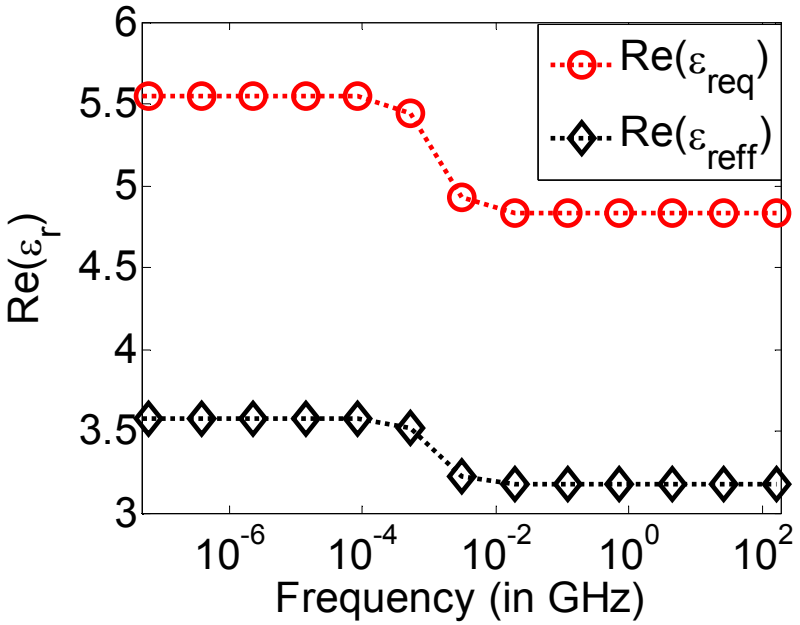

(b) ϵ_{reff} and ϵ_{req} vs testing frequency

Figure 4.16 ϵ_{reff} and ϵ_{req} as a function of testing frequency for two layered shielded microstrip with air above the signal metal and parameters $\mu_r = 1, h_1 = h_2 = 5\mu\text{m}, w = 2\mu\text{m}, a = 50\mu\text{m}, d = 40\mu\text{m}, c = a/2$ with $h = h_1 + h_2$, $\epsilon_{r1} = 4, \epsilon_{r2} = 11.7$ and conductivities (a) σ_1=0.001 S/m, σ_2=0 (b) σ_1=0, σ_2=.001 S/m.

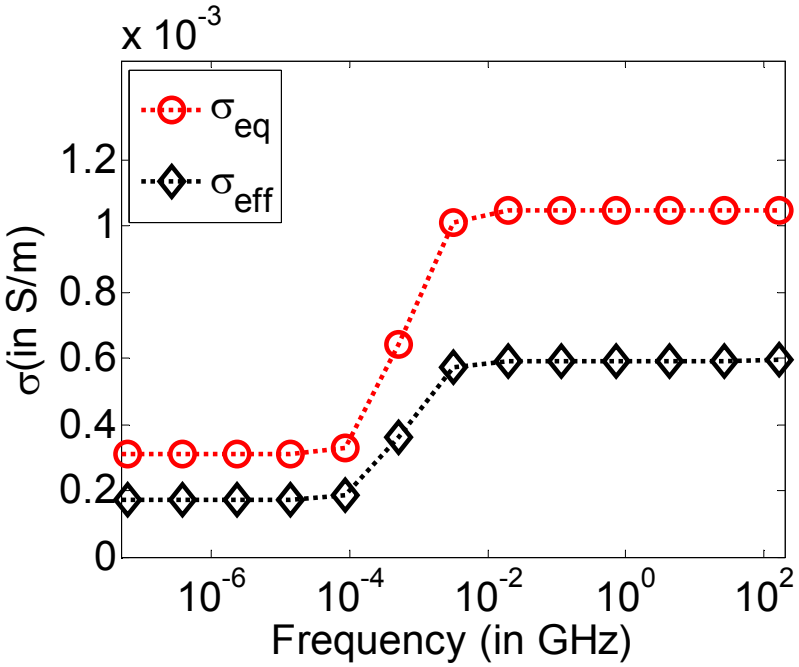

(a) σ_{reff} and σ_{req} vs testing frequency

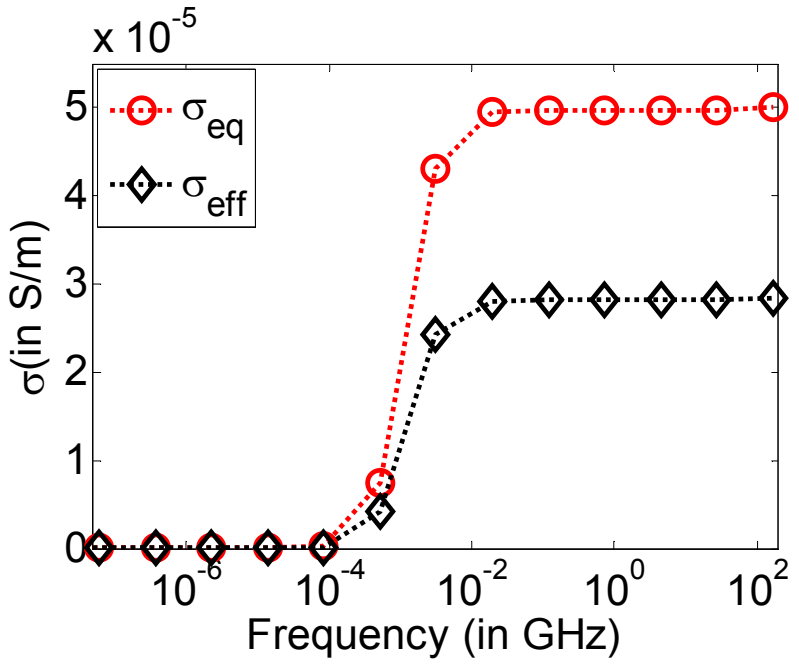

(b) σ_{reff} and σ_{req} vs testing frequency

Figure 4.17 σ_{reff} and σ_{req} as a function of testing frequency for two layered shielded microstrip with air above the signal metal and parameters $\mu_r = 1, h_1 = h_2 = 5\mu\text{m}, w = 2\mu\text{m}, a = 50\mu\text{m}, d = 40\mu\text{m}, c = a/2$ with $h = h_1 + h_2$, $\epsilon_{r1} = 4, \epsilon_{r2} = 11.7$ and conductivities (a) σ_1=0.001 S/m, σ_2=0 (b) σ_1=0, σ_2=.001 S/m.

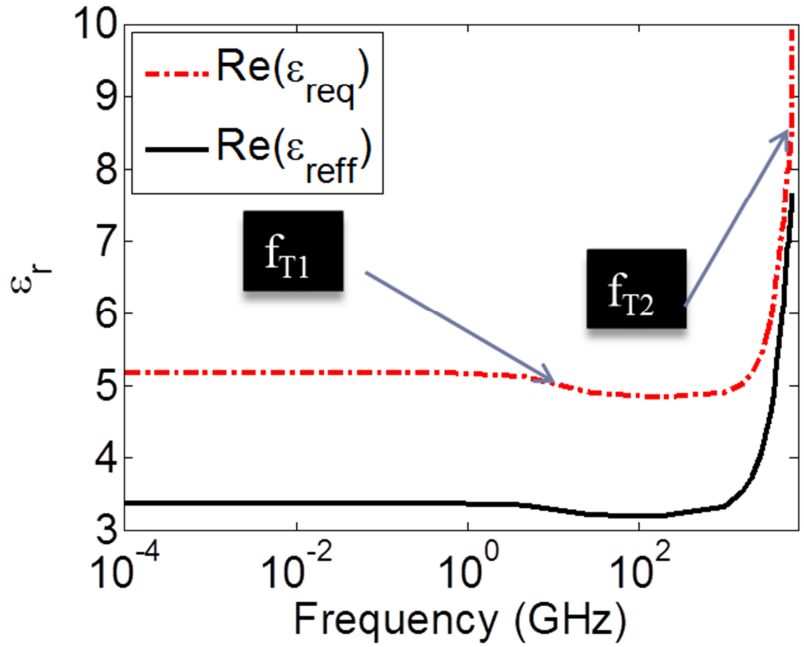

(a) ϵ_{reff} and ϵ_{req} vs testing frequency

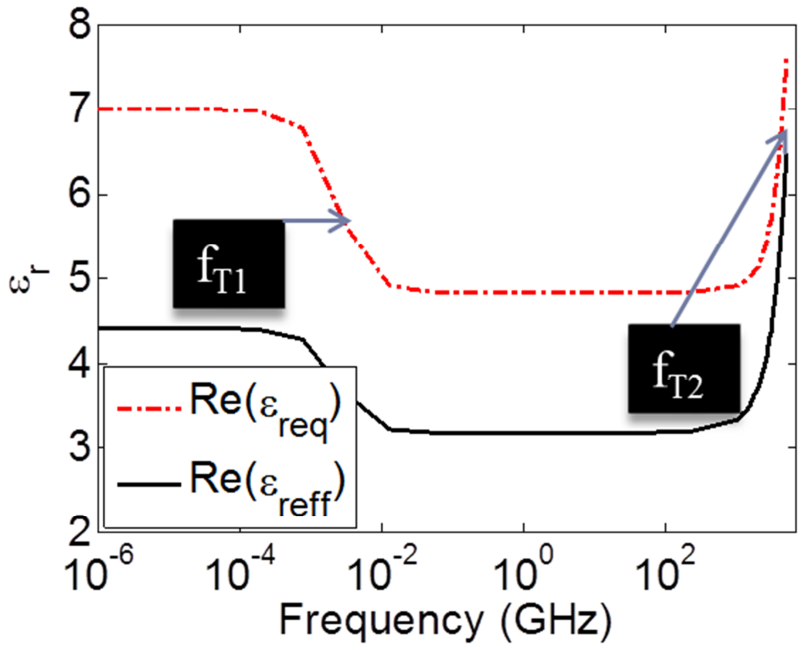

(b) ϵ_{reff} and ϵ_{req} vs testing frequency

Figure 4.18 ϵ_{reff} and ϵ_{req} as a function of testing frequency for two layered shielded microstrip with air above the signal metal and parameters $\mu_r = 1, w = 2\mu$m, $a = 50\mu$m, $d = 40\mu$m, $c = a/2$ with $h = h_1 + h_2$, $\epsilon_{r1} = 4, \epsilon_{r2} = 11.7$ and (a) σ_1=1 S/m, σ_2=10 S/m, $h_1 = h_2 = 5\mu$m (b) σ_1=1/640 S/m, σ_2=.001 S/m, $h_1 = 5\mu$m, $h_2 = 5\mu$m

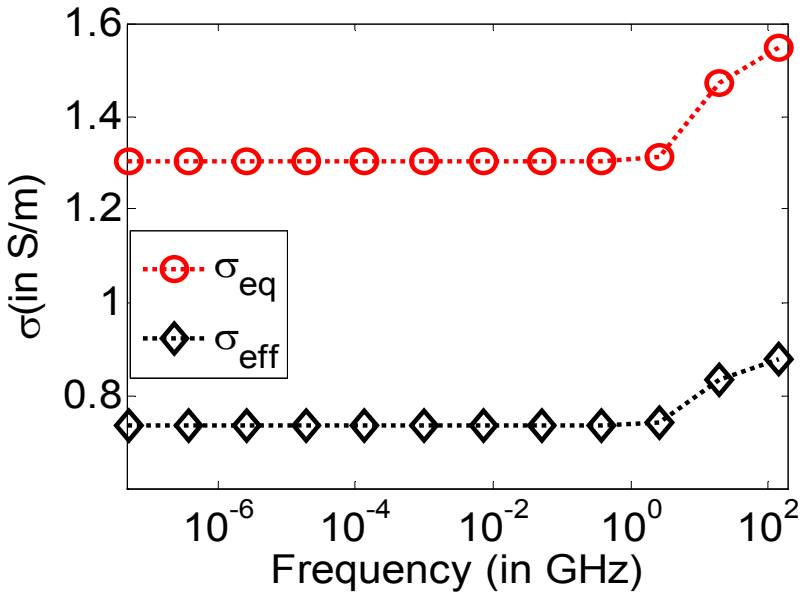

(a) σ_{reff} and σ_{req} vs testing frequency

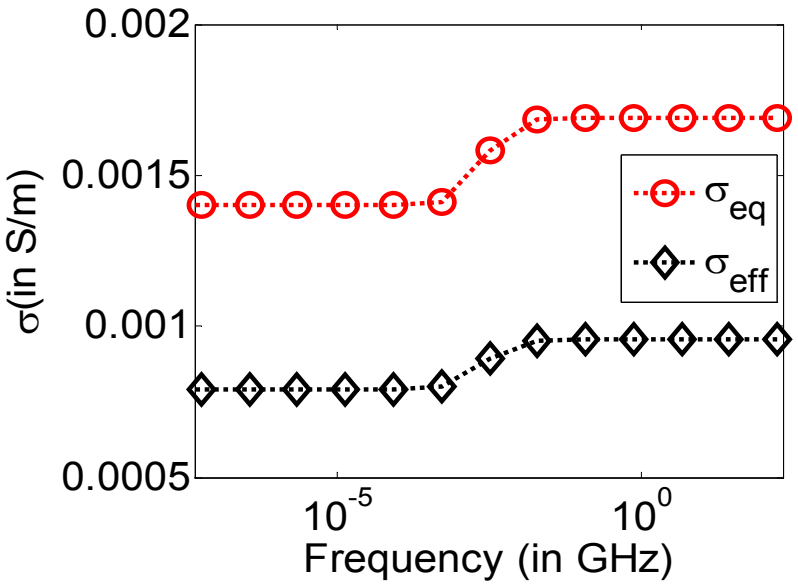

(b) σ_{reff} and σ_{req} vs testing frequency

Figure 4.19 σ_{reff} and σ_{req} as a function of testing frequency for two layered shielded microstrip with air above the signal metal and parameters $\mu_r = 1, w = 2\mu\text{m}, a = 50\mu\text{m}, d = 40\mu\text{m}, c = a/2$ with $h = h_1 + h_2$, $\epsilon_{r1} = 4, \epsilon_{r2} = 11.7$ and (a) σ_1=.001 S/m, σ_2=10 S/m, $h_1 = h_2 = 5\mu$m (b) σ_1=1 S/m, σ_2=10 S/m, $h_1 = 5\mu$m, $h_2 = 5\mu$m

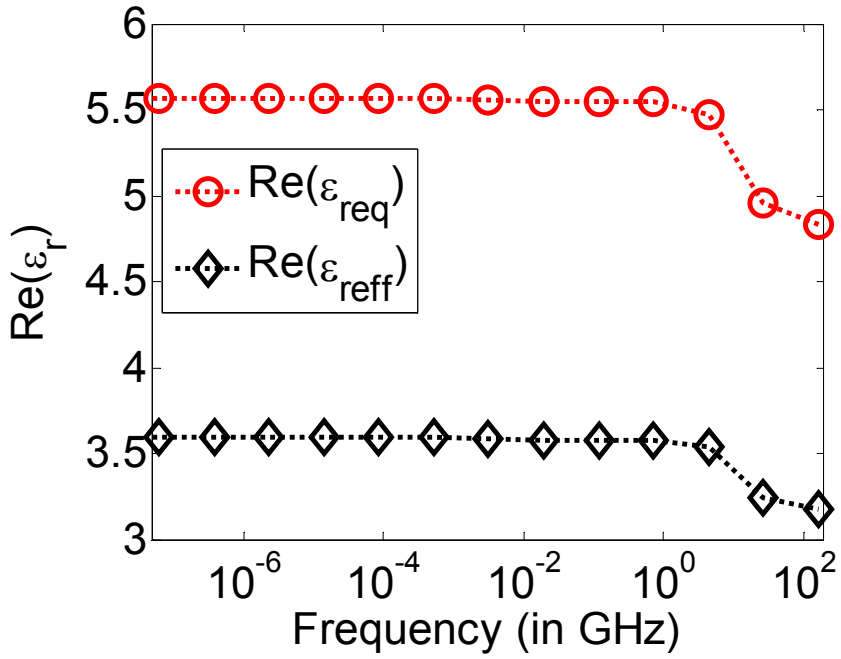

(a) ϵ_{reff} and ϵ_{req} vs testing frequency

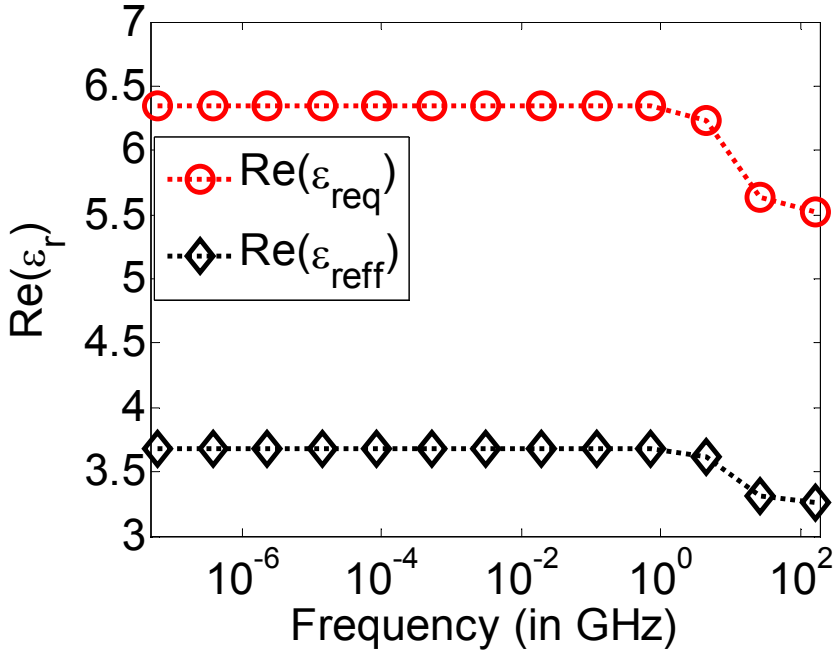

(b) ϵ_{reff} and ϵ_{req} vs testing frequency

Figure 4.20 ϵ_{reff} and ϵ_{req} as a function of testing frequency for two layered shielded microstrip with air above the signal metal and parameters $\mu_r = 1, w = 2\mu\text{m}, a = 50\mu\text{m}, d = 40\mu\text{m}, c = a/2$ with $h = h_1 + h_2$, $\epsilon_{r1} = 4, \epsilon_{r2} = 11.7$ and (a) σ_1=.001 S/m, σ_2=10 S/m, $h_1 = h_2 = 5\mu$m (b) σ_1=1 S/m, σ_2=10 S/m, $h_1 = 5\mu$m, $h_2 = 500\mu$m

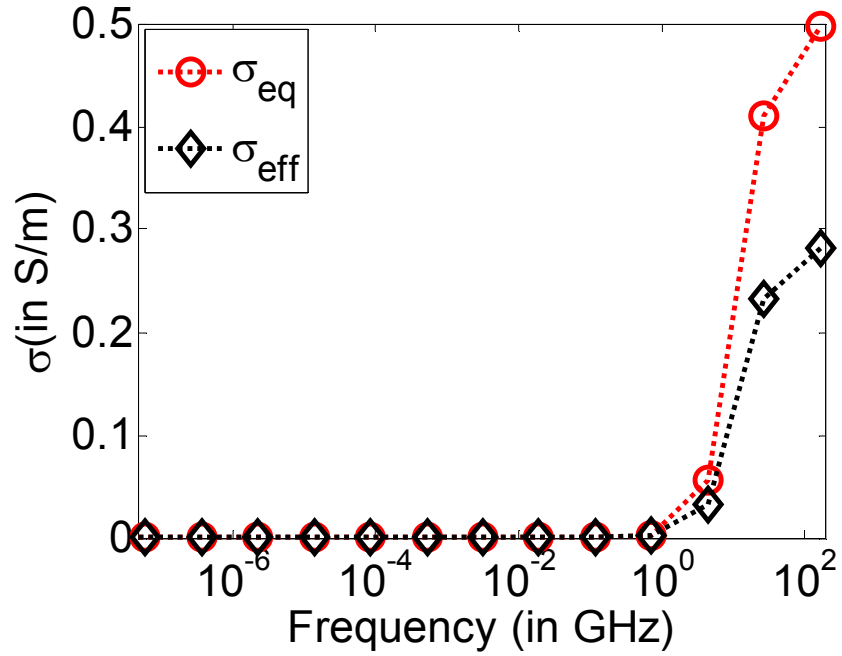

(a) σ_{reff} and σ_{req} vs testing frequency

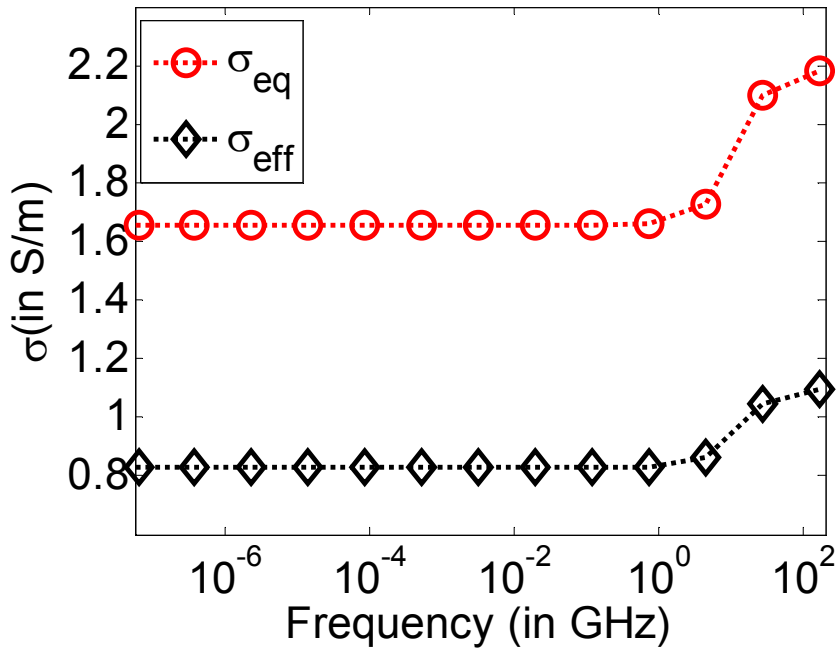

(b) σ_{reff} and σ_{req} vs testing frequency

Figure 4.21 σ_{reff} and σ_{req} as a function of testing frequency for two layered shielded microstrip with air above the signal metal and parameters $\mu_r = 1, w = 2\mu\text{m}, a = 50\mu\text{m}, d = 40\mu\text{m}, c = a/2$ with $h = h_1 + h_2$, $\epsilon_{r1} = 4, \epsilon_{r2} = 11.7$ and (a) σ_1=.001 S/m, σ_2=10 S/m, $h_1 = h_2 = 5\mu$m (b) σ_1=1 S/m, σ_2=10 S/m, $h_1 = 5\mu$m, $h_2 = 500\mu$m

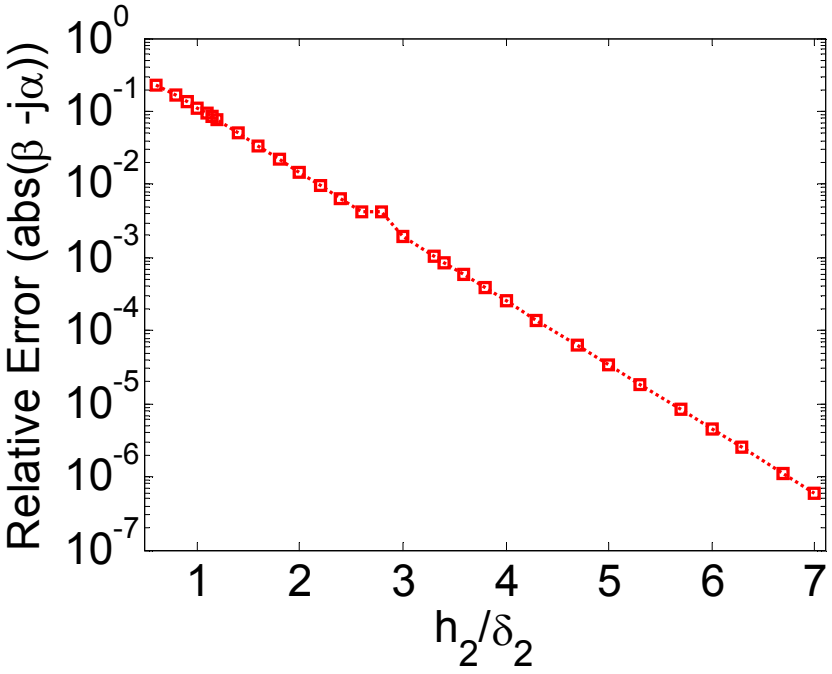

Figure 4.22 Relative error in $\beta - j\alpha$ vs thickness of semiconductor layer in terms of number of skin depths for a shielded MIS transmission line with parameters $\mu_r = 1, h_1 = 1\mu$m$, h_2 = 250\mu$m$, w = 80\mu$m$, a = 1$cm$, d = 1$cm$, c = a/2, \epsilon_{r1} = 4, \epsilon_{r2} = 12, \sigma_1 = 0$ and $\sigma_2 = 10000$ S/m at 100GHz.

CHAPTER 5. Approaches to Handle Finite Thickness and Conductivity of Metal Lines

There are several approaches which have been proposed for dealing with the finite thickness of metal lines. But in order to incorporate them into the spectral domain approach one has to be very careful about the choice of the basis functions. This is because while using these approximations one needs to subtract a constant term from the Green's function, therefore, basis functions with convergence $1/\sqrt{\alpha_n}$ or slower will lead to a nonconvergent infinite summation in the elements of the MoM matrix. Therefore, Chebyshev polynomial, sine cosine basis functions, etc. will lead to a non convergence in the elements of the MoM matrix. However, basis like triangular basis which converge as $1/\alpha_n^2$ are more suitable for the currents in the x direction. While for the longitudinal currents one can also use pulse basis although triangular basis will have a faster convergence. Figure 5.1 shows the triangle-triangle basis, the pulse-triangle basis and the Chebyshev basis.

5.1 Current Basis Functions

5.1.1 Chebyshev Polynomial

The formulation for the Chebyshev basis functions has been described in detail in Chapter 2.

5.1.2 Pulse-Pulse Basis

Divide the strip into $N = M_z$ parts each of width $T = 2w/N$ as shown in Figure 5.1. Both the longitudinal and the transverse current on the strip can be written as a linear combination of

pulse basis functions. The Fourier transform for the p^{th} $(p = 1, 2, ...N)$ pulse function for the longitudinal and transverse current can be written as:

$$\tilde{J}_z^p(\delta_w) = 2w/\delta_w \sin(\delta_w/N) \sin\{\alpha[c - w + (p-1)2w/N + w/N]\} \tag{5.1}$$

$$\tilde{J}_x^p(\delta_w) = 2w/\delta_w \sin(\delta_w/N) \cos\{\alpha[c - w + (p-1)2w/N + w/N]\} \tag{5.2}$$

where $\delta_w = \alpha w$.

5.1.3 Pulse-Triangle Basis

Divide the strip into $N = M_x = M_z - 1$ parts each of width $T = 2w/N$ as shown in Figure 5.1. The longitudinal current on the strip can be written as a linear combination of pulse basis functions and the transverse current as a linear combination of triangle basis functions. The Fourier transform for the p^{th} basis can be written as:

$$\tilde{J}_z^p(\delta_w) = 2w/\delta_w \sin(\delta_w/N) \sin[\alpha\{c - w + (p-1)2w/N + w/N\}] \tag{5.3}$$

$$\tilde{J}_x^p(\delta_w) = 2w/\delta_w^2 [\sin(\delta_w/N)]^2 \cos[\alpha(c - w + 2pw/N)] \tag{5.4}$$

5.1.4 Triangle-Triangle Basis

In the triangular basis for the longitudinal current we need to include two half triangles to increase the convergence because of the edge singularity in the current on the two ends of the strip. Divide the strip into $N = M_z - 2$ parts each of width $T = 2w/N$ as shown in Figure 5.1. Choose $M_x = M_z - 2$. Both the longitudinal and the transverse current on the strip can be written as a linear combination of triangle basis functions. The Fourier transform for the p^{th} $(p = 1, 2, ...N)$ triangle function for the longitudinal and transverse current can be written as:

$$\tilde{J}_z(\delta_w) = 2w/\delta_w^2 [\sin(\delta_w/N)]^2 \sin[\alpha(c - w + 2pw/N)] \tag{5.5}$$

$$\tilde{J}_x(\delta_w) = 2w/\delta_w^2[\sin(\delta_w/N)]^2\cos[\alpha(c-w+2pw/N)] \tag{5.6}$$

The Fourier transform of the first basis for the longitudinal current can be written as:

$$\tilde{J}_z^0(\delta_w) = 2w^2/N/\delta_w^2\{\alpha\cos[\alpha(c-w)] + N/(2w)(\sin[\alpha(c-w)] - \sin[\alpha(c-w+2w/N)])\} \tag{5.7}$$

and for the last one can be written as:

$$\tilde{J}_z^{N+1}(\delta_w) = 2w^2/N/\delta_w^2\{\alpha\cos[\alpha(c+w)] + N/(2w)(\sin[\alpha(c+w)] - \sin[\alpha(c+w-2w/N)])\} \tag{5.8}$$

Figure 5.2 and 5.3 show the convergence of the triangle-triangle and pulse-triangle and the Chebyshev polynomials basis, respectively. It can be seen that Chebyshev polynomial being an entire domain basis has a very fast convergence compared to the subdomain basis. Also, the triangle-triangle basis has a good convergence although it is a subdomain basis and very accurate results up to three digits can be obtained using nearly six basis functions and about 1000 terms of the summation.

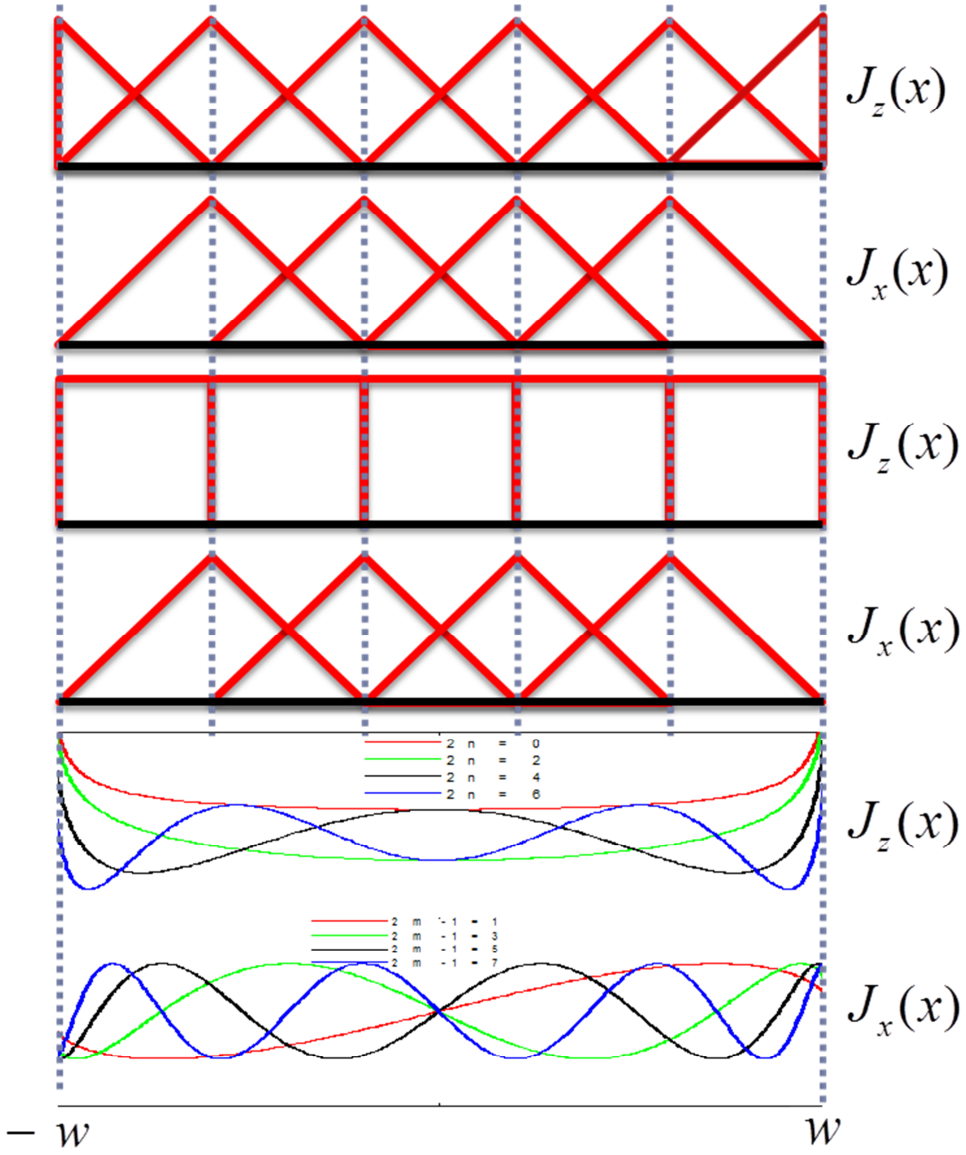

Figure 5.1 Basis Functions (top) Triangle-triangle basis (middle) Pulse-triangle basis (bottom) Chebyshev polynomial

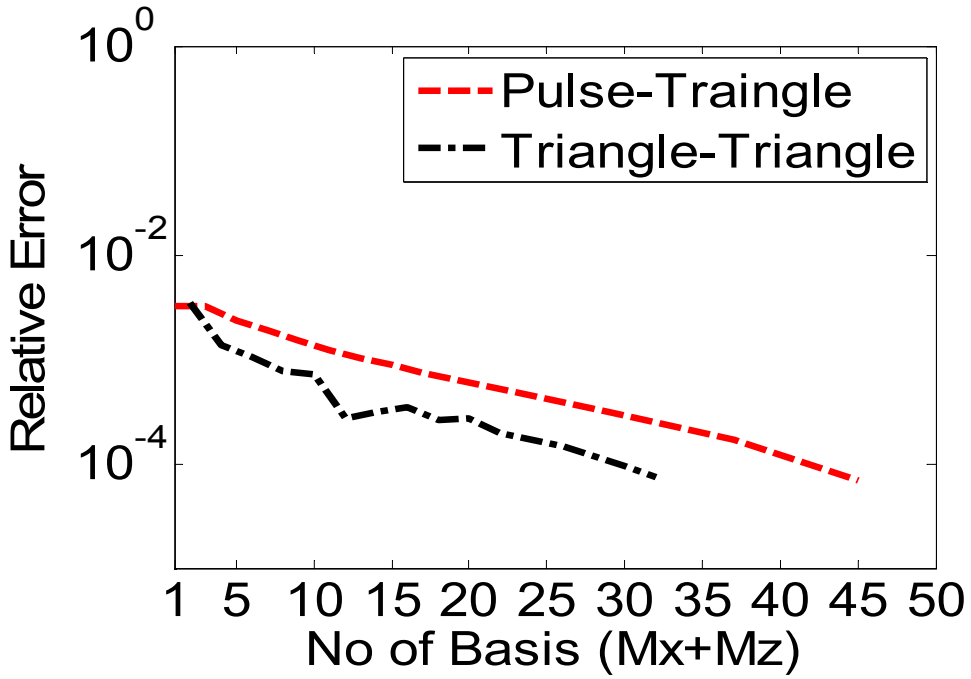

Figure 5.2 Convergence of the triangle-triangle and the pulse-triangle basis for a single layered shielded microstrip with parameters $\epsilon_{r_{-1}} = 8.875$, $\epsilon_{r_1} = 1$, $\mu_{r_i} = 1$, $f = 20$GHz, $D_{-1} = 1.27$mm, $D_1 = 11.43$mm, $2w = 1.27$mm, $a = 12.7$mm, $c = a/2$ at $\beta = 2k_0$.

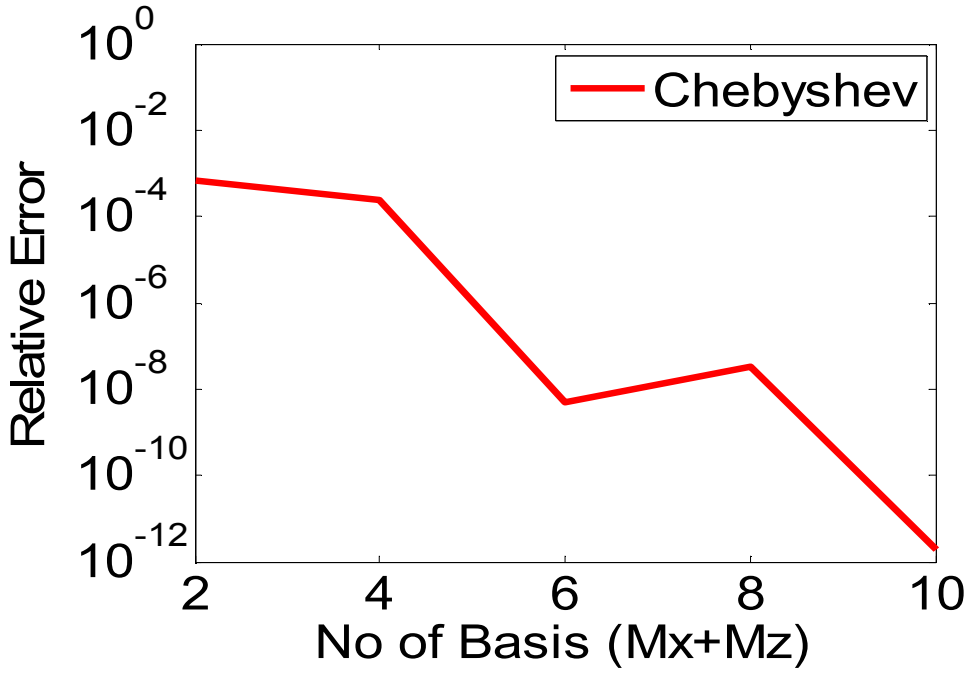

Figure 5.3 Convergence of the Chebyshev polynomial basis for the same single layered shielded microstrip as in Figure 5.2

5.2 Including the Finite thickness and Conductivity Approximations into the Spectral Domain Approach

Several approaches to approximate the finite thickness and conductivity of metal lines have been proposed in [58]. Although, R-card approximation is good for small thickness and impedance boundary condition approximation works well for thickness much greater than skin depth. It is difficult to get an accurate approximation for the intermediate thickness.

5.2.1 Resistive Thin Sheet Approximation (R-card)

We know that for the volume current J_v:

$$J_v = \sigma_s E \tag{5.9}$$

If the thickness of the strip is very small compared to the skin depth we can write $J_v = J_g/t$.

$$E_g = R_s J_g \tag{5.10}$$

where $R_s = 1/(\sigma_s t)$ J_g is the surface current density and $g \in (x, z)$.

5.2.2 R-Card with Finite Thickness (Tedjini's Approximation)

In [59] a model to approximate the finite thickness has been proposed if the approximate current distribution in the strip is known in the vertical direction. This model has been utilized for superconducting lines by Tounsi et al. [60]. In the spectral domain approach after using the boundary conditions the Fourier transform of the current and the electric field are related as:

$$\tilde{J}(\alpha_n) = Y(\alpha_n, \beta)\tilde{E}(\alpha_n) \tag{5.11}$$

Consider an elementary strip located at a distance s from the bottom surface of the signal strip, having a thickness ds and conductivity σ_s as shown in Figure 5.4. If the current distribution

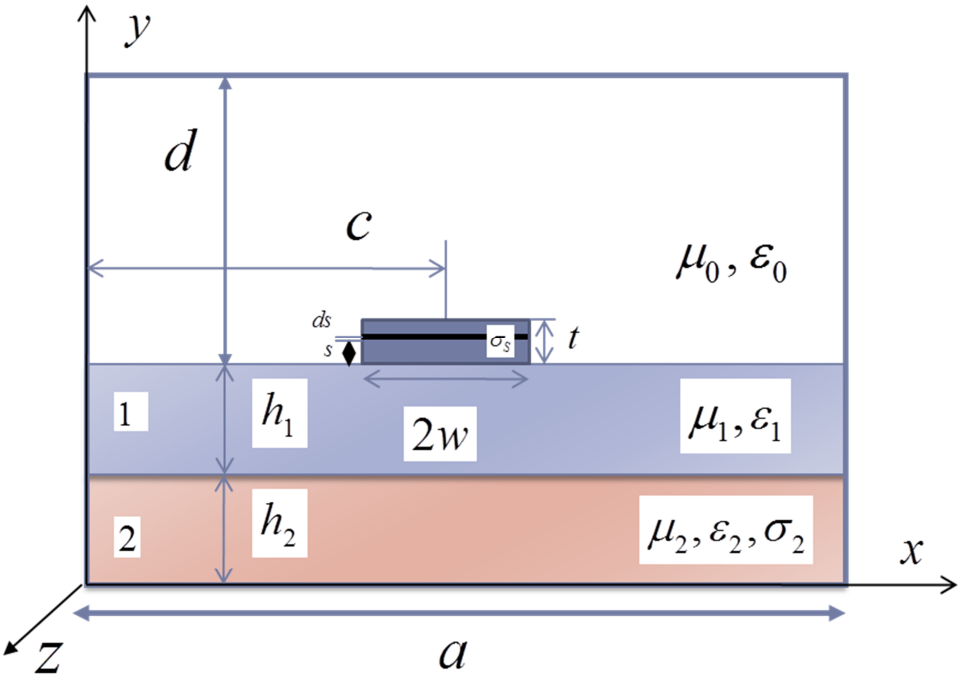

Figure 5.4 A three layered shielded microstrip with single metal strip of thickness t and conductivity σ_s. $\epsilon_{r1} = 4$; $\sigma_1 = 0$; $\epsilon_{r2} = 12$; $\sigma_2 = 5$ S/m; $\mu_{r1} = \mu_{r2} = 1$; $\sigma_s = 5.88 \times 10^7$ S/m, $t = 1\mu$m, $h_1 = 1\mu$m, $h_2 = 250\mu$m; $w = 80\mu$m; $a = 4000\mu$m; $d = 3200\mu$m; $c = a/2$. Strip is divided into elementary strips with thickness ds and located at a distance s from the bottom of the strip.

(normalized with thickness of the strip) in the vertical direction is $f(s)$. Then the current $d\tilde{J}(\alpha_n, s)$ in the strip ds can be written as:

$$d\tilde{J}(\alpha_n, s) = \tilde{J}(\alpha_n) f(s) ds \tag{5.12}$$

We know that the Greens function decreases exponentially in the vertical direction [56]. Therefore, at the y=constant plane at a distance s from the bottom of the strip the relationship between the differential current ($d\tilde{J}(\alpha_n, s)$) and the differential electric field can be written as:

$$d\tilde{J}(\alpha_n, s) = Y(\alpha_n, \beta) e^{\gamma_n s} d\tilde{E}(\alpha_n, s) \tag{5.13}$$

Integrating over the width of the strip we obtain:

$$\tilde{J}(\alpha_n) = Y(\alpha_n, \beta) S(\alpha_n) \tilde{E}(\alpha_n) \tag{5.14}$$

where

$$S(\alpha_n) = \Big[\int_0^t f(s) e^{-\gamma_n s} ds \Big]^{-1} \tag{5.15}$$

where

$$\gamma_n^2 + \beta^2 + \alpha_n^2 = \epsilon \mu \omega^2 \tag{5.16}$$

ϵ and μ are the permittivity and permeability of the material in which the strip is located. Thus, we can write

$$[\tilde{E}] = [G_s][\tilde{J}] \tag{5.17}$$

where

$$[G_s] = ([Y][S])^{-1} \tag{5.18}$$

For broader strips in a microstrip where $w/h >> 1$ and $t > \delta$ the current can be assumed to be concentrated on the lower surface of the strip and the expression for the distribution function can be written as [59]:

$$f(s) = (1/t) e^{(-s/\delta)} \tag{5.19}$$

For strips with smaller w/h ratio the current densities on the top and the bottom surface are comparable and can be approximated by [59]:

$$f(s) = (1/t) \cosh[(s - t/2)/\delta] / \cosh[t/(2\delta)] \tag{5.20}$$

Therefore, we can include the effect of finite thickness by multiplying the Green's function for the zero thickness case by the transformation term $[S]^{-1}$. In order to include the effect of finite conductivity of the metal line, we assume that the conductivity is very large so that the magnetic current can be neglected. Then, the tangential component of the electric field can be written as:

$$\tilde{E}_g = \tilde{J}_{vg}/\sigma_s = 1/(\sigma_s t) J_g \tag{5.21}$$

where J_{vg} is the volume current density and $g \in (x, z)$.

5.2.3 Impedance Boundary Condition (IBC) Approximation

This approximation was first proposed by Itoh in [9]. Several generalized IBC approximations have also been proposed but it is not feasible to include them in the SDA [61],[62]. It works well when the thickness of the strip is greater than about three times the skin depth. It is based on the fact that the current decays exponentially from the surface of the strip to inside the metal and drops down to 37% at one skin depth from the surface. So for a thick strip we can approximate this with a strip of width equal to the skin depth carrying a uniform current density equal to that on the surface. Also, it assumes that the thickness of the strip is much smaller than its width. Using Maxwell's equations we can obtain:

$$E_x = Z_s H_z \tag{5.22}$$

where $Z_s = (1+j)/(\sigma\delta)$, $\delta = \sqrt{2/(\omega\mu\sigma)}$. Using the fact that the tangential component of the electric field is very small and hence neglecting the magnetic current we can write:

$$E_x = Z_s J_x \tag{5.23}$$

Similarly,

$$E_z = Z_s J_z \tag{5.24}$$

5.2.4 R-card/IBC Approximation

A generalized R-card/IBC formulation was reported by [11]. This is derived assuming that all the current is existing on the bottom surface of the metal strip. This can be obtained by putting the terms corresponding to the J_{top} in the derivation for the two surface approximation given in the next section equal to zero. Therefore

$$Z_s = \frac{1}{\sigma_s t}\frac{(1+j)t/\delta}{\tanh[(1+j)t/\delta]} \tag{5.25}$$

Thus

$$E_g = Z_s J_g \tag{5.26}$$

When we consider the above four approximations the product of the electric field and the current on the left hand side of the integral equation while using the Galerkin method is not zero. Because the tangential component of the electric field on the metal strip is no longer zero. Therefore, by substituting the value of the E_g depending on the approximation we want to use, the inner product of the electric field with the testing functions can be written as:

$$\langle \tilde{E}_g, \tilde{J}_{gi} \rangle = \langle Z_s J_g, \tilde{J}_{gi} \rangle = Z_s \sum_{n=1}^{\infty} \tilde{J}_g \tilde{J}_{gi} = Z_s \sum_{k=1}^{M_g} a_{gk} \sum_{n=1}^{\infty} \tilde{J}_{gk} \tilde{J}_{gi} \tag{5.27}$$

Thus for the R-Card, Tedjini, IBC and R-Card/IBC approximations we can accommodate this term by subtracting it from the Green's function as follows:

$$G^s_{gg}(\alpha_n) = G_{gg} - Z_s \tag{5.28}$$

where $Z_s = 1/(\sigma_s t)$ for R-Card and the Tedjini's approximation, $Z_s = (1+j)/(\sigma_s \delta)$ for IBC approximation and $Z_s = \frac{1}{\sigma_s t} \frac{(1+j)t/\delta}{\tanh[(1+j)t/\delta]}$ for the R-card/IBC approximation.

5.2.5 Generalized Two Surface Approximation

Morsey et al. [63] have developed a generalized approximation for the finite thickness and conductivity of metal lines which considers the currents on the top as well as at the bottom surface of the strip. It reduces to the IBC approximation when the thickness of the conductor is large and to the R-card approximation when thickness is less than the skin depth on two parallel strips separated by a distance t.

Assuming that the width to thickness ratio of the conductor is large. The tangential components of the electric field can be written as:

$$E_p(y) = E_p^+ e^{-\gamma y} + E_p^- e^{+\gamma y} \tag{5.29}$$

Using the Faraday's law at the top and bottom surface we can solve for the coefficients. The relationship between the tangential components of the current and the magnetic field can be written as [63]:

$$\begin{bmatrix} E_{p,top} \\ E_{p,bot} \end{bmatrix} = \frac{Z_0}{j\sin(j\gamma t)} \begin{bmatrix} -\cos(j\gamma t) & 1 \\ -1 & \cos(j\gamma t) \end{bmatrix} \times \begin{bmatrix} H_{q,top} \\ H_{q,bot} \end{bmatrix} \tag{5.30}$$

where $q = x$ for $p = z$ and $q = z$ for $p = x$. For the case when the conductivity of the conductor is large, the tangential component of electric field on the surface of the conductor will be very small. Therefore, the contribution of the magnetic current can be neglected as it will be much smaller than the electric current. Thus, using the boundary condition for the tangential magnetic field ($J = \hat{n} \times H$) we get:

$$\begin{bmatrix} E_{p,top} \\ E_{p,bot} \end{bmatrix} = -\frac{Z_0}{\sinh(\gamma t)} \begin{bmatrix} \cosh(\gamma t) & 1 \\ 1 & \cosh(\gamma t) \end{bmatrix} \times \begin{bmatrix} J_{p,top} \\ J_{p,bot} \end{bmatrix} \tag{5.31}$$

where $\gamma = \sqrt{j\omega\mu\sigma}$ and $Z_0 = \sqrt{\frac{j\omega\mu}{\sigma}}$

5.3 Numerical Results

Figures 5.5(a) and 5.6(a) show the slow wave ratio (β/k_0) for two shielded MIS transmission lines. It can be concluded that the R-card/IBC model works same as R-card model when the thickness of the strip is less than 1δ and behaves similar to the IBC model for strip thickness greater than 3δ. Also the Tedjini's approach which includes the effect of thickness behave quite different from the R-card model as the thickness increases.

Figures 5.5(b) and 5.6(b) show the loss α for the same two MIS transmission lines and the same observations can be made as from the plot of SWR but it makes it more clear that the R-card/IBC model approaches the IBC model for large values of strip thickness.

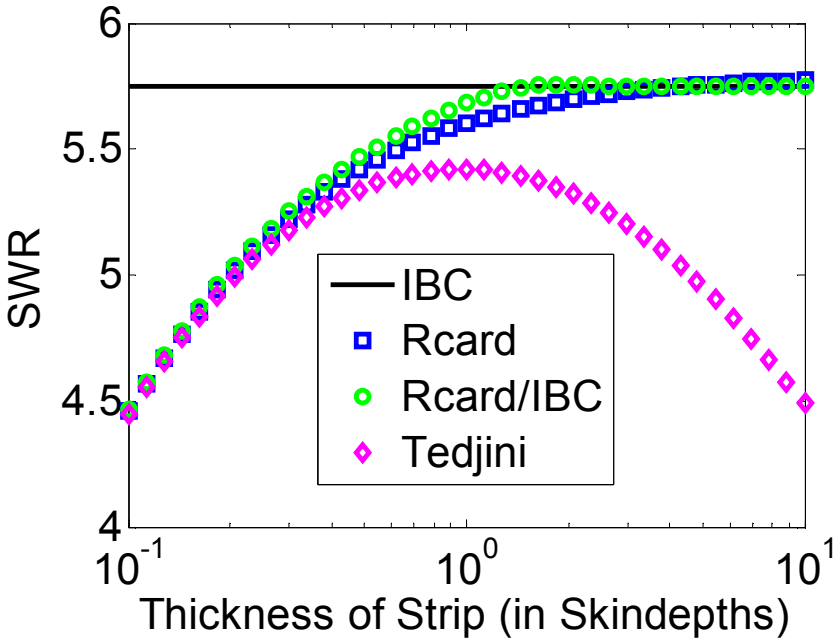

(a) SWR vs Strip Thickness (t)

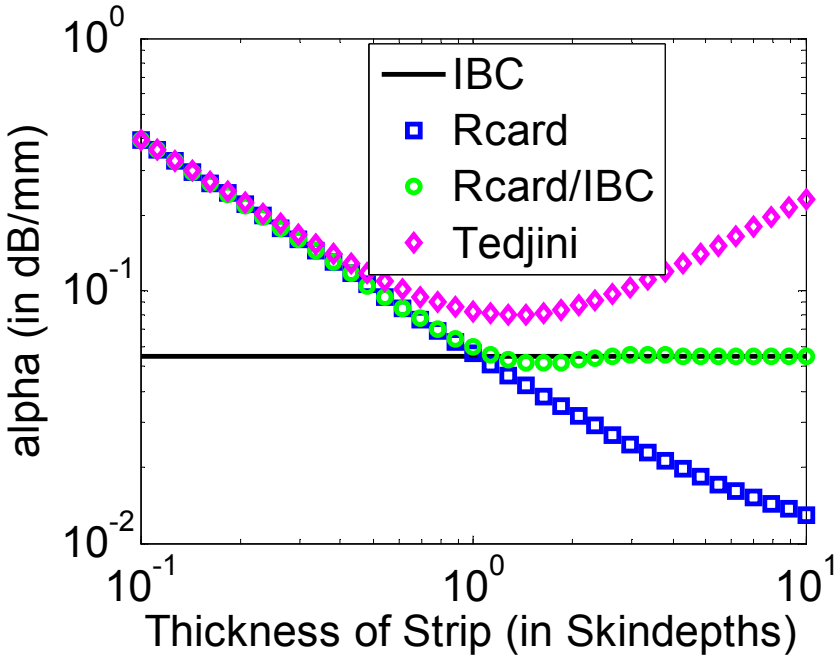

(b) α (dB/mm) vs Strip Thickness (t)

Figure 5.5 (a) Slow wave Ratio (SWR) (b) α (dB/mm) as a function of frequency for a shielded MIS transmission line with parameters $\mu_r = 1, h_1 = 1\mu$m$, h_2 = 250\mu$m$, w = 80\mu$m$, a = 4$mm, $d = 3.2$mm$, c = a/2, \epsilon_{r1} = 4, \epsilon_{r2} = 12, \sigma_1 = 0, \sigma_2 = 5$S/m, $\sigma_s = 5.88 \times 10^7$, skin depth $\delta = 2.075\mu$m$, f = 1$GHz using four different approximate models for finite thickness and conductivity of metal strip and triangle-triangle basis ($M_z = 4$ and $M_x = 2$)

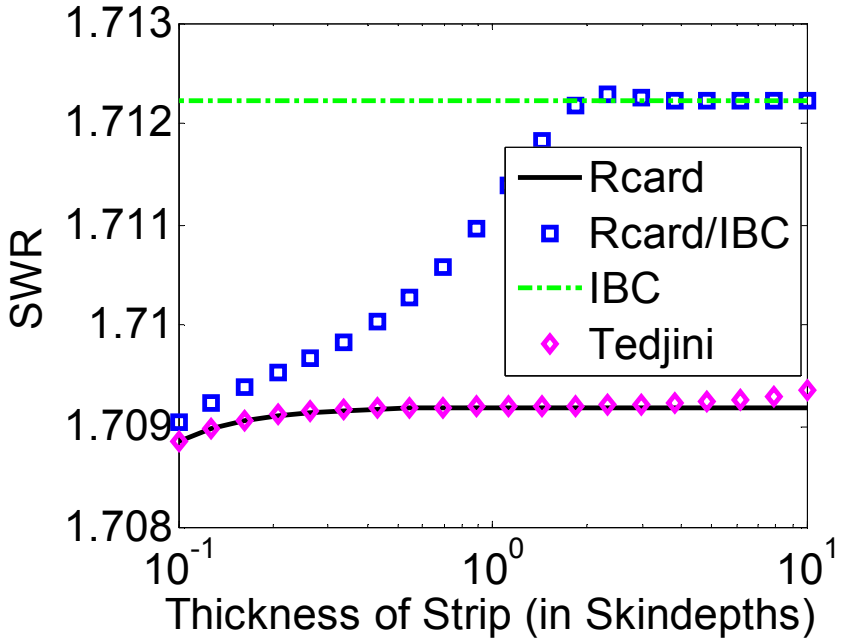

(a) SWR vs Strip Thickness (t)

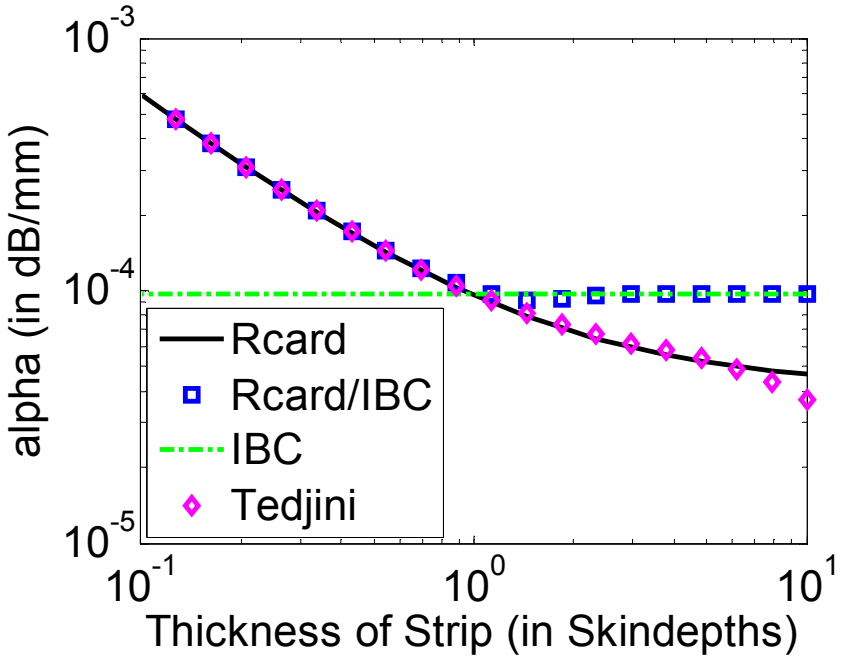

(b) α (dB/mm) vs Strip Thickness (t)

Figure 5.6 (a) Slow wave ratio (SWR) (b) α (dB/mm) as a function of frequency for a shielded MIS transmission line with parameters $\mu_r = 1, h_1 = 5\text{mm}, h_2 = 5\text{mm}, w = 1\text{mm}, a = 20\text{mm}, d = 10\text{mm}, c = a/2, \epsilon_{r1} = 4, \epsilon_{r2} = 12, \sigma_1 = 0, \sigma_2 = 5\text{S/m}, \sigma_s = 5.88 \times 10^7, \delta = 6.562\mu\text{m}, f = 100\text{MHz}$ using four different approximate models for finite thickness and conductivity of metal strip.

CHAPTER 6. Extension of the Spectral Domain Immittance Approach for Multiple Metal Lines on the Same Plane and its Acceleration Using Two Super Convergent Series

6.1 Extending the Spectral Domain Immittance Approach

In Chapter 3 we presented a technique to speed up the analysis of multilayered shielded microstrip with single metal line which is displaced from the edge by a distance c. In this Chapter, we extend the same technique for a multilayered shielded microstrip with multiple metal lines in the same plane. The derivation for the Green's function is the same because all the metal lines are located in the same layer. Figure 6.1 shows a multilayered shielded microstrip with M metal lines with a unique width $2w_i$ ($i = 1, ..., M$) displaced by a distance c_i from the left wall located on $y = 0$ plane and extending infinitely in the z direction. The side walls are perfect electric conductor (PEC) or perfect magnetic conductor (PMC). The m^{th} layer is defined by ϵ_m, μ_m and $k_m = \omega\sqrt{\epsilon_m\mu_m}$. The size of the box is a. The layers above the signal metal strip are numbered from 1 to $q + 1$ and the layers below are numbered from -1 to $-l - 1$. The top and bottom cover layers can be PEC, PMC or dielectric extending upto infinity. In order to extend the SDIA for this case we need to assume the current on all the strips using suitable basis functions. Also, we need to consider the cross coupling between the metal lines. If we use the same number of basis functions (M_z for the longitudinal current and M_x for the transverse current) for each strip then this would result in a matrix of size $[No.of strips \times (M_x + M_z)])^2$. Therefore, the need for fast and accurate evaluation of the matrix elements increases even more. The elements of the MoM

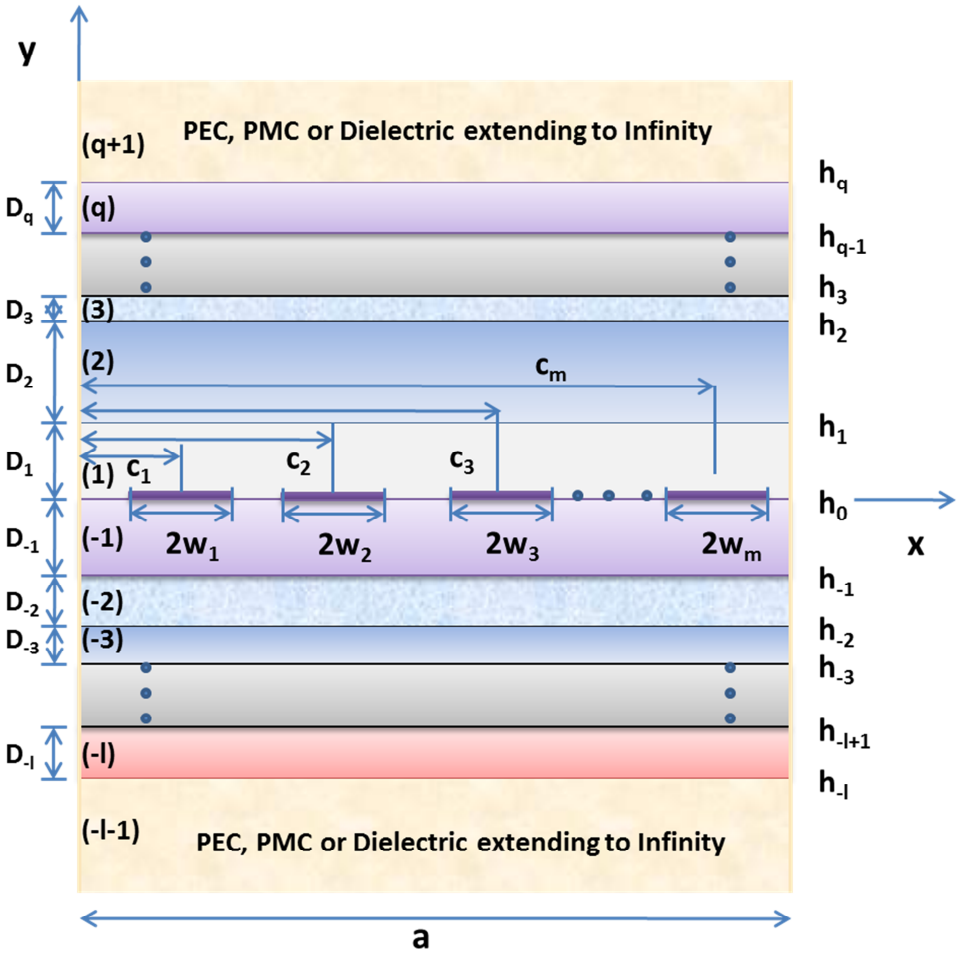

Figure 6.1 Shielded multilayered interconnects with multiple metal lines in one of the layers

matrix can be written as:

$$K^{uv}_{mnpq} = \sum_{k=1}^{\infty} G_{pq} \tilde{J}^{p}_{um}(w_p \alpha_k) \tilde{J}^{q}_{vn}(w_q \alpha_k) \tag{6.1}$$

where $(u, v) \in (x, z)$, $\tilde{J}^{p}_{um}$ refers to u component of the m^{th} basis for the p^{th} metal line. Thus, we can assume the unknown current in the form of suitable basis functions and then following the same procedure as in Chapter 3 we can obtain the value of the normalized propagation constant.

6.2 Acceleration Using Asymptotic Approximation and Two Super Convergent Series

In order to evaluate the elements of the K matrix as given in (6.1) we need to truncate the infinite summation which consists of slowly converging spectral series. If we choose Chebyshev polynomials as the basis functions the Fourier transform of the basis function will be a Bessel function as seen in the Chapter 3. Therefore, we need to deal with the product of Bessel functions. In order to accelerate the infinite summation we use the same technique as in Chapter 3 i.e. the asymptotic expansion of the basis functions and the Green's functions. Using (2.71) the asymptotic expansion for the product of the Bessel functions can be written as:

$$J_u^p(w_p z)J_v^q(w_q z) = \frac{2}{\pi z\sqrt{w_p w_q}}\left[L_0 + \frac{1}{8z}L_1 + \frac{1}{(8z)^2}L_2 + \frac{1}{(8z)^3}L_3 + \frac{1}{(8z)^4}L_4 + \frac{1}{(8z)^5}L_5\right] \tag{6.2}$$

where $z = \alpha_n$ and

$$L_0 = A_{uv}^{pq} \tag{6.3}$$

$$L_1 = -B_{uv}^{pq}C_u^1/w_p - C_{uv}^{pq}C_v^1/w_q \tag{6.4}$$

$$L_2 = -A_{uv}^{pq}C_v^2/w_q^2 + D_{uv}^{pq}C_v^1C_u^1/(w_p w_q) - A_{uv}^{pq}C_u^2/w_p^2 \tag{6.5}$$

$$L_3 = B_{uv}^{pq}(C_u^3/w_p^3 + C_u^1C_v^2/(w_p w_q^2)) + C_{uv}^{pq}(C_v^3/w_q^3 + C_v^1C_u^2/(w_p^2 w_q)) \tag{6.6}$$

$$L_4 = A_{uv}^{pq}(C_u^2C_v^2/(w_p^2w_q^2) + C_u^4/w_p^4 + C_v^4/w_q^4) - D_{uv}^{pq}(C_v^3C_u^1/(w_q^3w_p) + C_v^1C_u^3/(w_p^3w_q)) \tag{6.7}$$

$$L_5 = -B_{uv}^{pq}C_u^3C_v^2/(w_p^3w_q^2) - C_{uv}^{pq}C_v^3C_u^2/(w_q^3w_p^2) \tag{6.8}$$

where $\tilde{J}_u^p$ refers to the m^{th} basis for the p^{th} metal line.

$$G_{zz} = G_{zz0}/(\alpha_n)(1 - y_{1zz}^2/\alpha_n^2 - y_{2zz}^2/\alpha_n^4) \tag{6.9}$$

$$F^{zz}_{mnpq} = 2G_{zz0}/(\alpha_n^2 \pi \sqrt{w_p w_q}) \Big[L_0 + \frac{1}{8\alpha_n} L_1 + \frac{1}{(8\alpha_n)^2}(L_2 - 64 y_{1zz}^2 L_0) + \frac{1}{(8\alpha_n)^3}(L_3 - 64 y_{1zz}^2 L_1) + \frac{1}{(8\alpha_n)^4}(L_4 - 64 y_{1zz}^2 L_2 - 4096 y_{2zz}^2 L_0) + \frac{1}{(8\alpha_n)^5}(L_5 - 64 y_{1zz}^2 L_3 - 4096 y_{2zz}^2 L_1) \Big] \tag{6.10}$$

Define

$$S_1 = \sin[(w_p + w_q + c_p + c_q)\, z] \tag{6.11}$$

$$S_2 = \sin[(w_p + w_q - c_p - c_q)\, z] \tag{6.12}$$

$$S_3 = \sin[(w_p + w_q + c_p - c_q)\, z] \tag{6.13}$$

$$S_4 = \sin[(w_p + w_q - c_p + c_q)\, z] \tag{6.14}$$

$$S_5 = \sin[(w_p - w_q + c_p + c_q)\, z] \tag{6.15}$$

$$S_6 = \sin[(w_p - w_q - c_p - c_q)\, z] \tag{6.16}$$

$$S_7 = \sin[(w_p - w_q + c_p - c_q)\, z] \tag{6.17}$$

$$S_8 = \sin[(w_p - w_q - c_p + c_q)\, z] \tag{6.18}$$

Similarly, $C_i (i = 1, 2...8)$ are defined by replacing sine by cosine in the expression for S_i. For $u = odd$ and $v = odd$

$$A^{pq}_{uv} = 1/8 \Big[(-1)^{(u+v)/2}(S_1 + S_2 + S_3 + S_4) + (-1)^{(u-v)/2}(C_5 + C_6 + C_7 + C_8) \Big] \tag{6.19}$$

$$D^{pq}_{uv} = 1/8 (-(-1)^{(u+v)/2} \Big[(S_1 + S_2 + S_3 + S_4) + (-1)^{(u-v)/2}(C_5 + C_6 + C_7 + C_8) \Big] \tag{6.20}$$

$$B^{pq}_{uv} = 1/8 \Big[-(-1)^{(u+v)/2}(C_1 + C_2 + C_3 + C_4) + (-1)^{(u-v)/2}(S_5 + S_6 + S_7 + S_8) \Big] \tag{6.21}$$

$$C^{pq}_{uv} = 1/8 \Big[-(-1)^{(u+v)/2}(C_1 + C_2 + C_3 + C_4) - (-1)^{(u-v)/2}(S_5 + S_6 + S_7 + S_8) \Big] \tag{6.22}$$

For $u = even$ and $v = even$

$$A^{pq}_{uv} = 1/8 \Big[(-1)^{(u+v)/2}(S_1 + S_2 - S_3 - S_4) + (-1)^{(u-v)/2}(C_5 + C_6 - C_7 - C_8) \Big] \tag{6.23}$$

$$D^{pq}_{uv} = 1/8 \Big[-(-1)^{(u+v)/2}(S_1 + S_2 - S_3 - S_4) + (-1)^{(u-v)/2}(C_5 + C_6 - C_7 - C_8) \Big] \tag{6.24}$$

$$B_{uv}^{pq} = 1/8\Big[-(-1)^{(u+v)/2}(C_1 + C_2 - C_3 - C_4) + (-1)^{(u-v)/2}(S_5 + S_6 - S_7 - S_8)\Big] \quad (6.25)$$

$$C_{uv}^{pq} = 1/8\Big[-(-1)^{(u+v)/2}(C_1 + C_2 - C_3 - C_4) - (-1)^{(u-v)/2}(S_5 + S_6 - S_7 - S_8)\Big] \quad (6.26)$$

For $u = odd$ and $v = even$

$$A_{uv}^{pq} = 1/8\Big[-(-1)^{(u+v)/2}(S_1 - S_2 - S_3 + S_4) + (-1)^{(u-v)/2}(-C_5 + C_6 + C_7 - C_8)\Big] \quad (6.27)$$

$$D_{uv}^{pq} = 1/8\Big[(-1)^{(u+v)/2}(S_1 - S_2 - S_3 + S_4) + (-1)^{(u-v)/2}(-C_5 + C_6 + C_7 - C_8)\Big] \quad (6.28)$$

$$B_{uv}^{pq} = 1/8\Big[-(-1)^{(u+v)/2}(-C_1 + C_2 + C_3 - C_4) - (-1)^{(u-v)/2}(S_5 - S_6 - S_7 + S_8)\Big] \quad (6.29)$$

$$C_{uv}^{pq} = 1/8\Big[-(-1)^{(u+v)/2}(-C_1 + C_2 + C_3 - C_4) + (-1)^{(u-v)/2}(S_5 - S_6 - S_7 + S_8)\Big] \quad (6.30)$$

For $u = even$ and $v = odd$

$$A_{uv}^{pq} = 1/8\Big[-(-1)^{(u+v)/2}(S_1 - S_2 + S_3 - S_4) + (-1)^{(u-v)/2}(-C_5 + C_6 - C_7 + C_8)\Big] \quad (6.31)$$

$$D_{uv}^{pq} = 1/8\Big[(-1)^{(u+v)/2}(S_1 - S_2 + S_3 - S_4) + (-1)^{(u-v)/2}(-C_5 + C_6 - C_7 + C_8)\Big] \quad (6.32)$$

$$B_{uv}^{pq} = 1/8\Big[-(-1)^{(u+v)/2}(-C_1 + C_2 - C_3 + C_4) - (-1)^{(u-v)/2}(S_5 - S_6 + S_7 - S_8)\Big] \quad (6.33)$$

$$C_{uv}^{pq} = 1/8\Big[-(-1)^{(u+v)/2}(-C_1 + C_2 - C_3 + C_4) + (-1)^{(u-v)/2}(S_5 - S_6 + S_7 - S_8)\Big] \quad (6.34)$$

All the terms of (6.10) are of the form sine/cosine function divided by k^s, where s=2,3,4,5... Therefore, its infinite summation can be easily evaluated using the two super convergent series as shown in Chapter 3. Thus following the same procedure as before we can obtain the value of the propagation constant.

6.3 Numerical Results

We have used this program to test the performance of different basis functions including pulse-triangle, triangle-triangle and Chebyshev polynomials. The detailed expression for the pulse-triangle and the triangle-triangle basis can be found in Chapter 5.

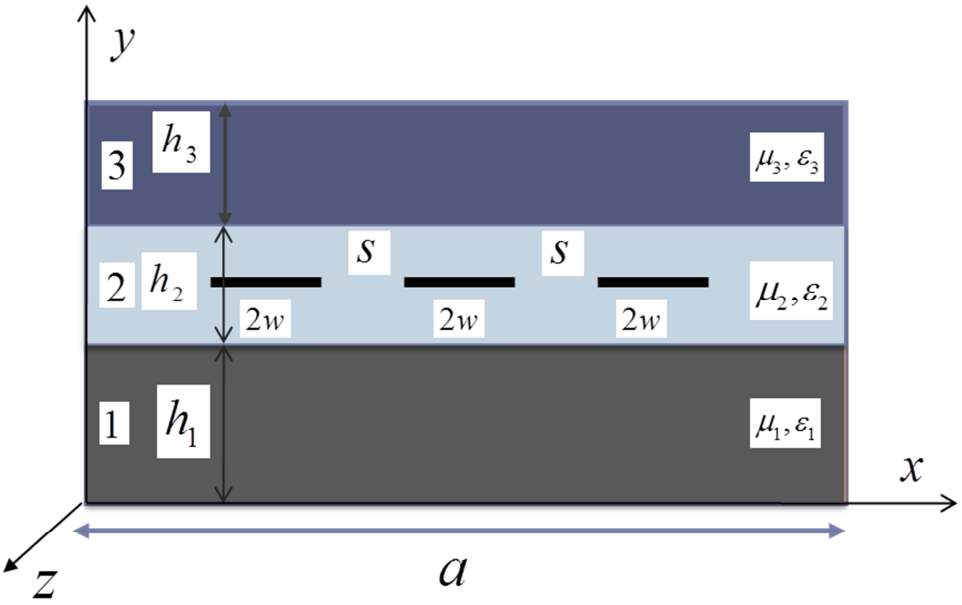

Figure 6.2 A three layered shielded microstrip with three metal lines in one of the layers and parameters ϵ_{r1} = ϵ_{r3}=9.7, ϵ_{r2} =4, μ_{r1} = μ_{r2} = μ_{r3}= 1, f= 3 GHz, h_1=h_2=h_3=h=1 mm, a=10 mm, $2w/h$ =1, s/h =0.1 [2]

Table 6.1 β/k_0 for different $N_{\max}$ for the dominant mode of a three layered shielded microstrip three metal lines with parameters as shown in Figure 6.2 using Chebyshev polynomials as basis

Mode No.	$N_{\max}$	M_z	M_x	ϵ_{reff}	ϵ_{reff}[2]
1	1000	2	2	6.0035	6.02
2	1000	2	2	4.7924	4.78
3	1000	2	2	4.3661	4.23

Table 6.2 β/k_0 for different $N_{\max}$ for the dominant mode of a three layered shielded microstrip three metal lines with parameters as shown in Figure 6.2 using Triangle-Triangle basis

Mode No.	$N_{\max}$	M_z	M_x	ϵ_{reff}
1	1000	3	1	5.9750
2	10000	7	5	4.7993
3	10000	3	1	4.3187

Table 6.3 β/k_0 for different $N_{\max}$ for the dominant mode of a three layered shielded microstrip three metal lines with parameters as shown in Figure 6.2 using Pulse-Triangle basis

Mode No.	$N_{\mathbf{max}}$	$M_{\mathbf{z}}$	$M_{\mathbf{x}}$	ϵ_{reff}
1	10000	2	1	5.9680
2	10000	10	9	4.7984
3	10000	6	5	4.2597

Tables 6.1, 6.2 and 6.3 show the comparison of the ϵ_{reff} for the first three modes of a three conductor shielded microstrip using three different basis functions. The results were compared with [2] which uses the finite difference method which is less accurate compared to the SDA.

Table 6.4 shows the comparison of the normalized propagation constant using different basis

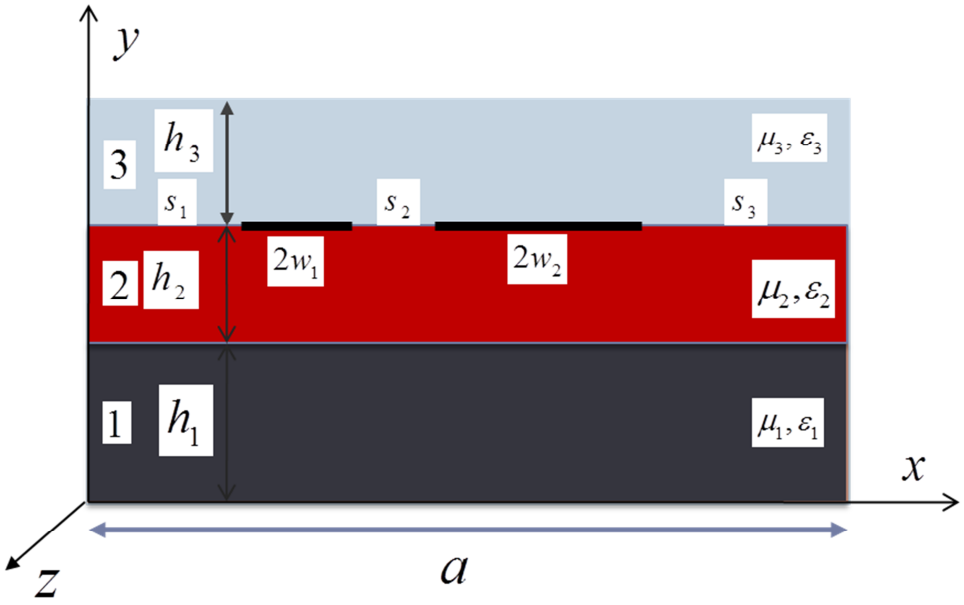

Figure 6.3 A Three layered shielded microstrip with two metal lines in one of the layers and parameters ϵ_{r1} =1, ϵ_{r2} =2.2, μ_{r1} = μ_{r2} = 1, f= 150 GHz, h_1= h_2=.254mm, h_3=.762mm a=2.54mm, s_2 = 0.0127mm, $s_1 : 2w_1 : s_2 : 2w_2 : s_3$ = 89.5 : 20 : 1 : 40 : 49.5[3].

Table 6.4 β/k_0 for different N_{max} for the dominant mode of a coupled suspended shielded microstrip with parameters as shown in Figure 6.3 using different basis functions

Basis	N_{max}	M_z	M_x	β/k_0
Chebychev-Chebychev	10000	8	8	1.260959
Triangle-Triangle	1000	5	3	1.260178
Pulse-Triangle	10000	6	5	1.260345

functions for a shielded microstrip with two metal lines. The results were compared with [3] which reports $\beta/k_0 = 1.26091$ for the same structure.

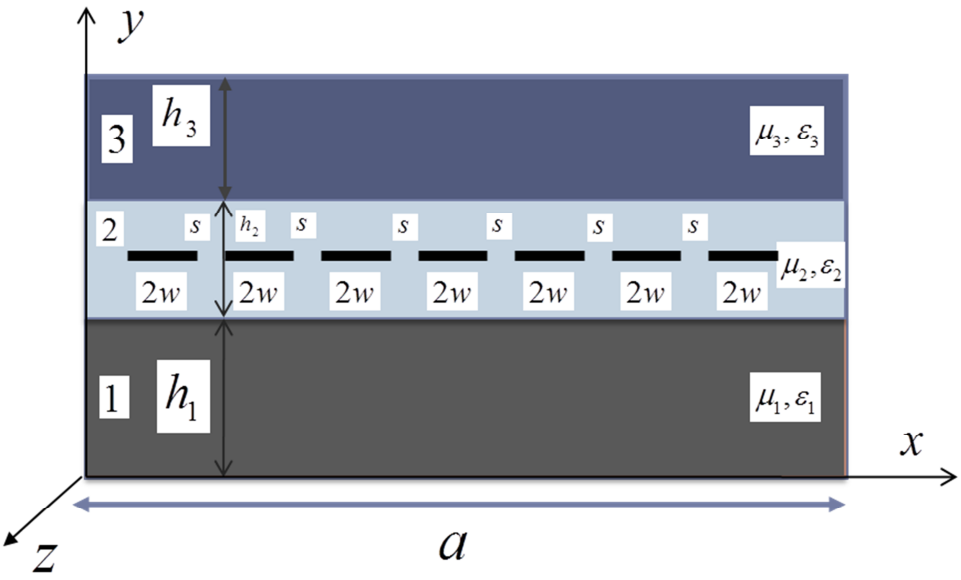

Figure 6.4 A three layered shielded microstrip with seven metal lines in one of the layers and parameters $\epsilon_{r1} = \epsilon_{r3}$=9.7, ϵ_{r2} =4, $\mu_{r1} = \mu_{r2} = \mu_{r3}$= 1, f= 3 GHz, h_1=h_2=h_3=h=1μm, a=20μm, $2w/h$ =1, s/h =0.1

Tables 6.5 and 6.6 shows that this approach can be used to obtain the first seven modes of a shielded microstrip with seven metal lines in the same plane using Chebyshev polynomial as basis and triangle-triangle basis, respectively. This confirms that the triangle-triangle basis has a reasonably good convergence even for this case although it is much slower than the Chebyshev polynomials.

Table 6.5 ϵ_{reff} for different N_{max} for the seven modes of a three layered shielded microstrip with seven metal lines with parameters as given in Figure 6.4 using Chebyshev polynomials as basis.

Mode No.	$N_{\mathbf{max}}$	$M_{\mathbf{z}}$	$M_{\mathbf{x}}$	$\beta/\mathbf{k_0}$
1	1000	4	4	4.7095
2	1000	4	4	4.8105
3	1000	4	4	4.9812
4	1000	4	4	5.2203
5	1000	4	4	5.5083
6	1000	4	4	5.8001
7	1000	4	4	6.0242

Table 6.6 ϵ_{reff} for different N_{max} for the seven modes of a three layered shielded microstrip with seven metal lines with parameters as given in Figure 6.4 using Triangle-Triangle basis.

Mode No.	$N_{\mathbf{max}}$	$M_{\mathbf{z}}$	$M_{\mathbf{x}}$	$\beta/\mathbf{k_0}$
1	1000	6	4	4.7114
2	1000	6	4	4.8131
3	1000	6	4	4.9838
4	1000	6	4	5.2195
5	1000	6	4	5.5017
6	1000	6	4	5.7857
7	1000	6	4	6.0024

The accelerated SDIA was verified for a layered shielded microstrip with two and three metal lines on the same interface. Tables 6.7 and 6.8 shows a comparison of the normalized propagation constant and the ϵ_{reff} for a shielded microstrip with two and three metal lines, respectively, using first four terms of the leading term extraction (LTE) and without using LTE (No LTE). It is observed that using about 200 terms of the summation one can get 6 digits of accuracy in the value of the normalized propagation constant. This would require nearly 10^6 terms without acceleration. Thus, this technique has accelerated the SDIA for the case of multiple metal lines by nearly four orders of magnitude. For a single strip microstrip line the CPU time for getting ϵ_{reff} correct up to 12 digits is nearly $.05$ seconds using a 2.66 GHz Intel processor. The finite difference approach proposed by Kaladhar and Chew [2] requires 12000 unknowns and a CPU time of about 90 seconds using the DEC Personal Workstation 600 for a similar microstrip to obtain less than 3 significant digits of accuracy.

Table 6.7 β/k_0 for different N_{max} for the dominant mode of a three layered shielded microstrip as shown in Figure 6.3

	$N_{\mathbf{max}}$	$M_{\mathbf{z}}$	$M_{\mathbf{x}}$	β/k_0
LTE	100	8	8	1.26253805
LTE	200	8	8	1.26095711
LTE	1000	8	8	1.26091722
LTE	2000	8	8	1.26091714
No LTE	100000	8	8	1.26091833

Table 6.8 β/k_0 for different $N_{\max}$ for the dominant mode of a three layered shielded microstrip with three metal lines and parameters as shown in Figure 6.2

	$N_{\mathbf{max}}$	$M_{\mathbf{z}}$	$M_{\mathbf{x}}$	$\epsilon_{\mathbf{reff}}$
LTE	100	4	4	5.97131978
LTE	200	4	4	5.97139435
No LTE	1000000	4	4	5.97139451
LTE	100	8	8	5.97140413
LTE	200	8	8	5.97123043
LTE	1000	8	8	5.97123338
No LTE	1000000	8	8	5.97123388

CHAPTER 7. Extension of Spectral Domain Immittance Approach for Multiple Metal Lines on Different Planes in Uniaxial Anisotropic Multilayered Shielded Interconnect

7.1 Introduction

In Chapter 6 the acceleration of the spectral domain immitance approach (SDIA) for solving the isotropic multilayered shielded interconnect problem with multiple metal lines on the same interface using superconvergent series has been discussed in detail. In this chapter we present an extension of the SDIA to solve the anisotropic multilayered shielded interconnect problem with arbitrarily spaced multiple metal lines in different layers. This is closer to what happens in modern interconnects where we have a number of arbitrary spaced metal lines accept the fact that for now we are assuming the metal lines to be zero thickness PEC. In Chapter 5 we have looked at some models to incorporate the finite thickness and conductivity of metal lines in the SDIA which can be easily integrated with this approach. So, this method can be used to obtain the equivalent medium parameters for an interconnect structure.

Consider a multilayered shielded microstrip with multiple metal lines in different layers as shown in Figure 7.1 consisting of M layers of lossy or dielectric material numbered from bottom to top. The side walls are perfect electric conductor (PEC) or perfect magnetic conductor (PMC). The m^{th} layer is defined by $[\epsilon_{mx}, \epsilon_{my}, \epsilon_{mz}]$, $[\mu_{mx}, \mu_{my}, \mu_{mz}]$ and σ_m. Interfaces m_i $i = 1, 2, ...N$ have multiple PEC strips on their surface each with a unique width $2w_{kmi}$ and at a distance c_{kmi} from the left side wall, extending infinitely in the z direction. ($k = 1, 2, .., N_{mi}$ and N_{mi} is the

number of strips on the m_i^{th} interface). The topmost and bottommost layers can be PEC, PMC or dielectric extending up to infinity.

All the field components can be written as a superposition of plane waves inhomogeneous in the y direction propagating at an angle θ with the z axis. For each θ the hybrid modes can be represented into two transmission line models (TE^y and TM^y) as shown in Figure 7.2. For the case when the the medium is uniaxially anisotropic i.e. $\epsilon_x = \epsilon_z$ the TE^y and TM^y modes are completely decoupled into two independent transmission line models. Therefore, J_u creates only the TE^y fields and J_v creates only the TM^y fields and the immittance matrix will be diagonal [54]. But for the biaxial anisotropic case the TE^y and TM^y modes cannot be completely decoupled as the fields E_v and H_v will be contributed by both the components of current (J_u and J_v). Thus, we will need to include an off diagonal term in the admittance matrix which is referred to us the conjoint admittance parameter in [64]. The parameters in (x, y, z) coordinates are related to (u, y, v) coordinates by the matrix transformation:

$$\begin{bmatrix} \tilde{P}_u \\ \tilde{P}_v \end{bmatrix} = \begin{bmatrix} -\cos\theta & \sin\theta \\ \sin\theta & \cos\theta \end{bmatrix} \times \begin{bmatrix} \tilde{P}_x \\ \tilde{P}_z \end{bmatrix} \tag{7.1}$$

where $\theta = \cos^{-1}(\beta/\sqrt{\alpha_n^2 + \beta^2})$ and P can be E or H.

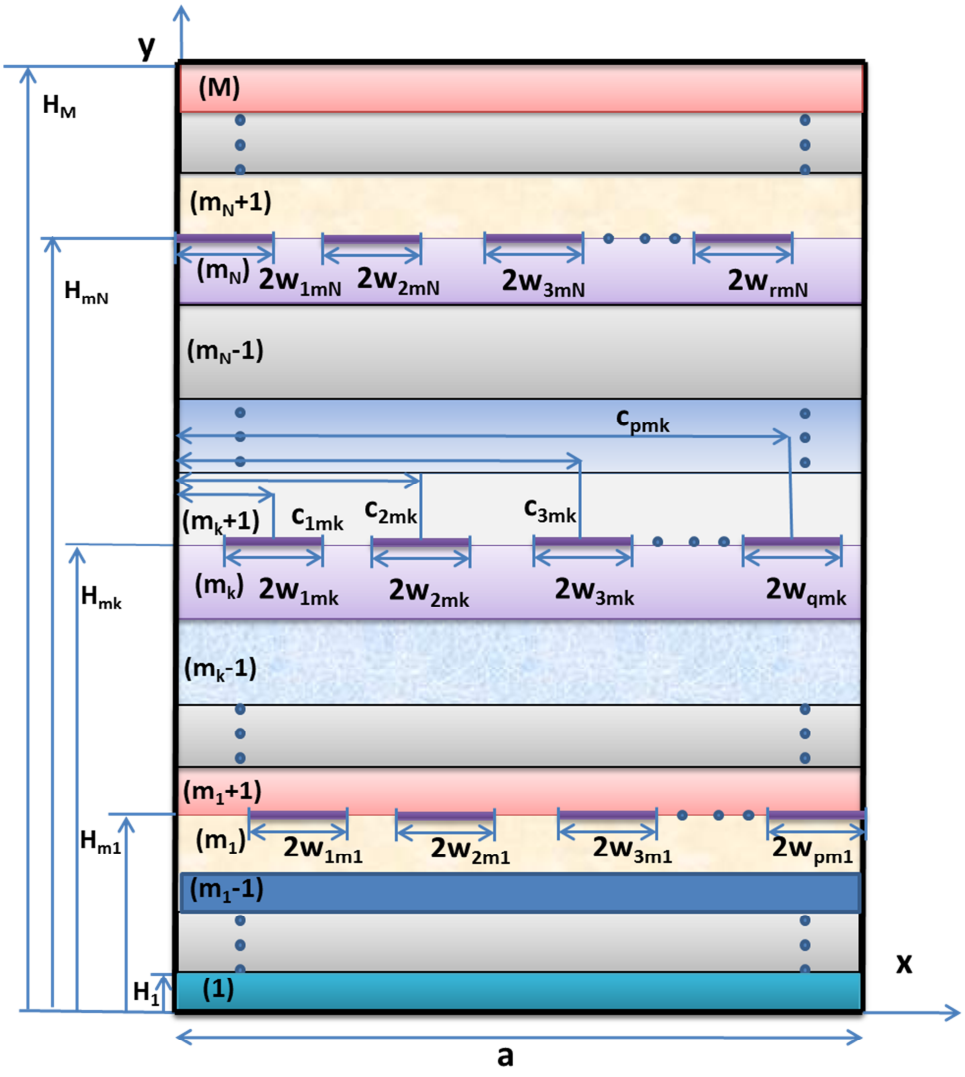

Figure 7.1 Shielded multilayered interconnects with multiple metal lines (zero thickness PEC) in different layers

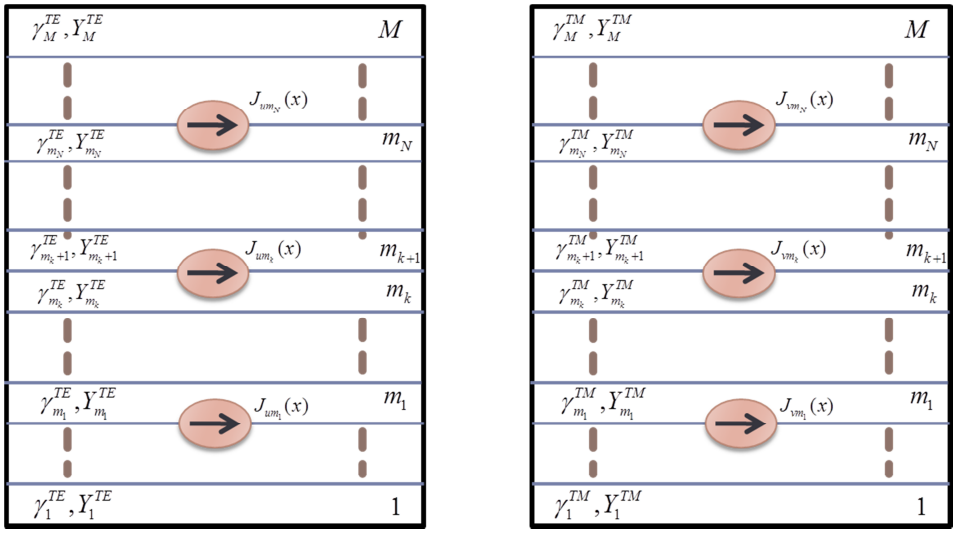

Figure 7.2 Transmission Line Model

For this general case of biaxial anisotropic medium, in the spectral domain the electric and magnetic fields will satisfy the following fourth degree propagation equations which can be obtained from the Maxwell's equations [64]:

$$\frac{\partial^4(\tilde{E}_y, \tilde{H}_y)}{\partial y^4} + (f^e_{1i}, f^h_{1i})\frac{\partial^2(\tilde{E}_y, \tilde{H}_y)}{\partial y^2} + (f^e_{2i}, f^h_{2i})(\tilde{E}_y, \tilde{H}_y) = 0 \tag{7.2}$$

where

$$f^e_{1i} = f^h_{1i} = k_0^2(\epsilon_{rxi}\mu_{rzi} + \epsilon_{rzi}\mu_{rxi}) - \alpha_n^2(\mu_{xi}/\mu_{yi} + \epsilon_{xi}/\epsilon_{yi}) - \beta^2(\mu_{zi}/\mu_{yi} + \epsilon_{zi}/\epsilon_{yi}) \tag{7.3}$$

$$f^e_{2i} = -[k_0^2\epsilon_{rxi}\epsilon_{rzi}\mu_{xi}/\mu_{yi} - \mu_{xi}(\alpha_n^2\epsilon_{xi} - \beta^2\epsilon_{zi})/(\epsilon_{yi}\mu_{yi})][\alpha_n^2 + \beta^2\mu_{zi}/\mu_{xi} - k_0^2\epsilon_{ryi}\mu_{rzi}] \tag{7.4}$$

The expression for f^h_{2i} can be obtained by interchanging ϵ and μ in the expression for f^e_{2i}. We can assume the solution of (7.2) to be of the form: For $i \leq m_q$:

$$\tilde{H}_{yi}(\alpha_n, y) = C_i \sinh[\gamma^a_{hi}(y - H_i)] + D_i \cosh[\gamma^b_{hi}(y - H_i)] \tag{7.5}$$

$$\tilde{E}_{yi}(\alpha_n, y) = A_i \sinh[\gamma^a_{ei}(y - H_i)] + B_i \cosh[\gamma^b_{ei}(y - H_i)] \tag{7.6}$$

For $i \geq m_q + 1$:

$$\tilde{H}_{yi}(\alpha_n, y) = C_i \sinh[\gamma^a_{hi}(H_i - y)] + D_i \cosh[\gamma^b_{hi}(H_i - y)] \tag{7.7}$$

$$\tilde{E}_{yi}(\alpha_n, y) = A_i \sinh[\gamma^a_{ei}(H_i - y)] + B_i \cosh[\gamma^b_{ei}(H_i - y)] \tag{7.8}$$

where $q = 1, 2, ...N_{\text{metal}}$ and $H_i = \Sigma_{k=1}^{i} h_k$ and

$$\gamma^a_{pi} = \sqrt{\{-f_1^p - [(f_1^p)^2 - 4f_2^p]^{1/2}\}/2} \tag{7.9}$$

$$\gamma^b_{pi} = \sqrt{\{-f_1^p + [(f_1^p)^2 - 4f_2^p]^{1/2}\}/2} \tag{7.10}$$

where $p = e, h$.

Note that the sign of the arguments for the two cases is opposite because looking from the m^{th} metal layer we would have to choose opposite signs for the γ for the layers above and below it.

The remaining tangential components of fields in the (u, y, v) coordinates for the i^{th} layer are expressed in terms of $\tilde{E}_{yi}$ and $\tilde{H}_{yi}$ as follows [65]:

$$\tilde{E}_{ui} = -\frac{\omega\mu_{yi}}{\delta_n}\tilde{H}_{yi} \tag{7.11}$$

$$\tilde{E}_{vi} = \frac{\omega\mu_{yi}\alpha_n\beta(\epsilon_{zi} - \epsilon_{xi})}{\delta_n\delta_{n\epsilon}^2}\tilde{H}_{yi} - j\frac{\epsilon_{yi}\delta_n}{\delta_{n\epsilon}^2}\frac{\partial\tilde{E}_{yi}}{\partial y} \tag{7.12}$$

$$\tilde{H}_{ui} = -\frac{\omega\epsilon_{yi}}{\delta_n}\tilde{E}_{yi} \tag{7.13}$$

$$\tilde{H}_{vi} = -j\frac{\mu_{yi}\delta_n}{\delta_{n\mu}^2}\frac{\partial\tilde{H}_{yi}}{\partial y} + \frac{\omega\epsilon_{yi}\alpha_n\beta(\mu_{xi} - \mu_{zi})}{\delta_n\delta_{n\mu}^2}\tilde{E}_{yi} \tag{7.14}$$

where

$$\delta_n = \sqrt{\alpha_n^2 + \beta^2} \tag{7.15}$$

$$\delta_{n\epsilon}^2 = \alpha_n^2\epsilon_{xi} + \beta^2\epsilon_{zi} \tag{7.16}$$

$$\delta_{n\mu}^2 = \alpha_n^2\mu_{xi} + \beta^2\mu_{zi} \tag{7.17}$$

7.2 Self Impedance

7.2.1 TM^y

In order to consider the effect of metal lines in the i^{th} layer we introduce current densities J_{ui} and J_{vi} which are responsible for generating the TM^y fields. Their Fourier transforms are $\tilde{J}_{ui}$ and $\tilde{J}_{vi}$, respectively. The TM^y self impedance corresponding to i^{th} metallization plane is defined as [64]:

$$\tilde{Z}_{vi}^e = \frac{\tilde{E}_{vi}}{\tilde{J}_{vi}} \tag{7.18}$$

It is obtained by taking the reciprocal of the sum of admittances looking up ($\tilde{Y}^e_{vi\ \text{up}}$) and down ($\tilde{Y}^e_{vi\ \text{down}}$) from the interface with the metallization assuming that there is no metallization present in any of the other layers.

$$\tilde{Z}^e_{vi} = \frac{1}{\tilde{Y}^e_{vi\ \text{up}} + \tilde{Y}^e_{vi\ \text{down}}} \tag{7.19}$$

$\tilde{Y}^e_{vi\ \text{up}}$ is determined by iterating from topmost layer to the $(i+1)^{th}$ layer and $\tilde{Y}^e_{vi\ \text{down}}$ by iterating from bottom most layer to the i^{th} layer using the recursive relation:

$$\tilde{Y}^e_{vi\pm} = y^e_{vi}\frac{\sinh(\gamma^a_{ei}h_i) + S^e_{vi\pm}\cosh(\gamma^b_{ei}h_i)}{\gamma^c_{ei}\cosh(\gamma^a_{ei}h_i) + S^e_{vi\pm}\sinh(\gamma^b_{ei}h_i)} \tag{7.20}$$

where

$$y^e_{vi} = \frac{j\omega\delta^2_{n\epsilon}}{\gamma^b_{ei}\delta^2_n},\ \gamma^c_{ei} = \frac{\gamma^a_{ei}}{\gamma^b_{ei}} \tag{7.21}$$

and

$$S^e_{vi\pm} = \tilde{Y}^e_{v(i\pm1)\pm}\frac{\gamma^c_{ei}}{y^e_{vi}}(i = 2, 3.., M-1) \tag{7.22}$$

with initial conditions $\tilde{Y}^e_{v1-} = y^e_{v1}\coth(\gamma^b_{e1}h_1)$ and $\tilde{Y}^e_{vM+} = y^e_{vM}\coth(\gamma^b_{eM}h_M)$ assuming that the top and bottom boundaries are PEC. Thus,

$$\tilde{Y}^e_{vi\ \text{up}} = \tilde{Y}^e_{v(i+1)+} \tag{7.23}$$

$$\tilde{Y}^e_{vi\ \text{down}} = \tilde{Y}^e_{vi-} \tag{7.24}$$

7.2.2 Conjoint Impedance Parameter

For the biaxial anisotropic materials it is not possible to decouple the TE^y and TM^y modes into two independent transmission lines as is possible for the uniaxial case [66]. Hence, a conjoint impedance parameter [64] is used in order to consider the remaining field components i.e. $\tilde{E}_v$ for the TE^y mode and $\tilde{H}_u$ for the TM^y mode. This conjoint parameter is nothing but the TM^y impedance at the interface with the metallization due to the presence of both J_u and J_v in its

equivalent circuit at the same time. The conjoint impedance parameter for the i^{th} metallization interface is defined as:

$$\tilde{Z}^e_{uvi} = \frac{\tilde{E}_{vi}}{\tilde{J}_{ui}} \tag{7.25}$$

$$\tilde{Z}^e_{uvi} = \frac{1}{\tilde{Y}^e_{uvi\ \text{up}} + \tilde{Y}^e_{uvi\ \text{down}}} \tag{7.26}$$

The admittances $\tilde{Y}^e_{uvi\ \text{up}}$ and $\tilde{Y}^e_{uvi\ \text{down}}$ are determined recursively similar to the TM^y admittances using the recursion relation [64]:

$$\tilde{Y}^e_{uvi\pm} = y^e_{uvi} \frac{\sinh(\gamma^a_{ei} h_i) + S^e_{uvi\pm} \cosh(\gamma^b_{ei} h_i)}{\gamma^c_{ei} \cosh(\gamma^a_{ei} h_i) + S^e_{uvi\pm} \sinh(\gamma^b_{ei} h_i)} \tag{7.27}$$

where

$$y^e_{uvi} = y^e_{vi} \frac{\alpha_n \beta (\mu_{xi} - \mu_{zi})}{\delta^2_{n\mu}} \tag{7.28}$$

and

$$S^e_{uvi\pm} = \tilde{Y}^e_{uv(i\pm1)\pm} \frac{\gamma^c_{ei}}{y^e_{uvi}} (i = 2, 3..., M-1) \tag{7.29}$$

with initial conditions $\tilde{Y}^e_{uv1-} = y^e_{uv1} \coth(\gamma^b_{e1} h_1)$ and $\tilde{Y}^e_{uvM+} = y^e_{uvM} \coth(\gamma^b_{eM} h_M)$ assuming the top and bottom boundary to be PEC.

7.2.3 TE^y

The current density $\tilde{J}_u$ is responsible for the TE^y fields. Similar to the TM^y case, the self impedance ($\tilde{Z}^h_{ui}$) corresponding to i^{th} metallization layer is defined as:

$$\tilde{Z}^h_{ui} = \frac{\tilde{E}_{ui}}{\tilde{J}_{ui}} \tag{7.30}$$

It is obtained by taking the reciprocal of the sum of the admittances looking up ($\tilde{Y}^h_{ui\ \text{up}}$) and down ($\tilde{Y}^h_{vi\ \text{down}}$) from the interface with the metallization assuming that there is no metallization present in any of the other layers.

$$\tilde{Z}^h_{ui} = \frac{1}{\tilde{Y}^h_{ui\ \text{up}} + \tilde{Y}^h_{ui\ \text{down}}} \tag{7.31}$$

$\tilde{Y}^h_{ui\ \text{up}}$ is determined by iterating from topmost layer to the $(i+1)^{th}$ layer and $\tilde{Y}^h_{ui\ \text{down}}$ by iterating from bottom most layer to the i^{th} layer using the recursive relation [64]:

$$\tilde{Y}^h_{ui\pm} = y^h_{ui} \frac{S^h_{ui\pm} \cosh(\gamma^a_{hi} h_i) + \gamma^d_{hi} \sinh(\gamma^b_{hi} h_i)}{S^h_{ui\pm} \sinh(\gamma^a_{hi} h_i) + \cosh(\gamma^b_{hi} h_i)} \tag{7.32}$$

where $\gamma^d_{hi} = \gamma^b_{hi}/\gamma^a_{hi}$,

$$y^h_{ui} = \frac{j\delta_n^2 \gamma^a_{hi}}{\omega \delta^2_{n\mu}},\ \gamma^c_{hi} = \frac{\gamma^a_{hi}}{\gamma^b_{hi}} \tag{7.33}$$

and

$$S^h_{ui\pm} = \frac{\tilde{Y}^h_{u(i\pm1)\pm}}{y^h_{ui}} (i = 2, 3.., M-1) \tag{7.34}$$

with initial conditions $\tilde{Y}^h_{u1-} = y^h_{u1} \coth(\gamma^a_{h1} h_1)$ and $\tilde{Y}^h_{uM+} = y^h_{uM} \coth(\gamma^a_{hM} h_M)$.

7.3 Transfer Impedance

7.3.1 TM^y

The transfer impedance corresponding to the TM^y mode ($\tilde{Z}^h_{vij}$) is defined assuming that there is no metallization in any layer accept the j^{th} as follows [65]:

$$\tilde{Z}^e_{vij} = \frac{\tilde{E}_{vi}}{\tilde{J}_{vj}} \tag{7.35}$$

For $i < j$

$$\tilde{Z}^e_{vij} = \tilde{Z}^e_{vj} \prod_{k=m_i+1}^{m_j} \frac{\tilde{E}_{vk}(\alpha_n, H_k)}{\tilde{E}_{vk}(\alpha_n, H_{k-1})} = \tilde{Z}^e_{vj} \prod_{k=m_{i+1}}^{m_j} \frac{\tilde{y}^e_{vk}}{\tilde{y}^e_{vk} \cosh(\gamma^b_{hk} h_k) + \tilde{Y}^e_{v(k-1)-} \sinh(\gamma^a_{hk} h_k)} \tag{7.36}$$

For $i > j$

$$\tilde{Z}^e_{vij} = \tilde{Z}^e_{vj} \prod_{k=m_j+1}^{m_i} \frac{\tilde{E}_{vk}(\alpha_n, H_{k-1})}{\tilde{E}_{vk}(\alpha_n, H_k)} = \tilde{Z}^e_{vj} \prod_{k=m_j}^{m_{i+1}} \frac{\tilde{y}^e_{vk}}{\tilde{y}^e_{vk} \cosh(\gamma^b_{hk} h_k) + \tilde{Y}^e_{v(k+1)+} \sinh(\gamma^a_{hk} h_k)} \tag{7.37}$$

7.3.2 TE^y

The transfer impedance corresponding to the TE^y mode ($\tilde{Y}^h_{uij}$) is defined assuming that there is no metallization in any layer accept the j^{th} as follows:

$$\tilde{Z}^h_{uij} = \frac{\tilde{E}_{ui}}{\tilde{J}_{uj}} \tag{7.38}$$

For $i < j$

$$\tilde{Z}^h_{uij} = \tilde{Z}^h_{uj} \prod_{k=m_i+1}^{m_j} \frac{\tilde{E}_{uk}(\alpha_n, H_k)}{\tilde{E}_{uk}(\alpha_n, H_{k-1})} = \tilde{Z}^h_{uj} \prod_{k=m_{i+1}}^{m_j} \frac{\tilde{y}^h_{uk}}{\tilde{y}^h_{uk}\cosh(\gamma^b_{hk}h_k) + \tilde{Y}^h_{u(k-1)-}\sinh(\gamma^a_{hk}h_k)} \tag{7.39}$$

For $i > j$

$$\tilde{Z}^h_{uij} = \tilde{Z}^h_{uj} \prod_{k=m_j+1}^{m_i} \frac{\tilde{E}_{uk}(\alpha_n, H_{k-1})}{\tilde{E}_{uk}(\alpha_n, H_k)} = \tilde{Z}^h_{uj} \prod_{k=m_j}^{m_{i+1}} \frac{\tilde{y}^h_{uk}}{\tilde{y}^h_{uk}\cosh(\gamma^b_{hk}h_k) + \tilde{Y}^h_{u(k+1)+}\sinh(\gamma^a_{hk}h_k)} \tag{7.40}$$

7.3.3 Conjoint Transfer Impedance Parameter

For the biaxial anisotropic materials it is not possible to decouple the TE^y and TM^y modes into two independent transmission lines as is possible for the uniaxial case [66]. Hence, we introduce a new conjoint transfer impedance parameter in order to consider the remaining field components i.e. $\tilde{E}_v$ for the TE^y mode and $\tilde{H}_u$ for the TM^y mode. This conjoint parameter is nothing but the TM^y transfer impedance expressing the coupling effect due to the source $\tilde{J}_{uj}$ to the field at the i^{th} metallization interface due to the presence of both $\tilde{J}_{uj}$ and $\tilde{J}_{vj}$ in its equivalent circuit at the same time. It is defined as:

$$\tilde{Z}^e_{uvij} = \frac{\tilde{E}_{vi}}{\tilde{J}_{uj}} \tag{7.41}$$

The derivation of the conjoint transfer impedance has been left as future work for those interested in biaxial anisotropic medium.

7.4 Green's Function

Using these impedances we can express the Fourier transform of electric field components in terms of the Fourier transform of current components. For the uniaxial anisotropic case this relation can be written as:

$$\begin{bmatrix} \tilde{E}_{u1} \\ \tilde{E}_{v1} \\ \tilde{E}_{u2} \\ \tilde{E}_{v2} \\ \dots \\ \tilde{E}_{uN} \\ \tilde{E}_{vN} \end{bmatrix} = \begin{bmatrix} \tilde{Z}^h_{u1} & 0 & \tilde{Z}^h_{u12} & 0 & \tilde{Z}^h_{u13} & \dots & \tilde{Z}^h_{u1N} & 0 \\ 0 & \tilde{Z}^e_{v1} & 0 & \tilde{Z}^e_{v12} & 0 & \dots & 0 & \tilde{Z}^e_{v1N} \\ \dots & \dots & \dots & \dots & \dots & \dots & \dots & \dots \\ \tilde{Z}^h_{uN1} & 0 & \tilde{Z}^h_{uN2} & 0 & \tilde{Z}^h_{uN3} & \dots & \tilde{Z}^h_{uN} & 0 \\ 0 & \tilde{Z}^e_{vN1} & 0 & \tilde{Z}^e_{vN2} & 0 & \dots & 0 & \tilde{Z}^e_{vN} \end{bmatrix} \times \begin{bmatrix} \tilde{J}_{u1} \\ \tilde{J}_{v1} \\ \tilde{J}_{u2} \\ \tilde{J}_{v2} \\ \dots \\ \tilde{J}_{uN} \\ \tilde{J}_{vN} \end{bmatrix} \tag{7.42}$$

But for the biaxial anisotropic medium we need to include terms corresponding to the conjoint self and transfer admittance in the admittance matrix so the current field relationship can be written as:

$$\begin{bmatrix} \tilde{E}_{u1} \\ \tilde{E}_{v1} \\ \tilde{E}_{u2} \\ \tilde{E}_{v2} \\ \dots \\ \tilde{E}_{uN} \\ \tilde{E}_{vN} \end{bmatrix} = \begin{bmatrix} \tilde{Z}^h_{u1} & 0 & \tilde{Z}^h_{u12} & 0 & \tilde{Z}^h_{u13} & \dots & \tilde{Z}^h_{u1N} & 0 \\ \tilde{Z}^e_{uv1} & \tilde{Z}^e_{v1} & \tilde{Z}^e_{uv12} & \tilde{Z}^e_{v12} & \tilde{Z}^e_{uv13} & \dots & \tilde{Z}^e_{uv1N} & \tilde{Z}^e_{v1N} \\ \dots & \dots & \dots & \dots & \dots & \dots & \dots & \dots \\ \tilde{Z}^h_{uN1} & 0 & \tilde{Z}^h_{uN2} & 0 & \tilde{Z}^h_{uN3} & \dots & \tilde{Z}^h_{uN} & 0 \\ \tilde{Z}^e_{uvN1} & \tilde{Z}^e_{vN1} & \tilde{Z}^e_{uvN2} & \tilde{Z}^e_{vN2} & \tilde{Z}^e_{uvN3} & \dots & \tilde{Z}^e_{uvN} & \tilde{Z}^e_{vN} \end{bmatrix} \times \begin{bmatrix} \tilde{J}_{u1} \\ \tilde{J}_{v1} \\ \tilde{J}_{u2} \\ \tilde{J}_{v2} \\ \dots \\ \tilde{J}_{uN} \\ \tilde{J}_{vN} \end{bmatrix} \tag{7.43}$$

Thus,

$$[E_{uv}] = [Z_{uv}][J_{uv}] \tag{7.44}$$

Having obtained the impedance matrix in the (u, v) coordinates we go back to the (x, z) using the following sequence of transformations.

$$[E_{xz}] = [T^{-1}][Z_{uv}][T][J_{xz}] \tag{7.45}$$

$$[E_{xz}] = [G_{xz}][J_{xz}] \tag{7.46}$$

where T is the transformation matrix (whose inverse is same as the matrix itself) with all elements zero except a repetition of the 2×2 matrix along it main diagonal as shown below:

$$T = T^{-1} = \begin{bmatrix} -\cos\theta & \sin\theta & 0 & 0 & .... & 0 & 0 \\ \sin\theta & \cos\theta & 0 & 0 & .... & 0 & 0 \\ 0 & 0 & -\cos\theta & \sin\theta & .... & 0 & 0 \\ 0 & 0 & \sin\theta & \cos\theta & .... & 0 & 0 \\ 0 & 0 & 0 & 0 & .... & -\cos\theta & \sin\theta \\ 0 & 0 & 0 & 0 & .... & \sin\theta & \cos\theta \end{bmatrix} \tag{7.47}$$

where $\theta = \cos^{-1}(\beta/\sqrt{\alpha_n^2 + \beta^2})$. Finally, in the (x, y) coordinates the matrix relation can be written as:

$$\begin{bmatrix} \tilde{E}_{x1} \\ \tilde{E}_{z1} \\ \tilde{E}_{x2} \\ \tilde{E}_{z2} \\ ... \\ \tilde{E}_{xN} \\ \tilde{E}_{zN} \end{bmatrix} = \begin{bmatrix} Z_{11} & Z_{12} & Z_{13} & ..... & Z_{1(2N)} \\ Z_{21} & Z_{22} & Z_{23} & ..... & Z_{2(2N)} \\ Z_{31} & Z_{32} & Z_{33} & ..... & Z_{3(2N)} \\ Z_{(2N)1} & Z_{(2N)2} & Z_{(2N)3} & ..... & Z_{(2N)(2N)} \end{bmatrix} \times \begin{bmatrix} \tilde{J}_{x1} \\ \tilde{J}_{v1} \\ \tilde{J}_{x2} \\ \tilde{J}_{v2} \\ ... \\ \tilde{J}_{xN} \\ \tilde{J}_{vN} \end{bmatrix} \tag{7.48}$$

7.5 Current Basis Function

Unknown current can be expanded in the form of suitable basis functions. Chebyshev polynomials are the best choice for the case when we are treating the metal as PEC. But if we use

other approximations for the finite thickness and conductivity a subdomain basis like the triangle-triangle basis would be a better choice. The unknown current on the k^{th} metal line on the m^{th} metallization interface can be expanded using suitable basis functions as follows:

$$\tilde{J}_{xmk}(x) = \sum_{r=1}^{P_{mk}} a_{rmk} \tilde{J}_{xrmr}(x) \tag{7.49}$$

$$\tilde{J}_{zmk}(x) = \sum_{r=1}^{Q_{mk}} b_{rmk} \tilde{J}_{zrmr}(x) \tag{7.50}$$

Using the Galerkin's method and Parseval's theorem the elements of the MoM matrix can be written as:

$$K_{pq}^{smk,tnr} = \sum_{n=1}^{\infty} G_{pq}^{mn}(\alpha_n, \beta) \tilde{J}_{psmk} \tilde{J}_{qtnr} \tag{7.51}$$

where $(p, q) \in (x, z)$, mk refers to the k^{th} metal line in the m^{th} metallization layer from the bottom and nr refers to the r^{th} metal line in the n^{th} metallization layer from the bottom. (s, t) are the s^{th} and t^{th} basis corresponding to p and q, respectively. The matrix $[K]$ will be a square matrix with side consisting of (Total metal lines $\times$ (Mx+Mz)) elements. Then by equating the determinant of the $[K]$ we can obtain the value of β. Once we know the β for a particular mode we can obtain the eigen vectors. And on getting the eigen vectors we can get the current distribution on the strip. From the current distribution we can obtain all the field components.

7.6 Numerical Results

Table 7.1 shows the normalized propagation constant for the shielded microstrip with two metal lines in different layers as shown in Figure 7.3 for different basis and different number of terms of the summation. Our results converge for different basis as well as different number of terms. The results are also in close agreement with the space domain approach used by [4].

Table 7.2 show a comparison of the normalized propagation constants for the shielded microstrip shown in Figure 7.4 as function of frequency with that obtained by Kaladhar and Chew

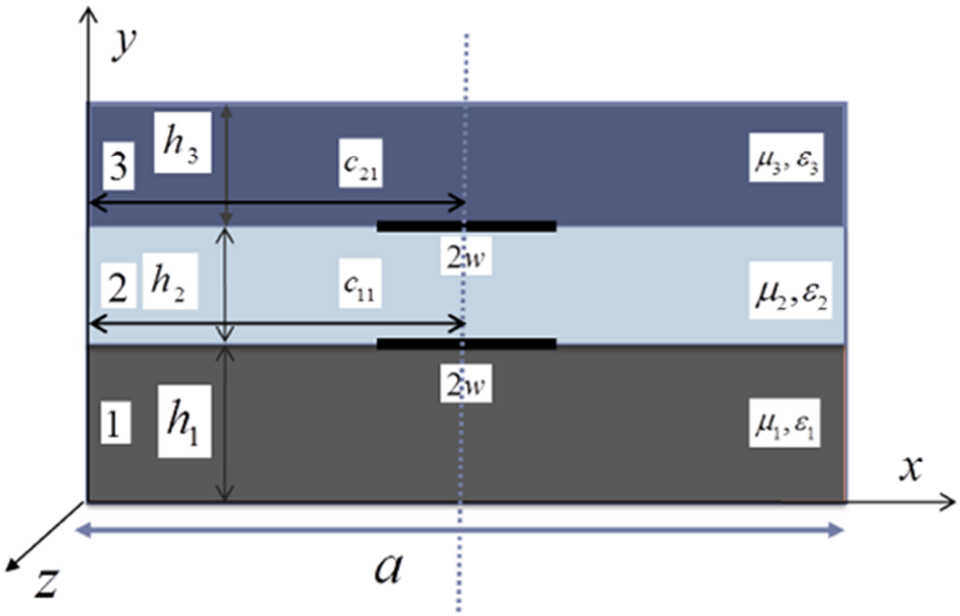

Figure 7.3 A three layered shielded microstrip with two metal lines in different layers and parameters ϵ_{r1} =ϵ_{r2}=[4 4 4], ϵ_{r3} =[1 1 1], μ_{r1} = μ_{r2} = μ_{r3} =[1 1 1], h_1= h_2=1mm, h_3=6mm, $2w$=1mm a=10mm [4].

[2] using the finite difference approach. The results show good agreement.

Table 7.1 β/k_0 for different $N_{\max}$ for the different modes of a three layered shielded microstrip with two metal lines in different layers with parameters as shown in Figure 7.3 at 31.59 GHz for $c_{11} = a/2$ and $c_{21} = a/2$.

			Normalized propagation constant				
$N_{\max}$	M_z	M_x	**Mode 1**	**Mode 2**	**Mode 3**	**Mode 4**	**Mode 5**
100	2	2	1.9829	1.8407	1.0700	0.8330	0.3420
100	8	8	1.9884	1.8469	1.0694	0.8331	0.3438
200	8	8	1.9834	1.8411	1.0703	0.8336	0.3419
300	8	8	1.9826	1.8401	1.0705	0.8338	0.3415
			1.963 [4]	1.854[4]	1.06[4]	0.835[4]	0.338[4]

Table 7.2 β/k_0 for different frequencies using $N_{\max}$=300, M_x=4 and M_z=4 for the dominant mode of a three layered uniaxial anisotropic shielded microstrip with parameters as shown in Figure 7.4

Frequency (in GHz)	$\beta/\mathbf{k_0}$	$\beta/\mathbf{k_0}$[2]
6	3.2320	3.2321
12	3.3028	3.2972
18	3.3344	3.3337
24	3.3585	3.3591
30	3.3801	3.3795

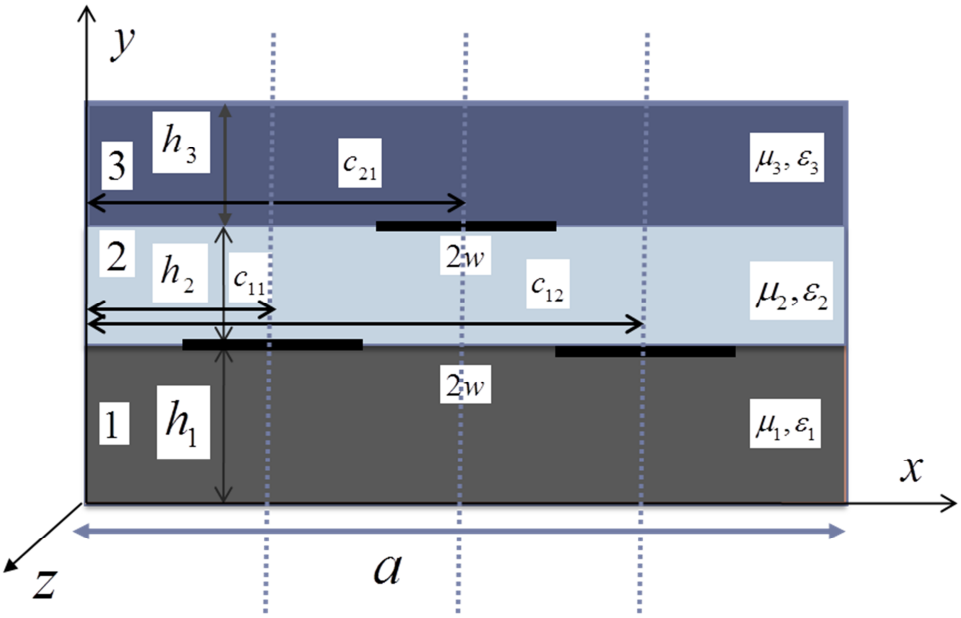

Figure 7.4 A three layered shielded microstrip with a total of three metal lines in two different layers and parameters ϵ_{r1} =ϵ_{r2}=[9.4 11.6 9.4], ϵ_{r3} =[1 1 1], μ_{r1} = μ_{r2} = μ_{r3} =[1 1 1], h_1= h_2=1mm, h_3=4mm, $2w$=1mm a=10mm, c_{11}=3.5 mm, c_{12}= 6.5 mm and c_{21}=5 mm [2].

7.7 Acceleration Using the Two Super Convergent Series Approach

Since, as the number of metal lines increases the size of the MoM increase very rapidly. So there is a need to speed up the computation of the matrix elements and there has not been any attempt to solve this problem to the best of our knowledge due to its sheer complexity. But using the approach developed in the previous chapter and the corresponding assumptions it is very easy to speed up the computation of the matrix elements by many orders of magnitude and obtain very accurate results for the propagation constant.

In that case we saw that the effect of all the layers accept the layer above and below the metal lines will be negligible for large values of α_n, similarly we can use the same approximation in the case when we have multiple metal lines in different layers. Therefore, we do not need to include the effect of interaction between metal lines which are separated by more than one layer after considering the minimum number of terms (N_{min}) in the summation. An expression of N_{min} has already been derived and presented in our earlier work.

So, for the terms of the Green's function which take care of the cross coupling we only need to find the leading term extraction for the case where the separation of the layers with the metal lines is equal to one layer. Other terms, will have very negligible effect which will change the result in the 9th digit of decimal of a value of N_{min} between $50 - 100$ for the dimensions of the order of interest in interconnects.

Also, the approach for the numerical extraction of the leading terms which we have developed can be very easily used to extract the asymptotic terms of the Green's function in this case because it is very tedious to extract even the first two leading terms analytically. Rest of the procedure will be the same as that for the shielded microstrip with multiple metal lines in the same layer.

CHAPTER 8. Summary and Contributions

The work reported in this thesis is summarized below.

1. A method to derive the Green's function for an open microstrip using the combination of TE^y, TM^y mode has been outlined.

2. Two novel approaches for fast convergence for series, namely, two super convergent series and mid point summation have been developed and applied to accelerate the SDA for shielded microstrip interconnects. A method for recursively calculating the coefficients in the MPS has been developed. This technique is one order faster than the existing Euler Maclaurin formula.

3. These combined with the leading term extraction for the Bessel's and Green's function have been used to accelerate the infinite series summation occurring the spectral domain approach for shielded microstrip problems. The speed of computation of the elements of the Galerkin matrix has been increased by nearly six orders of magnitude compared to the SDA without acceleration. And a solutions for the propagation constant correct up to twelve significant digits can be obtained using a few hundred terms of the summation which would otherwise take 10^{12} terms of the infinite summation.

4. SDIA for shielded multilayered microstrip has been accelerated by nearly six orders of magnitude using two super convergent series approach to speed up the infinite summation occurring in the elements of the Galerkin Matrix. Closed form formula for choosing the parameters to further speed up the second type of super convergent series have been derived. Also,

a formula to choose the number of terms of the second super convergent series for a given accuracy has been derived.

5. A simple and fast numerical technique to obtain higher order leading terms of the Green's function has been developed. It can be very handy in obtaining the asymptotic expansion when it is difficult to do it analytically.

6. An equivalent model for multilayered lossy shielded microstrip has been developed using the accelerated SDIA. The model can be used to reduce multiple lossy as well as lossless layers to a single layer and also retains the inhomogeneity of the shielded microstrip. The model is frequency independent for frequencies below the transition frequency. For frequencies higher than the transition frequency the equivalent model is not frequency independent but it gives good results for the higher order mode although it is derived using the dominant mode.

7. If one of the layers is semiconductor or metallic with finite conductivity. Using h equal to the sum of the thickness of all the layers above it and n skin depths of this layer, if it is thick enough, we can obtain approximately $n-1$ significant digits in the value of complex ϵ_{reff} and hence the ϵ_{req}. The layers below this will have negligible effect on the equivalent model and can be neglected.

8. Several interesting frequency independent characteristics of multilayered lossy and lossless microstrip have been found both at low as well as high frequencies. One very interesting result is that when we have a multilayered microstrip where some or all the layers have a finite conductivity σ_i. For this case, we observe two transition frequencies. The first transition frequency depends on the layer with the highest value of σ_i/ϵ_{ri} irrespective of its location w.r.t the signal metal and the transition occurs when the ratio $(\sigma_i/\epsilon_i)_{\text{max}}/\omega$ becomes equal to 1. The second transition frequency occurs when the thickness of the layer with the highest value of ϵ_{ri} becomes comparable to the wavelength. Between the first and the second

transition frequencies we see the near field effect and the ϵ_{reff} and σ_{reff} depend highly on the layers nearest to the signal metal.

9. SDIA was extended to handle multiple metal lines in the same layer for a multilayered shielded microstrip. Then, the SDIA for this case was accelerated using the two super convergent series approach which was used for single metal line to obtain a speed up of more than four order of magnitude compared to the standard SDIA.

10. The convergence of different basis functions including the pulse-triangle basis, the triangle-triangle basis and the Chebyshev polynomials has been compared

11. SDIA was further extended to handle multiple metal lines in different layers for the uniaxial anisotropic medium. Also, some ideas have been proposed to accelerate it using the same asymptotic extraction followed by the use of two super convergent series approach used before.

12. Several existing techniques for modeling the finite thickness and conductivity of metal lines including IBC approximation, R-Card approximation and the IBC/R-Card approximation and the two strip approximation have been studied. Also pulse-triangle basis and the triangle-triangle basis have been implemented so as to integrate these approximation into the spectral domain immitance approach.

8.1 Future Work

1. Accelerating the SDIA for multiple metal lines in different layers using the two super convergent series approach and integrating the approximations for the finite thickness and conductivity into the SDIA for this case.

2. Developing an equivalent model for finding the effective medium parameters for the case when we have multiple metal lines in different layers.

3. Extending the SDIA to a multilayered biaxial anisotropic medium with multiple metal lines in different layers.

4. Solving the 3D problem so that we can deal with interconnects which are perpendicular to each other and also metal patches with finite thickness and conductivity and then accelerating it using the two superconvergent series approach.

APPENDIX A. Super Convergent Series for Higher Orders

$$\sum_{n=1,3,5,..}^{\infty} \cos(nz)/n^3 = 1.051799790264645 + z^2/4\ln(z/2) - 3z^2/8 + z^4/288 + 7z^6/86400 + 31z^8/10160640 + 127z^{10}/870912000 + 73z^{12}/9032601600 + .. \quad \text{(A.1)}$$

$$\sum_{n=1,3,5,..}^{\infty} \sin(nz)/n^4 = 1.051799790264645z + z^3/12\ln(z/2) - 11z^3/72 + z^5/1440 + z^7/86400 + 31z^9/91445760 + 127z^{11}/9580032000 + 73z^{13}/117423820800 + .. \quad \text{(A.2)}$$

$$\sum_{n=1,3,5,..}^{\infty} \cos(nz)/n^5 = 1.004523762795139 - (0.525899895132322z^2 + z^4/48\ln(z/2) - 25z^4/576 + z^6/8640 + 7z^8/4838400 + 31z^{10}/914457600 + 127z^{12}/114960384000 + 73z^{14}/1643933491200 + ..) \quad \text{(A.3)}$$

$$\sum_{n=1}^{\infty} \cos(nz)/n^3 = 1.202056903159594 + z^2/2\ln z - 3z^2/4 - z^4/288 - z^6/86400 - z^8/10160640 - .. \quad \text{(A.4)}$$

$$\sum_{n=1}^{\infty} \sin(nz)/n^4 = 1.2020569031595942z + z^3/6\ln z - 11z^3/36 - z^5/1440 - z^7/604800 - z^9/(91445760) - .. \quad \text{(A.5)}$$

$$\sum_{n=1}^{\infty} \cos(nz)/n^5 = 1.036927755143370 - (1.2020569031595942 z^2/2 + z^4/24 \ln z - 11z^4/144 - z^4/96 - z^6/8640 - z^8/4838400) - .. \quad \text{(A.6)}$$

APPENDIX B. Spectral Domain Analysis of Open Microstrip Using TE^y and TM^y Modes

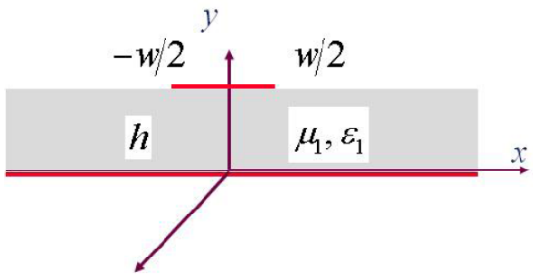

B.1 Spectral Domain Analysis

The structure cannot support pure TEM modes. The solutions are hybrid modes which are superpositions of TE^y and TM^y.

B.2 Vector Potentials

The vector potential of TE^y modes is

$$F_y(x,y,z) = \frac{1}{2\pi} e^{-j\beta z} \int_{-\infty}^{\infty} d\alpha\, f(\alpha,y) e^{-j\alpha x}$$

and the vector potential of TM^y modes is

$$A_y(x,y,z) = \frac{1}{2\pi} e^{-j\beta z} \int_{-\infty}^{\infty} d\alpha\, g(\alpha,y) e^{-j\alpha x}$$

where

$$f(\alpha, y) = \begin{cases} f_1(\alpha, y) & y \leq h \\ \\ f_2(\alpha, y) & y > h \end{cases}$$

$$g(\alpha, y) = \begin{cases} g_1(\alpha, y) & y \leq h \\ \\ g_2(\alpha, y) & y > h \end{cases}$$

They satisfy homogeneous Helmholtz equation in source free region ($y \neq h$),

$$\nabla_t^2 \Phi_i^{(p)}(x, y) + (k_i^2 - \beta^2)\Phi_i^{(p)}(x, y) = 0$$

where $\tilde{\Phi}_i^{(h)}(\alpha, y) = f_i(\alpha, y)$, $\tilde{\Phi}_i^{(e)}(\alpha, y) = g_i(\alpha, y)$, $k_i^2 = \omega^2 \epsilon_i \mu_i$, $i = 1, 2$ and $p = e, h$

The general solution can be written as:

$$\begin{aligned} \tilde{\Phi}_i^{(p)}(\alpha, y) &= A_i^{(p)}(\alpha) e^{\gamma_i y} + B_i^{(p)}(\alpha) e^{-\gamma_i y} \\ &= A_i^{(p)}(\alpha) \sinh(\gamma_i y) + B_i^{(p)}(\alpha) \cosh(\gamma_i y) \end{aligned}$$

where $\gamma_i^2 = \alpha^2 + \beta^2 - k_i^2$ and $i = 1, 2$.

The fields for TM and TE modes can be written as

$$\begin{aligned} E_{xi}(x, y) &= \frac{1}{\epsilon_i} \frac{\partial F_y}{\partial z} - \frac{j}{\omega \mu_i \epsilon_i} \frac{\partial^2 A_y}{\partial x \partial y} \\ E_{yi}(x, y) &= -\frac{j}{\omega \mu_i \epsilon_i} \left(\frac{\partial^2}{\partial y^2} + k_i^2 \right) A_y \\ E_{zi}(x, y) &= -\frac{1}{\epsilon_i} \frac{\partial F_y}{\partial x} - \frac{j}{\omega \mu_i \epsilon_i} \frac{\partial^2 A_y}{\partial y \partial z} \end{aligned}$$

$$H_{xi}(x,y) = -\frac{j}{\omega\mu_i\epsilon_i}\frac{\partial^2 F_y}{\partial x \partial y} - \frac{1}{\mu_i}\frac{\partial A_y}{\partial z}$$
$$H_{yi}(x,y) = -\frac{j}{\omega\mu_i\epsilon_i}\left(\frac{\partial^2}{\partial y^2} + k_i^2\right) F_y$$
$$H_{zi}(x,y) = -\frac{j}{\omega\mu_i\epsilon_i}\frac{\partial^2 F_y}{\partial y \partial z} + \frac{1}{\mu_i}\frac{\partial A_y}{\partial x}$$

In the spectral domain after dropping the $e^{-j\beta z}$ the fields can be written as:

$$\tilde{E}_{xi}(\alpha,y) = -\frac{j\beta}{\epsilon_i} f(\alpha,y) - \frac{\alpha}{\omega\mu_i\epsilon_i}\frac{\partial g(\alpha,y)}{\partial y}$$
$$\tilde{E}_{yi}(\alpha,y) = -\frac{j}{\omega\mu_i\epsilon_i}\left(\frac{\partial^2}{\partial y^2} + k_i^2\right) g(\alpha,y)$$
$$\tilde{E}_{zi}(\alpha,y) = \frac{j\alpha}{\epsilon_i} f(\alpha,y) - \frac{\beta}{\omega\mu_i\epsilon_i}\frac{\partial g(\alpha,y)}{\partial y}$$

$$\tilde{H}_{xi}(\alpha,y) = -\frac{\alpha}{\omega\mu_i\epsilon_i}\frac{\partial f(\alpha,y)}{\partial y} + \frac{j\beta}{\mu_i} g(\alpha,y)$$
$$\tilde{H}_{yi}(\alpha,y) = -\frac{j}{\omega\mu_i\epsilon_i}\left(\frac{\partial^2}{\partial y^2} + k_i^2\right) f(\alpha,y)$$
$$\tilde{H}_{zi}(\alpha,y) = -\frac{\beta}{\omega\mu_i\epsilon_i}\frac{\partial f(\alpha,y)}{\partial y} - \frac{j\alpha}{\mu_i} g(\alpha,y)$$

B.3 Boundary Conditions

At infinity the fields must vanish, so we have

$$f_2(\alpha,y) = A_2^{(h)}(\alpha) e^{-\gamma_2(y-h)}$$

$$g_2(\alpha,y) = A_2^{(e)}(\alpha) e^{-\gamma_2(y-h)}$$

At $y = 0$

$$E_{x1}(x,0) = 0 \implies \tilde{E}_{x1}(\alpha,0) = 0$$

$$\frac{-j\beta}{\epsilon_1} B_1^{(h)}(\alpha) - \frac{\alpha\gamma_1}{\omega\epsilon_1\mu_1} A_1^{(e)}(\alpha) = 0$$

$$A_1^{(e)}(\alpha) = -\frac{j\beta\omega\mu_1}{\gamma_1\alpha} B_1^{(h)}(\alpha)$$

$$E_{z1}(x,0) = 0 \implies \tilde{E}_{z1}(\alpha,0) = 0$$

$$\frac{j\alpha}{\epsilon_1} B_1^{(h)}(\alpha) - \frac{\beta\gamma_1}{\omega\epsilon_1\gamma_1} A_1^{(e)}(\alpha) = 0$$

$$A_1^{(e)}(\alpha) = \frac{j\alpha\omega\mu_1}{\gamma_1\beta} B_1^{(h)}(\alpha)$$

$$A_1^{(e)}(\alpha) = B_1^{(h)}(\alpha) = 0$$

Therefore

$$f_1(\alpha, y) = A_1^{(h)} \sinh(\gamma_1 y)$$

$$g_1(\alpha, y) = B_1^{(e)} \cosh(\gamma_1 y)$$

The tangential components of electric field must be continuous across the boundary.

Put

$$A(\alpha) = \frac{A_1^{(h)}(\alpha)}{\epsilon_r}$$

and

$$B(\alpha) = \frac{B_1^{(e)}(\alpha)}{\epsilon_r\mu_r}$$

The tangential components of electric field must be continuous across the boundary.

$$E_{x1}(x,h) = E_{x2}(x,h), \implies \tilde{E}_{x1}(\alpha,h) = \tilde{E}_{x2}(\alpha,h), \implies$$

$$\frac{-j\beta}{\epsilon_0}\left(B_2^{(h)}(\alpha)-\frac{A_1^{(h)}(\alpha)\sinh(\gamma_1 h)}{\epsilon_r}\right)-\frac{\alpha}{\omega\mu_0\epsilon_0}\left(-\gamma_2 B_2^{(e)}(\alpha)-\frac{\gamma_1 B_1^{(e)}(\alpha)\sinh(\gamma_1 h)}{\mu_r\epsilon_r}\right)=0$$

$$E_{z1}(z,h)=E_{z2}(z,h)\implies \tilde{E}_{z1}(\alpha,h)=\tilde{E}_{z2}(\alpha,h),\Longrightarrow$$

$$\frac{-j\alpha}{\epsilon_0}\left(B_2^{(h)}(\alpha)-\frac{A_1^{(h)}(\alpha)\sinh(\gamma_1 h)}{\epsilon_r}\right)-\frac{\beta}{\omega\mu_0\epsilon_0}\left(-\gamma_2 B_2^{(e)}(\alpha)-\frac{\gamma_1 B_1^{(e)}(\alpha)\sinh(\gamma_1 h)}{\mu_r\epsilon_r}\right)=0$$

Hence from above two equations we get:

$$B_2^{(h)}(\alpha)=\frac{A_1^{(h)}(\alpha)\sinh(\gamma_1 h)}{\epsilon_r}$$

$$B_2^{(e)}(\alpha)=-\frac{\gamma_1 B_1^{(e)}(\alpha)\sinh(\gamma_1 h)}{\gamma_2\mu_r\epsilon_r}$$

$$f(\alpha,y)=\begin{cases}\epsilon_r A(\alpha)\sinh(\gamma_1 y) & y\le h\\ A(\alpha)\sinh(\gamma_1 h)e^{-\gamma_2(y-h)} & y>h\end{cases}$$

$$g(\alpha,y)=\begin{cases}\epsilon_r\mu_r B(\alpha)\cosh(\gamma_1 y) & y\le h\\ -\frac{\gamma_1 B(\alpha)}{\gamma_2}\sinh(\gamma_1 h)e^{-\gamma_2(y-h)} & y>h\end{cases}$$

Applying the boundary conditions for the magnetic field

$$H_{z2}(x,h)-H_{z1}(x,h)=J_x(x)\implies \tilde{H}_{z2}(\alpha,h)-\tilde{H}_{z1}(\alpha,h)=\tilde{J}_x(\alpha),\Longrightarrow$$

$$-\frac{\beta}{\omega\mu_2\epsilon_2}\frac{\partial f(\alpha,y)}{\partial y}\bigg|_{y=h^+}-\frac{j\alpha}{\mu 2}g(\alpha,h^+)+\frac{\beta}{\omega\mu_1\epsilon_1}\frac{\partial f(\alpha,y)}{\partial y}\bigg|_{y=h^-}+\frac{j\alpha}{\mu 1}g(\alpha,h^-)=\tilde{J}_x\implies$$

$$\frac{\beta A(\alpha)}{\omega\mu_2\epsilon_2\mu_1}\Delta_h+\frac{j\alpha B(\alpha)}{\mu_2\epsilon_2\gamma_2}\Delta_l=\tilde{J}_x$$

where

$$\Delta_h=\left[\mu_1\gamma_2\sinh(\gamma_1 h)+\mu_2\gamma_1\cosh(\gamma_1 h)\right]$$

$$\Delta_l=\left[\epsilon_2\gamma_1\sinh(\gamma_1 h)+\epsilon_1\gamma_2\cosh(\gamma_1 h)\right]$$

$$H_{x2}(x,h)-H_{x1}(x,h)=-J_z(x)\implies \tilde{H}_{x2}(\alpha,h)-\tilde{H}_{x1}(\alpha,h)=-\tilde{J}_z(\alpha),\Longrightarrow$$

$$-\frac{\alpha}{\omega\mu_2\epsilon_2}\frac{\partial f(\alpha,y)}{\partial y}\bigg|_{y=h^+}+\frac{j\beta}{\mu 2}g(\alpha,h^+)+\frac{\alpha}{\omega\mu_1\epsilon_1}\frac{\partial f(\alpha,y)}{\partial y}\bigg|_{y=h^-}-\frac{j\beta}{\mu 1}g(\alpha,h^-)=-\tilde{J}_z \implies$$

$$\frac{\alpha A(\alpha)}{\omega\mu_2\epsilon_2\mu_1}\Delta_h-\frac{j\beta B(\alpha)}{\mu_2\epsilon_2\gamma_2}\Delta_l=-\tilde{J}_z$$

Solving the equations we get

$$A(\alpha)=\frac{\omega\mu_1\epsilon_2\mu_2}{(\alpha^2+\beta^2)\Delta_h}(\beta\tilde{J}_x-\alpha\tilde{J}_z)$$

$$B(\alpha)=-\frac{j\mu_2\epsilon_2\gamma_2}{(\alpha^2+\beta^2)\Delta_l}(\alpha\tilde{J}_x+\beta\tilde{J}_z)$$

$$\begin{aligned}E_{x2}(\alpha,h)&=-\frac{j\beta\epsilon_r}{\epsilon_1}A\alpha\sinh(\gamma_1 h)-\frac{\alpha\gamma_1\epsilon_r\mu_r}{\omega\mu_1\epsilon_1}B\alpha\sinh(\gamma_1 h)\\&=G_{xx}(\alpha,\beta)\tilde{J}_x(\alpha)+G_{xz}(\alpha,\beta)\tilde{J}_z(\alpha)\end{aligned}$$

$$\begin{aligned}\tilde{E}_{z2}(\alpha,h)&=-\frac{j\alpha\epsilon_r}{\epsilon_1}A\alpha\sinh(\gamma_1 h)-\frac{\beta\gamma_1\epsilon_r\mu_r}{\omega\mu_1\epsilon_1}B\alpha\sinh(\gamma_1 h)\\&=G_{zx}(\alpha,\beta)\tilde{J}_x(\alpha)+G_{zz}(\alpha,\beta)\tilde{J}_z(\alpha)\end{aligned}$$

where

$$\epsilon_r=\epsilon_1/\epsilon_2$$

$$\mu_r=\mu_1/\mu_2$$

$$\begin{aligned}G_{xx}(\alpha,\beta)&=\left[\frac{-j\beta^2\omega\mu_1\mu_2}{(\alpha^2+\beta^2)\Delta_h}+\frac{j\alpha^2\gamma_2\gamma_1}{\omega(\alpha^2+\beta^2)\Delta_l}\right]\sinh(\gamma_1 h)\\&=\frac{j}{(\alpha^2+\beta^2)}\left(\frac{-\beta^2\omega\mu_1\mu_2}{\mu_1\gamma_2+\mu_2\gamma_1\coth(\gamma_1 h)}+\frac{\alpha^2\gamma_2\gamma_1\tanh(\gamma_1 h)}{\omega(\epsilon_2\gamma_1\tanh(\gamma_1 h)+\epsilon_1\gamma_2)}\right)\\&=\frac{j}{(\alpha^2+\beta^2)\omega\Delta}\left[(-\beta^2k_2^2+\alpha^2\gamma_2^2)\mu_1\gamma_1\tanh(\gamma_1 h)+(-\beta^2k_1^2+\alpha^2\gamma_1^2)\mu_2\gamma_2\right]\end{aligned}$$

where

$$\Delta = \left[\epsilon_2\gamma_1 \tanh(\gamma_1 h) + \epsilon_1\gamma_2\right]\left[\mu_1\gamma_2 + \mu_2\gamma_1 \coth(\gamma_1 h)\right]$$

Substituting $\gamma_2^2 = \alpha^2 + \beta^2 - k_2^2$ we get

$$\begin{aligned} G_{xx}(\alpha,\beta) &= \frac{j}{(\alpha^2+\beta^2)\omega\Delta}\left[(\alpha^2+\beta^2)(\alpha^2-k_2^2)\mu_1\gamma_1\tanh(\gamma_1 h) + (\alpha^2+\beta^2)(\alpha^2-k_1^2)\mu_2\gamma_2\right] \\ &= \frac{j}{\omega\Delta}\left[(\alpha^2-k_2^2)\mu_1\gamma_1\tanh(\gamma_1 h) + (\alpha^2-k_1^2)\mu_2\gamma_2\right] \end{aligned}$$

$$\begin{aligned} G_{xz}(\alpha,\beta) &= \frac{j\alpha\beta\omega\mu_1\mu_2}{(\alpha^2+\beta^2)\Delta_h}\sinh(\gamma_1 h) + \frac{j\alpha^2\gamma_1\gamma_2}{(\alpha^2+\beta^2)\omega\Delta_l}\sinh(\gamma_1 h) \\ &= \frac{j\alpha\beta}{(\alpha^2+\beta^2)\Delta\omega}\left[\omega^2\mu_1\mu_2(\epsilon_2\gamma_1\tanh(\gamma_1 h) + \epsilon_1\gamma_2) + \gamma_1\gamma_2\tanh(\gamma_1 h)(\mu_1\gamma_2 + \mu_2\gamma_1\coth(\gamma_1 h))\right] \\ &= \frac{j\alpha\beta}{(\alpha^2+\beta^2)\Delta\omega}\left[\mu_1\gamma_1(\gamma_2^2+k_2^2)\tanh(\gamma_1 h) + \mu_2\gamma_2(\gamma_1^2+k_1^2)\right] \\ &= \frac{j\alpha\beta}{\Delta\omega}\left[\mu_1\gamma_1\tanh(\gamma_1 h) + \mu_2\gamma_2\right] \end{aligned}$$

Substituting $\gamma_2^2 + k_2^2 = \alpha^2 + \beta^2$ and $\gamma_1^2 + k_1^2 = \alpha^2 + \beta^2$, we have

$$G_{xz}(\alpha,\beta) = \frac{j\alpha\beta}{\Delta\omega}\left[\mu_1\gamma_1\tanh(\gamma_1 h) + \mu_2\gamma_2\right]$$

$$\begin{aligned} \tilde{E}_{z2}(\alpha,h) &= \frac{j\alpha\epsilon_r}{\epsilon_1}A\alpha\sinh(\gamma_1 h) - \frac{\beta\gamma_1\epsilon_r\mu_r}{\omega\mu_1\epsilon_1}B\alpha\sinh(\gamma_1 h) \\ &= G_{zx}(\alpha,\beta)\tilde{J}_x(\alpha) + G_{zz}(\alpha,\beta)\tilde{J}_z(\alpha) \end{aligned}$$

Similarly we can find

$$G_{zx}(\alpha,\beta) = \frac{j\alpha\beta}{\Delta\omega}\left[\mu_1\gamma_1\tanh(\gamma_1 h) + \mu_2\gamma_2\right]$$
$$G_{zz}(\alpha,\beta) = \frac{j}{\omega\Delta}\Big[\mu_1\gamma_1(\beta^2 - k_2^2) + \mu_2\gamma_2(\beta^2 - k_1^2)\tanh(\gamma_1 h)\Big]$$

where

$$\Delta = \Big[\epsilon_2\gamma_1 + \epsilon_1\gamma_2\tanh(\gamma_1 h)\Big]\Big[\mu_2\gamma_1 + \mu_1\gamma_2\coth(\gamma_1 h)\Big]$$

Dividing numerator and denominator by ϵ_2 and μ_2 the Greens function can be written as:

$$G_{xx}(\alpha,\beta) = \frac{j\eta_2}{k_2\tilde{\Delta}}\Big[\gamma_2(\alpha^2 - k_1^2) + \mu_r\gamma_1(\alpha^2 - k_2^2)\tanh(\gamma_1 h)\Big]$$
$$G_{xz}(\alpha,\beta) = G_{zx}(\alpha,\beta) = \frac{j\eta_2\alpha\beta}{k_2\tilde{\Delta}}\Big[\gamma_2 + \mu_r\gamma_1\tanh(\gamma_1 h)\Big]$$
$$G_{zz}(\alpha,\beta) = \frac{j\eta_2}{k_2\tilde{\Delta}}\Big[\gamma_2(\beta^2 - k_1^2) + \mu_r\gamma_1(\beta^2 - k_2^2)\tanh(\gamma_1 h)\Big]$$
$$\tilde{\Delta} = \Big[\epsilon_r\gamma_2 + \gamma_1\tanh(\gamma_1 h)\Big]\Big[\mu_r\gamma_2 + \gamma_1\coth(\gamma_1 h)\Big]$$

BIBLIOGRAPHY

[1] G. Cano, F. Medina, and M. Horno, "Efficient spectral domain analysis of generalized multistrip lines in stratified media including thin, anisotropic, and lossy substrates," *IEEE Transactions on Microwave Theory and Techniques*, vol. 40, no. 2, pp. 217–227, Feb. 1992.

[2] K. Radhakrishnan and W. C. Chew, "Full-wave analysis of multiconductor transmission lines on anisotropic inhomogeneous substrates," *IEEE Transactions on Microwave Theory and Techniques*, vol. 47, no. 9, pp. 1764–1770, Sep. 1999.

[3] G. Cano, F. Medina, and M. Horno, "On the efficient implementation of sda for boxed strip-like and slot-like structures," *IEEE Transactions on Microwave Theory and Techniques*, vol. 46, no. 11 pt 1, pp. 1801–1806, Nov. 1998.

[4] E. Hassan, "Modal solution of generalised planar transmission lines," *IEE Proceedings - Microwaves, Antennas and Propagation*, vol. 150, no. 3, pp. 131–136, 2003.

[5] *www.ansys.com*.

[6] L. Dunleavy and P. Katehi, "Shielding effects in microstrip discontinuities," *IEEE Transactions on Microwave Theory and Techniques*, vol. 36, no. 12, pp. 1767–1774, Dec. 1988.

[7] R. Faraji-Dana and Y. Chow, "Accurate and efficient cad tool for the design of optimum packaging for (m)mics," *IEE Proceedings - Microwaves, Antennas and Propagation*, vol. 142, no. 2, pp. 81–88, Apr 1995.

[8] J. Song, *Lecture Notes on Computational Methods in Electromagnetics, 2009*.

[9] C.-W. Kuo and T. Itoh, "A flexible approach combining the spectral domain method and impedance boundary condition for the analysis of microstrip lines," *IEEE Microwave and Guided Wave Letters*, vol. 1, no. 7, pp. 172 –174, Jul. 1991.

[10] D. Nghiem, J. Williams, and D. Jackson, "A general analysis of propagation along multiple-layer superconducting stripline and microstrip transmission lines," *IEEE Transactions on Microwave Theory and Techniques*, vol. 39, no. 9, pp. 1553–1565, Sep. 1991.

[11] C. Krowne, "Dyadic green's function modifications for obtaining attenuation in microstrip transmission layered structures with complex media," *IEEE Transactions on Microwave Theory and Techniques*, vol. 50, no. 1, pp. 112–122, Jan. 2002.

[12] J. L. Tsalamengas and G. Fikioris, "Rapidly converging spectral-domain analysis of rectangularly shielded layered microstrip lines," *IEEE Transactions on Microwave Theory and Techniques*, vol. 51, no. 6, pp. 1729–1734, Jun. 2003.

[13] W. Shu, *Electromagnetic waves in double negative metamaterials and study on numerical resonances in the method of moments*. USA: Phd thesis - Iowa State University, 2008.

[14] F. Medina and M. Horno, "Quasi-analytical static solution of the boxed microstrip line embedded in a layered medium," *IEEE Transactions on Microwave Theory and Techniques*, vol. 40, no. 9, pp. 1748–1756, Sep. 1992.

[15] W. D. Munro, "Note on the euler-maclaurin formula," *The American Mathematical Monthly*, vol. 65, no. 3, pp. 201–203, Mar. 1958.

[16] *http://en.wikipedia.org/wiki/Euler%E2%80%93Maclaurin_formula*.

[17] V. Sheinin and D. ke He, "On the performance of uniform threshold quantization for a sum of independent memoryless laplacian sources," *IEEE International Conference on Acoustics, Speech and Signal Processing (ICASSP)*, vol. 3, pp. 1485–1488, Apr. 2007.

[18] S. Singh and R. Singh, "On the use of shank's transform to accelerate the summation of slowly converging series," *IEEE Transactions on Microwave Theory and Techniques*, vol. 39, no. 3, pp. 608 –610, Mar. 1991.

[19] J. R. Mosig and A. Alvarez Melcon, "The summation-by-parts algorithm - a new efficient technique for the rapid calculation of certain series arising in shielded planar structures," *IEEE Transactions on Microwave Theory and Techniques*, vol. 50, no. 1, pp. 215 – 218, Jan. 2002.

[20] A. Sidi, "The richardson extrapolation process with a harmonic sequence of collocation points," *SIAM Journal on Numerical Analysis*, vol. 37, no. 5, pp. 1729–1746, 2000.

[21] A. Verma and G. Sadr, "Unified dispersion model for multilayer microstrip line," *IEEE Transactions on Microwave Theory and Techniques*, vol. 40, no. 7, pp. 1587–1591, Jul. 1992.

[22] A. K. Verma and R. Kumar, "New empirical unified dispersion model for shielded-, suspended-, and composite-substrate microstrip line for microwave and mm-wave applications," *IEEE Transactions on Microwave Theory Techniques*, vol. 46, pp. 1187–1192, Aug. 1998.

[23] J. Zhu and D. Jiao, "A unified finite-element solution from zero frequency to microwave frequencies for full-wave modeling of large-scale three-dimensional on-chip interconnect structures," *IEEE Transactions on Advanced Packaging*, vol. 31, no. 4, pp. 873–881, Nov. 2008.

[24] P. Crespo-Valero, M. Mattes, I. Sievanovic, and J. Mosig, "Analysis of multilayer boxed printed circuits," *IEEE Mediterranean Electrotechnical Conference (MELECON)*, pp. 206–209, May 2006.

[25] Y.-S. Xu and A. Omar, "Rigorous solution of mode spectra for shielded multilayer microstrip lines," *IEEE Transactions on Microwave Theory and Techniques,*, vol. 42, no. 7, pp. 1213–1222, Jul. 1994.

[26] T. Kitazawa and T. Itoh, "Propagation characteristics of coplanar-type transmission lines with lossy media," *IEEE Transactions on Microwave Theory and Techniques*, vol. 39, no. 10, pp. 1694–1700, Oct. 1991.

[27] T. Kitazawa, "Loss calculation of single and coupled strip lines by extended spectral domain approach," *IEEE Microwave and Guided Wave Letters*, vol. 3, no. 7, pp. 211–213, Jul. 1993.

[28] R. Pucel, D. Masse, and C. Hartwig, "Losses in microstrip," *IEEE Transactions on Microwave Theory and Techniques*, vol. 16, no. 6, pp. 342–350, Jun. 1968.

[29] G. Plaza, R. Marques, and F. Medina, "Quasi-tm mol/mom approach for computing the transmission-line parameters of lossy lines," *IEEE Transactions on Microwave Theory and Techniques*, vol. 54, no. 1, pp. 198–209, Jan. 2006.

[30] T. Demeester and D. De Zutter, "Quasi-tm transmission line parameters of coupled lossy lines based on the dirichlet to neumann boundary operator," *IEEE Transactions on Microwave Theory and Techniques*, vol. 56, no. 7, pp. 1649–1660, Jul. 2008.

[31] W. Heinrich, "Full-wave analysis of conductor losses on mmic transmission lines," *IEEE Transactions on Microwave Theory and Techniques*, vol. 38, no. 10, pp. 1468–1472, Oct. 1990.

[32] J.-F. Lee, "Finite element analysis of lossy dielectric waveguides," *IEEE Transactions on Microwave Theory and Techniques*, vol. 42, no. 6, pp. 1025–1031, Jun. 1994.

[33] F. Alessandri, G. Baini, G. D'Inzeo, and R. Sorrentino, "Conductor loss computation in multiconductor mic's by transverse resonance technique and modified perturbational method," *IEEE Microwave and Guided Wave Letters*, vol. 2, no. 6, pp. 250–252, Jun. 1992.

[34] R. E. Collin, *Field Theory of Guided Waves, 2nd ed.* Piscataway ,New Jersey: IEEE Press, 1991.

[35] J. Pond, C. Krowne, and W. Carter, "On the application of complex resistive boundary conditions to model transmission lines consisting of very thin superconductors," *IEEE Transactions on Microwave Theory and Techniques*, vol. 37, no. 1, pp. 181–190, Jan. 1989.

[36] S. Amari and J. Bornemann, "Lse- and lsm-mode sheet impedances of thin conductors," *IEEE Transactions on Microwave Theory and Techniques*, vol. 44, no. 6, pp. 967–970, Jun. 1996.

[37] J.-Y. Ke and C. Chen, "Modified spectral-domain approach for microstrip lines with finite metallisation thickness and conductivity," *IEE Proceedings - Microwaves, Antennas and Propagation*, vol. 142, no. 4, pp. 357–363, Aug. 1995.

[38] J. Kiang, "Integral equation solution to the skin effect problem in conductor strips of finite thickness," *IEEE Transactions on Microwave Theory and Techniques*, vol. 39, no. 3, pp. 452–460, Mar. 1991.

[39] M. Farina and T. Rozzi, "Spectral domain approach to 2d-modelling of open planar structures with thick lossy conductors," *IEE Proceedings - Microwaves, Antennas and Propagation*, vol. 147, no. 5, pp. 321–324, Oct. 2000.

[40] J.-Y. Ke and C. Chen, "A new approach to the microstrip lines with finite strip thickness and conductivity," *IEEE MTT-S International Microwave Symposium*, vol. 2, pp. 931–934, May 1993.

[41] J. Rautio and V. Demir, "Microstrip conductor loss models for electromagnetic analysis," *IEEE Transactions on Microwave Theory and Techniques*, vol. 51, no. 3, pp. 915–921, Mar. 2003.

[42] C. A. Balanis, *Advanced Engineering Electromagnetics*. New York: Wiley, John and Sons, May 1989.

[43] J. Song, *Lecture Notes on Advanced Electromagnetic Field Theory II, 2010*.

[44] Z. Zeng, J. Song, and L. Zhang, "Dc limit of microstrip analysis using the spectral domain approach with both transverse and longitudinal currents," *IEEE Antennas and Wireless Propagation Letters*, vol. 6, pp. 560–563, 2007.

[45] G. N. Watson, *A treatise on the theory of Bessel functions*. United Kingdom: Cambridge University Press, 1995.

[46] M. Abramowitz and I. A. S. (Eds), *Handbook of Mathematical Functions*. New York: Dover Publications, 1970.

[47] *MATHCAD Software*. Engineering Calculation Software-PTC.

[48] H. M. Edwards, *Riemann's Zeta Function*. N. Chemsford, MA: Courier Dover Publications, 2001.

[49] J. Song and S. Jain, "Midpoint summation: A method for accurate and efficient summation of series appearing in electromagnetics," *IEEE Antennas and Wireless Propagation Letters*, vol. 9, pp. 1084–1087, 2010.

[50] *http://en.wikipedia.org/wiki/Bernoulli_numbers*.

[51] S. Jain and J. Song, "Accelerated spectral domain approach for shielded microstrip lines by approximating summation with super convergent series," *IEEE Conference on Electromagnetic Field Computation (CEFC), Paper 1364*, May 2010.

[52] *http://en.wikipedia.org/wiki/Speed_of_light*.

[53] J. L. Tsalamengas, *Email communication*.

[54] T. Itoh, "Spectral domain immitance approach for dispersion characteristics of generalized printed transmission lines," *IEEE Transactions on Microwave Theory Techniques*, vol. 28, no. 7, pp. 733–736, Jul. 1980.

[55] S. Jain and J. Song, "Numerical acceleration of spectral domain approach for shielded microstrip lines by approximating summation with corrected integral," *IEEE Electrical Performance of Electronic Packaging and Systems (EPEPS)*, vol. pp. 223-226, Oct. 2009.

[56] N. Das and D. Pozar, "A generalized spectral-domain green's function for multilayer dielectric substrates with application to multilayer transmission lines," *IEEE Transactions on Microwave Theory and Techniques*, vol. 35, no. 3, pp. 326–335, Mar. 1987.

[57] S. Jain and J. Song, "Efficient and accurate approximation of infinite series summation using asymptotic approximation and super convergent series," *Progress In Electromagnetics Research (PIER)*, 2011 (accepted).

[58] L. Zhang, *Accurate electromagnetic full-wave modeling for interconnects in semiconductor integrated circuits*. USA: Phd Thesis - Iowa State University, 2007.

[59] S. Tedjini, N. Daoud, D. Rauly, and E. Pic, "Analysis of mmics with finite strip thickness and conductivity," *Electronics Letters*, vol. 24, no. 15, pp. 965–966, Jul. 1988.

[60] M. Tounsi and M. Yagoub, "Hybrid-mode analysis of high-tc thick superconducting microwave circuits on multilayered anisotropic layers," *Journal of Electromagnetic Waves and Applications*, vol. 22, no. 17-18, pp. 2497–2510, 2008.

[61] Z. Qian, M. Tong, and W. Chew, "Conductive medium modeling with an augmented gibc formulation," *Progress In Electromagnetics Research*, vol. 99, pp. 261–272, 2009.

[62] Z. G. Qian, W. C. Chew, and R. Suaya, "Generalized impedance boundary condition for conductor modeling in surface integral equation," *IEEE Transactions on Microwave Theory and Techniques*, vol. 55, no. 11, pp. 2354–2364, Nov. 2007.

[63] J. Morsey, V. Okhmatovski, and A. Cangellaris, "Finite-thickness conductor models for full-wave analysis of interconnects with a fast integral equation method," *IEEE Transactions on Advanced Packaging*, vol. 27, no. 1, pp. 24–33, Feb. 2004.

[64] M. Tounsi, R. Touhami, and M. C. Yagoub, "Generic spectral immittance approach for fast design of multilayered bilateral structures including anisotropic media," *IEEE Microwave and Wireless Components Letters*, vol. 17, no. 6, pp. 409–411, Jun. 2007.

[65] ——, "Analysis of the mixed coupling in bilateral microwave circuits including anisotropy for mics and mmics applications," *Progress In Electromagnetics Research*, vol. 62, pp. 281–315, Jun. 2006.

[66] T. Ho, B. Beker, Y. Shih, and Y. Chen, "Microstrip resonators on anisotropic substrates," *IEEE Transactions on Microwave Theory and Techniques*, vol. 40, no. 4, pp. 762–765, Apr. 1992.

List of Publications

[1] S. Jain and J. Song, "Numerical acceleration of spectral domain approach for shielded microstrip lines by approximating summation with corrected integral," *IEEE 18th Conference on Electrical Performance of Electronic Packaging and Systems (EPEPS)*, pp. 223 –226, Oct. 2009.

[2] ——, "Accelerated spectral domain approach for shielded microstrip lines by approximating summation with super convergent series," *IEEE Conference on Electromagnetic Field Computation (CEFC), Paper 1364*, May 2010.

[3] J. M. Song and S. Jain, "A novel approach for approximation of summation to integral with mid-point summation to speed up the spectral domain approach for shielded microstrip lines," *IEEE Antennas and Propagation Society International Symposium, Paper 409.10*, Jul. 2010.

[4] J. Song and S. Jain, "Midpoint summation: A method for accurate and efficient summation of series appearing in electromagnetics," *IEEE Antennas and Wireless Propagation Letters*, vol. 9, pp. 1084–1087, 2010.

[5] S. Jain and J. Song, "Efficient and accurate approximation of infinite series summation using asymptotic approximation and super convergent series," *Progress in Electromagnetics Research (PIER)*, 2011 (accepted).

[6] J. Song and S. Jain, "A novel technique for approximation of summation with corrected inte-

gral (asci) to accelerate the spectral domain approach for shielded microstrip lines," *Progress in Electromagnetics Research Symposium (PIERS)*, p. 482, Jul. 2010.

[7] S. Jain, J. Song, T. Kamgaing, and Y. Mekonnen, "Equivalent model for shielded microstrip transmission lines over lossy layered substrates," *IEEE Electronic Components and Technology Conference (ECTC)*, pp. 195–201, Jun. 2011.

[8] ——, "Efficient spectral domain analysis of multilayered shielded microstrip using two super convergent series," *IEEE 20th Conference on Electrical Performance of Electronic Packaging and Systems (EPEPS)*, Oct. 2011.

[9] ——, "Efficient and accurate modeling of effective medium for interconnects in lossy shielded layered medium using fast convergent series," *IEEE Electronic Components and Technology Conference (ECTC) 2012*, (accepted).

[10] S. Jain, J. Song, and T. Kamgaing, "Acceleration of spectral domain approach for generalized multilayered shielded microstrip interconnects using two super convergent series," *IEEE Transactions on Components, Packaging and Manufacturing Technology*, (submitted).